



University of Kentucky  
UKnowledge

---

Theses and Dissertations--Chemical and  
Materials Engineering

Chemical and Materials Engineering

---

2023

## **DROP WETTING AND SLIDING ON SOFT, SWOLLEN ELASTOMERS**

Zhuoyun Cai

*University of Kentucky*, zhuoycai@gmail.com

Digital Object Identifier: <https://doi.org/10.13023/etd.2023.033>

Right click to open a feedback form in a new tab to let us know how this document benefits you.

### **Recommended Citation**

Cai, Zhuoyun, "DROP WETTING AND SLIDING ON SOFT, SWOLLEN ELASTOMERS" (2023). *Theses and Dissertations--Chemical and Materials Engineering*. 148.  
[https://uknowledge.uky.edu/cme\\_etds/148](https://uknowledge.uky.edu/cme_etds/148)

This Doctoral Dissertation is brought to you for free and open access by the Chemical and Materials Engineering at UKnowledge. It has been accepted for inclusion in Theses and Dissertations--Chemical and Materials Engineering by an authorized administrator of UKnowledge. For more information, please contact [UKnowledge@lsv.uky.edu](mailto:UKnowledge@lsv.uky.edu).

**STUDENT AGREEMENT:**

I represent that my thesis or dissertation and abstract are my original work. Proper attribution has been given to all outside sources. I understand that I am solely responsible for obtaining any needed copyright permissions. I have obtained needed written permission statement(s) from the owner(s) of each third-party copyrighted matter to be included in my work, allowing electronic distribution (if such use is not permitted by the fair use doctrine) which will be submitted to UKnowledge as Additional File.

I hereby grant to The University of Kentucky and its agents the irrevocable, non-exclusive, and royalty-free license to archive and make accessible my work in whole or in part in all forms of media, now or hereafter known. I agree that the document mentioned above may be made available immediately for worldwide access unless an embargo applies.

I retain all other ownership rights to the copyright of my work. I also retain the right to use in future works (such as articles or books) all or part of my work. I understand that I am free to register the copyright to my work.

**REVIEW, APPROVAL AND ACCEPTANCE**

The document mentioned above has been reviewed and accepted by the student's advisor, on behalf of the advisory committee, and by the Director of Graduate Studies (DGS), on behalf of the program; we verify that this is the final, approved version of the student's thesis including all changes required by the advisory committee. The undersigned agree to abide by the statements above.

Zhuoyun Cai, Student

Dr. Jonathan T. Pham, Major Professor

Dr. Fuqian Yang, Director of Graduate Studies

# DROP WETTING AND SLIDING ON SOFT, SWOLLEN ELASTOMERS

---

## DISSERTATION

---

A dissertation submitted in partial fulfillment of the  
requirements for the degree of Doctor of Philosophy in the  
College of Engineering  
at the University of Kentucky

By  
Zhuoyun Cai  
Lexington, Kentucky

Director: Dr. Jonathan T. Pham, Professor of Materials Science and Engineering  
And Co-director Dr. Matthew J. Beck, Professor of Materials Science and Engineering  
Lexington, Kentucky  
2022

Copyright © Zhuoyun Cai 2022  
[<https://orcid.org/0000-0001-2345-6789>]

## ABSTRACT OF DISSERTATION

### DROP WETTING AND SLIDING ON SOFT, SWOLLEN ELASTOMERS

Soft, slippery surfaces have gained increasing attention due to their wide range of potential applications, for example in self-cleaning, anti-fouling, liquid collection, and more. One design approach in creating slippery surfaces is using a swollen elastomer, which is a polymer network swollen with a lubricant. This type of surface may be beneficial for longer-term use than standard lubricant-infused surfaces, and provides a versatile surface with tunable mechanical properties. Hence, understanding the physics of soft surface interactions is important for fundamental soft matter physics, biomaterials, adhesives, and coatings. This research experimentally investigates wetting on soft infused networks, with the aim of providing insight towards a physical description of wetting on a low-modulus, swollen elastomer.

In principle, when a water drop is deposited on a soft surface, the surface tension of water can pull up the surface and form a wetting ridge at the drop periphery. However, when the soft material surfaces are also swollen with a fluid, the imbibed fluid may separate from the surface at the drop periphery to minimize the elastic energy that is caused by network stretching. Although significant efforts have been put into understanding the wetting ridge formation on soft crosslinked solids, as well as designing slippery, lubricant-infused porous surfaces (SLIPS), there is limited knowledge on soft and swollen surfaces. We bridge soft crosslinked solids and SLIPS by studying how infusing a soft crosslinked network with lubricant affects drop interactions, with a focus on low modulus elastomers (e.g. ~100 kPa or less). Specifically, by using silicone oil–swollen polydimethylsiloxane (PDMS) elastomers, we investigate situations of both static and dynamic wetting. My research is mainly divided into two integrated sections, briefly described below.

In the first part of this work, we present an approach to visualize a crosslinked network and its swelling fluid separately by employing fluorescent molecules and confocal microscopy. We can vividly see the PDMS network and the oil phases separately at the contact line. We systematically investigate how the degrees of crosslinking and swelling affect fluid separation and network deformation during wetting on swollen networks. The degree of swelling is varied from  $Q=1$  (dry) to saturation (maximum swelling) for four different degrees of crosslinking. Upon swelling the network to lower swelling ratios, the height of the wetting ridge increases due to the decreased modulus from swelling. As the degree of swelling increases further however, fluid clearly separates from the network. By continuing to increase the degree of swelling towards saturation, the amount of fluid separation increases. Qualitatively, the general trend of an initially increasing wetting ridge height followed by fluid separation is universal, regardless of the degree of crosslinking. Our experiments reveal that the static wetting ridge of a soft and swollen network can comprise both a region of network pullup and a region of pure fluid; this suggests that the swelling fluid, commonly found in soft networks, can play a critical role

on surface wetting properties.

In the second part, we transfer our focus from static wetting to dynamic wetting conditions to investigate the slippery properties of soft, swollen elastomers. In the dynamic wetting state, we study how the polymer network density and degree of swelling related to the pinning force and friction of a water drop. We first study when a water drop sticks or slides on a vertical, silicone oil–swollen PDMS elastomer, where gravity drives the drop to slide down while surface interactions promote drop sticking. Hence, a critical drop volume exists directly when gravity overcomes drop-surface adhesion forces. We find that the critical water drop volume for sliding decreases when increasing the degree of swelling, nearly independently from crosslinking for very soft elastomers. This is likely associated with oil separating from the bulk substrate when it encounters a water drop, lubricating the surface and decreasing the pinning force. Additionally, we develop a cantilever-based approach to measure lateral friction forces between drops and soft surfaces, while observing the water-elastomer contact line with confocal microscopy. Results show the friction force decreases when increasing the degree of swelling, which is a function of velocity.

In summary, the results demonstrate the importance of considering the fluid inside of gels when investigating wetting of soft surfaces, offering fundamental insight into soft wetting, and into the slippery properties of soft, oil-swollen elastomers.

**KEYWORDS:** Adaptive, Swollen, Wetting, Phase separation, Drop Sliding, Confocal Microscope

---

Zhuoyun Cai

---

[12/14/2022]

---

Date

DROP WETTING AND SLIDING ON SOFT, SWOLLEN ELASTOMERS

By

Zhuoyun Cai

Dr. Jonathan T. Pham

---

Director of Dissertation

Dr. Matthew J. Beck

---

Co-Director of Dissertation

Dr. Fuqian Yang

---

Director of Graduate Studies

[12/14/2022]

---

Date

## ACKNOWLEDGMENTS

My last four year's graduate study and life at UK have been enriched by interactions with many people. I appreciate everyone deeply.

My advisor, Prof. Jonathan T. Pham, who is one of the best advisors in the world, has been my role model by being encouraging, considerate, knowledgeable, energetic, and curious about everything. I wouldn't have gone this far without his guidance, support, patience and understanding. I enjoyed and will miss the delightful, inspiring, and fruitful discussions we had in the pasted four years.

I would like to thank former and current group members and visiting scholars: Dr. Krishnaroop Chaudhuri, Dr. Justin Glover, Daniel Darby, MD Sazzadul Rahat, Kyujin Ko, Lukas Hauer and Junyong Park for their great help and friendship. In addition, I would like to thank staff members: Nicholas Cprek and Paula Ackerman for their instrumental support, patience and assistance. I would also like to thank my collaborators: Dr. Artem Skabeev for his synthetic fluorescent dye that helps to visualize the oil phase in the wetting study; Dr. Svetlana Morozova for the helpful discussions for theoretical model development in the static wetting study; Lukas Hauer and Dr. Doris Vollmer for their help and discussion in experiments, theoretical model development and paper writing in the study of velocity-dependent water drop sliding on swollen elastomers.

I would like to thank Prof. Matthew Beck, Prof. Bradley Berron and Prof. Christine Trinkle for serving as my dissertation committee members and Prof. Chad Risko for being my outside examiner.

I also received equally important support from my family and friends, a special gratitude

goes to my boyfriend, Shengdong Xiao, for always providing me with unconditional and priceless love and support.

Finally, I would like to thank US National Science Foundation through award number 2043732, National Science Foundation KY-EPSCoR award 1849213, the Naval Research Lab via DTRA, and startup funds from the University of Kentucky for the financial support.

## TABLE OF CONTENTS

ACKNOWLEDGMENTS .....	iii
LIST OF FIGURES .....	viii
CHAPTER 1. INTRODUCTION.....	1
1.1 <i>Liquid-repellent surfaces</i> .....	1
1.1.1     Lotus effect.....	1
1.1.2     Slippery liquid-infused porous surfaces (SLIPS) .....	3
1.1.3     Lubricant-infused gels (swollen elastomers) .....	4
1.2 <i>Wetting on soft surfaces</i> .....	5
1.2.1     Force balance on the contact line of soft surface.....	5
1.2.2     Lubricant layer formation on infused elastomer gels .....	8
1.2.3     Phase separation at the contact line .....	10
1.3 <i>Dissertation organization</i> .....	12
CHAPTER 2. SWOLLEN ELASTOMER PREPARATION.....	13
2.1 <i>Background</i> .....	13
2.2 <i>Experimental plan</i> .....	14
2.3 <i>Preparation of bulk, as-prepared PDMS</i> .....	15
2.3.1     Extraction of uncrosslinked (free) PDMS chains .....	16
2.3.2     Swelling of extracted (dry) PDMS network with silicone oil.....	18
2.4 <i>Characterization of oil-swollen PDMS elastomer</i> .....	21
2.4.1     The degree of swelling measurement .....	21
2.4.2     Rheological measurements .....	24
2.5 <i>Summary</i> .....	28
CHAPTER 3. STATIC WETTING ON SOFT, SWOLLEN ELASTOMERS .....	30
3.1 <i>Background and introduction</i> .....	30

3.2	<i>Visualizing the fluid separation</i> .....	33
3.2.1	Special sample preparation of thin samples.....	34
3.2.2	Visualizing the wetting ridge with confocal microscopy .....	36
3.2.3	Modulus and degree of swelling variation.....	39
3.3	<i>Characterization of contact angles and fluid separation</i> .....	42
3.3.1	Contact angles .....	42
3.3.2	Wetting ridge quantification .....	44
3.3.3	Network wetting ridge height .....	47
3.3.4	Proposed fluid separation mechanism .....	50
3.3.5	Discussion .....	56
3.4	<i>Summery and conclusion</i> .....	59
CHAPTER 4. DYNAMIC WETTING ON SOFT, SWOLLEN ELASTOMERS.....		60
4.1	<i>Background and introduction</i> .....	60
4.2	<i>Drop pinning and sliding on soft swollen elastomers</i> .....	62
4.2.1	Experimental set up .....	62
4.2.2	Pinning/sliding on dry elastomers .....	63
4.2.3	Sliding on swollen elastomers .....	66
4.2.4	Calculation of critical drop volume .....	67
4.2.5	Rinsing, aging and re-lubrication .....	73
4.2.6	Oil leaching mechanism .....	76
4.3	<i>Effects of drop sliding velocity on wetting ridges</i> .....	79
4.3.1	Experimental set up .....	80
4.3.2	Kinetic friction force of a sliding water drop .....	82
4.3.3	Fluid separation during sliding .....	84
4.4	<i>Summary and conclusion</i> .....	88
CHAPTER 5. CONCLUSION AND FUTURE WORK .....		90
5.1	<i>Conclusions</i> .....	90

5.2	<i>Future work</i>	92
REFERENCES		94
VITA		106

## LIST OF FIGURES

- Figure 1.1. Scanning electron micrographs of the *Nelumbo nucifera* adaxial leaf surface (a), (b) contaminating particle on a regularly sculptured wing surface and (c) mercury droplet on the papillose adaxial epidermal surface.<sup>1</sup> (Scale bar = 1 $\mu$ m) \_\_\_\_\_ 2
- Figure 1.2. Wetting status on lotus-effect surfaces. (a) The Cassie–Baxter model and (b) the Wenzel model wetting status.<sup>3</sup> \_\_\_\_\_ 2
- Figure 1.3. Slippery lubricant-infused porous substrate (SLIPS) (a) Scheme of SLIPS<sup>8</sup> (b) optical micrographs demonstrating the mobility of a low-surface-tension liquid sliding off from SLIPS.<sup>14</sup> \_\_\_\_\_ 4
- Figure 1.4. Schematic showing under a mechanical stretch, a droplet of test liquid changes from sliding to pinning when lubricant layer cannot overcoat the substrate.<sup>16</sup> \_\_\_\_\_ 4
- Figure 1.5. Schematics illustrating a liquid drop on a rigid surface (a) and (b) on a soft deformable polymer (PDMS), (c) Neumann's triangle relating the surface tensions and contact angles of (b) in static equilibrium \_\_\_\_\_ 7
- Figure 1.6. Droplet on soft (gel-like) substrate. (a) Line force balance conditions for surface stresses. (b) Line force balance conditions with elastic force.<sup>29</sup> \_\_\_\_\_ 7
- Figure 1.7. Deformation of PDMS after water drop deposited: (a) via X-ray microscopy.<sup>32</sup> and (b) PDMS contact line via confocal microscopy.<sup>31</sup> \_\_\_\_\_ 8
- Figure 1.8 (a) Weight loss of a PDMS gel with different lubricants, green singles lubricant in graph with positive  $\Delta G$  and pink lubricant with negative  $\Delta G$ .<sup>33</sup> (b) SEM images showing the surface microtexture morphology of PDMS material infused with 15% 1000 cSt oil after aging for three months at room temperature.<sup>34</sup> \_\_\_\_\_ 9
- Figure 1.9 Schematic of the four-phase contact zone. (a) (Inset) Schematic of the surface tension balance at each of the contact lines A, B, and C.<sup>35</sup> (b) Schematic of force balance based on Equation 1.1<sup>25</sup> \_\_\_\_\_ 11
- Figure 2.1. PDMS mass loss as a function of washing time.<sup>54</sup> \_\_\_\_\_ 17
- Figure 2.2. A 20:1 example showing sample volume increases with increasing silicone oil swelling. \_\_\_\_\_ 18
- Figure 2.3. Schematic of oil-swollen PDMS with high and low network density. The PDMS with lower network density can be swollen with more oil than the one with higher network density. \_\_\_\_\_ 21

Figure 2.4. Examples of 5:1, 30:1, and 60:1 PDMS mass increasing with lubricant immersing time.	23
Figure 2.5. Saturated oil swelling/infusing weight as a function of PDMS base/crosslinker ratio.	24
Figure 2.6. Storage modulus vs. frequency. Plots of shear storage modulus ( $G$ ) vs. frequency for the different degrees of swelling $Q$ with as-prepared mixing ratios of (a) 60:1, (b) 50:1, (c) 40:1 and (d) 30:1.	26
Figure 2.7. Shear storage modulus. Plots of shear modulus vs. swelling ratio of (a) 60:1, (b) 50:1, (c) 40:1 and (d) 30:1 base/crosslinker mixing ratios. The dashed lines are calculated values given by $G = G_{\text{dry}}\phi^{0.56}$ .	27
Figure 2.8. Stress vs. strain. A plot of stress vs. strain for dry 60:1, 50:1, 40:1, and 30:1 samples with at a frequency of 10 Hz. The samples remain in the linear region up to 10% strain, which is used for the frequency sweeps to quantify modulus values.	28
Figure 3.1 Schematic illustration of possible outcomes for soft wetting on a swollen network. (a) Prior to drop deposition, the surface is homogeneous and flat. (b-c) Schematic of two possible wetting ridges upon placing a water drop on the surface: (b) a homogeneous ridge and (c) a fluid separating ridge.	32
Figure 3.2. Schematic of interfacial extraction and swelling method. The as-prepared PDMS films are released on a water surface by dissolving the sacrificial PAA underlayer. For extraction, hexane was then carefully added to the petri dishes to swell the network and allow uncrosslinked molecules to migrate into the surrounding media. During this procedure, the film remains at the hexane–water interface. To swell the sample with the desired silicone oil fluid, drops of dyed silicone oil are added directly onto the extracted film when it is still floating on the water surface.	35
Figure 3.3. Emission spectrum. Fluorescein in PDMS is excited with a 488 nm laser (black line) and Perylene monoimide in silicone oil is excited with 638 nm laser (red line). This shows a non-overlapping emission of the two dyes.	37
Figure 3.4. Thickness measurements by optical profilometry and confocal microscopy. A plot of the comparison of the thickness measurements from confocal microscopy to optical profilometry. $t_{\text{op}}$ : the thickness measured by the optical profilometry, and $t_{\text{cm}}$ : the thickness measured by the confocal microscopy. Optical profilometry measurements were taken on a Filmetrics Profilm 3D.	38
Figure 3.5. Visualizing the network and fluid parts separately at the contact line. (a) Schematics of a water drop on a swollen surface, and (b) the PDMS elastomer, where the network is dyed with fluorescein and the silicone oil is dyed with PMI. (c-h) Schematics and corresponding confocal images of a wetting ridge for swollen network with a water drop deposited on the surface. (c), (d) Channel 1 shows the PDMS network (green), (e),	

(f) channel 2 shows the silicone oil (red), and (g), (h) the combination of channels 1 and 2 show both parts (yellow). Scale bars: 20  $\mu\text{m}$ . \_\_\_\_\_ 39

Figure 3.6. Qualitative map of cross-sectional confocal images of contact line with varying degrees of crosslinking and swelling. Each row of pictures from top to bottom corresponds to samples with a dry modulus ranging from 17 kPa to 234 kPa, and a base/crosslinker ratio from 60:1 to 30:1, respectively. Orange numbers inside each image indicate the degree of swelling and blue numbers indicate the macroscopic modulus. Column A and B display the dry and saturated conditions, respectively. Scale bar: 20  $\mu\text{m}$ .

41

Figure 3.7. Apparent contact angle ( $\theta_{\text{app}}$ ) and wetting ridge tip angle ( $\theta_{\text{tip}}$ ). (a-b) The apparent contact angle for substrates with different degrees of swelling and base/crosslinker mixing ratios. Scale bar: 1 mm. (c) Examples of tip-aligned xz profiles for 50:1 and 60:1 samples, both with and without clear fluid separation. (d) Zoomed-in xz profiles for three samples with no fluid separation (red), a small amount of fluid separation (purple), and a significant amount of fluid separation (green). The open data points are for the fluid profile and the filled data points are for the network profile. \_\_\_\_\_ 44

Figure 3.8. Quantifying the wetting ridge heights. (a) Example of a cross-sectional confocal image of a water drop on swollen 60:1 PDMS ( $h_f$  and  $h_n$  are the fluid and network tip heights relative to the unperturbed surface). Note that several images are stitched together to obtain a larger field of view. Scale bar: 20  $\mu\text{m}$ . (b-d) Graphs of fluid height ( $h_f$ , open data points) and network height ( $h_n$ , filled data points) as a function of degree of swelling ( $Q$ ) with mixing ratios of (b) 60:1, (c) 50:1, (d) 40:1, and 30:1. (e) The network height for different degrees of swelling and crosslinking, where the solid curves are predictions given by  $\approx \gamma_w \sin\theta/E$ . Error bars denote standard deviations. \_\_\_\_\_ 46

Figure 3.9. Height of wetting ridge as a function of substrate thickness. Examples of wetting ridge heights for 60:1 and 50:1 as-prepared samples. The red line shows that the height of the wetting ridge is first increasing with thickness and then remains constant at thickness values larger than ~50  $\mu\text{m}$  for 60:1 and ~40  $\mu\text{m}$  for 50:1. \_\_\_\_\_ 47

Figure 3.10. Network height vs. modulus. A plot of the network height ( $h_n$ ) vs. modulus ( $E$ ) for 60:1 (black squares), 50:1 (blue circles), 40:1 (red diamonds), and 30:1 (green triangles) samples. The solid lines are calculated values given by  $h_n = \gamma_w \sin\theta/E$ . \_\_\_\_\_ 48

Figure 3.11. Possible wetting ridge height mechanisms. Confocal images show the surface/interfacial tensions pulling up the network for (a) dry, (b) low swelling ratio, and (c) high swelling ratio 60:1 samples. (d) Cross-sectional confocal images of four 50:1 samples with different levels of swelling and fluid separation, and (e) the corresponding profiles aligned at the network-fluid-water contact line on the right side. Interfacial tensions are shown as vectors with magnitude given in mN/m. Scale bar: 20  $\mu\text{m}$ . \_\_\_\_\_ 49

Figure 3.12. Surface/interfacial tensions. A pendant water drop in (a) air, (b) silicone oil, (c) PMI dyed silicone oil and (d) n-hexadecane. Scale bars: 1mm. (e) A bar plot showing

the surface/interfacial tensions of water-air, water-oil, water-PMI dyed oil, and water-hexadecane. \_\_\_\_\_ 51

Figure 3.13. Comparison of experiment to approximate theory. (a) Schematic describing the balance of elastic, mixing, and interfacial energy.  $h_n$ ,  $h_f$ , and  $\Delta h$  are also described in the schematic. (b-e) Plots of the experimental (filled black points) and theoretical (Equation 1, orange open points and lines) separation heights as a function of degree of swelling with mixing ratios of (b) 60:1, (c) 50:1, (d) 40:1 and (e) 30:1. Insets show zoomed-in data of lower swelling for clarity. f Separation height as a function of degree of swelling of hexadecane swollen 60:1 PDMS. The dotted line is at  $\Delta h = 0$ . Error bars denote standard deviations. \_\_\_\_\_ 54

Figure 3.14. Hexadecane swollen samples. (a) A plot of network height  $h_n$  and fluid height  $h_f$  as a function of the degree of swelling ( $Q$ ) of hexadecane swollen samples. (b) Confocal image showing a small excess hexadecane droplet on a saturated network. (c) The hexadecane droplets can be found near a wetting ridge. The fluid zone of the wetting ridge likely comes from the excess droplets. Scale bars: 20  $\mu\text{m}$ . \_\_\_\_\_ 56

Figure 4.1. A water drop is deposited on a vertical PDMS elastomer. (a) A schematic of experimental setup. (b) An image of a water drop sticking to a surface and (c) of a water drop sliding on the surface. Note that four images are overlaid in (c) to illustrate drop sliding. Scale bars: 5 mm. \_\_\_\_\_ 63

Figure 4.2. Water drop sliding percentage on dry surfaces with base/crosslinker ratios of (a) 60:1 and 50:1, and (b) 40:1 and 30:1. The horizontal dashed line represents the sliding percentage of 50%. The star shows the 50% point of our fit, which is taken as  $V_c$ . Each data point includes at least 5 drops. (c) The critical volume  $V_c$  as function of base/crosslinker ratio for dry samples. \_\_\_\_\_ 65

Figure 4.3. Water drop sliding percentage on surfaces with various degrees of swelling for (a) 60:1 and 50:1 samples and for (b) 40:1 and 30:1 samples. The horizontal dashed line represents the sliding percentage of 50%. (c) The critical volume  $V_c$  as a function of degree of swelling  $Q$  for the 30:1, 40:1, 50:1 and 60:1 samples. \_\_\_\_\_ 67

Figure 4.4. Water volume  $V$  as a function of contact diameter cubed  $D^3$  on different elastomers. The dashed line is a linear fit of all data points with a resulting slope of 0.17. \_\_\_\_\_ 69

Figure 4.5. Advancing and receding contact angles, as well as the contact angle hysteresis of water on (a) 30:1, (b) 40:1, (c) 50:1 and (d) 60:1 samples with different degrees of swelling from dry to saturated. \_\_\_\_\_ 71

Figure 4.6. Plots of the experimental data for  $V_c$  vs.  $Q$  (filled black data points) overlaid with calculated values from Equation 4.5 for (a) 30:1, (b) 40:1, (c) 50:1 and (d) 60:1 swollen elastomers. The open black circles and dashed lines are the calculated from Equation 4.5 with  $k = 0.5$ , and the open red circles and dashed lines for  $k = 1.57$ . \_\_\_\_\_ 72

Figure 4.7. The critical water volume as a function of aging days for a swollen 40:1 ( $Q = 5.5$ ) elastomer. Each box represents one rinse and aging cycle using the same sample. 74

Figure 4.8. The critical water drop volume as a function of aging days for a 50:1 ( $Q = 7.0$ ) elastomer (a) and a silicone elastomer prepared from Gelest starting materials (b). The highly swollen 50:1 sample shows a decrease in  $V_c$  with aging, consistent with the 40:1 tests in Figure 4.7. 75

Figure 4.9. (a) A schematic of rinsing, aging, and re-lubrication of highly swollen PDMS. (b-e) Paper stain test with a highly swollen 40:1 ( $Q = 5.5$ ) sample. (b-c) A water-rinsed sample and (d-e) a sample aged for 7 days. No stain is left on the paper for water-rinsed samples (c), while an oil stain is observed on the paper for the 7 day aged sample (e). Scale bars: 5 mm. 76

Figure 4.10. Schematic of a potential mechanism that drive the oil separates from the swollen PDMS 78

Figure 4.11. (a) Critical water volume as a function of aging days for 40:1 ( $Q = 2.1$ ) elastomers. For the substrate aged for 134 days, (b) it is put into contact with paper for 10 s, and (c) no stain is left on the paper. Scale bars: 5 mm. 79

Figure 4.12. Drop sliding set-up and wetting ridge visualization. Macroscopic side view of affixed drop, substrate moves left while drop is stationary. Inset, set-up schematic. 81

Figure 4.13. Force measurement by using a metal wire. The swollen PDMS substrate ( $Q = 14.5$ ) moves with a velocity of 5  $\mu\text{m}/\text{s}$ . The wire bends with a displacement  $\Delta x$  (b) from the original position (a) while the underneath substrate moves. (c) A plot of momentary friction force vs sliding time, the friction force is calculated with the equation  $F = k\Delta x$ . 83

Figure 4.14. Kinetic friction force  $F$  as a function of sliding velocity  $v$  for swollen samples with degree of swelling  $Q$  of (a) 7 and (b) 16. 84

Figure 4.15. Wetting ridge visualization during drop sliding at 5  $\mu\text{m}/\text{s}$  on a swollen PDMS network ( $Q = 14.5$ ). Substrate moves left while the drop is stationary. (a) Temporal averaged ( $n = 158$ ) confocal microscopy image of a phase-separated wetting ridge. Red shows silicone oil and orange shows swollen PDMS network. (c) Extracted interfaces of silicone oil (red points) and PDMS network (yellow points). Inset, blown up section of the phase-separated zone in the wetting ridge. Standard errors are smaller than symbol size. 85

Figure 4.16. Dynamic wetting ridge shape for different sliding speeds and swelling ratios (a), (b)  $Q = 16$ , (c), (d)  $Q = 14.5$ , (e), (f)  $Q = 10$ . (a), (c), (e) Dynamic ridge profiles of liquid silicone oil (and network PDMS as insets). (a), (c) For silicone oil, the ridge height gradually decreases for increasing drop speed,  $v = 5, 10, 50, 100, 300, 800 \mu\text{m}/\text{s}$ . Top row images are representative confocal microscopy images for  $v = 5 \mu\text{m}/\text{s}$  and  $v = 800 \mu\text{m}/\text{s}$  (scale bar 20  $\mu\text{m}$ ). (b), (d), (f) Maximum height of dynamic ridges of silicone

oil (red) and network PDMS (yellow). Data shows average of min.  $n = 3$  repetitions together with standard deviations. Dashed lines mark dynamic elastocapillary height  $\lambda \sim \gamma \sin \theta_{\text{adv}} / E$ , which are (b) 21  $\mu\text{m}$  ( $E \approx 3 \text{ kPa}$ ) (d) 16  $\mu\text{m}$  ( $E \approx 3.9 \text{ kPa}$ ) (f) 13  $\mu\text{m}$  ( $E \approx 4.8 \text{ kPa}$ ). 

---

 87

# CHAPTER 1. INTRODUCTION

## 1.1 Liquid-repellent surfaces

### 1.1.1 Lotus effect

The lotus is used as a symbol of purity due to its ability to clean itself even from muddy water. In order to understand and dig into the science behind the magical properties of lotus, in the 1990s, Barthlott, Wilhelm, and Christoph Neinhuis<sup>1</sup> used scanning electron microscopy (SEM). They investigated the surface of the lotus leaves, and revealed that leaves were covered with a surface microstructure. As Figure 1.1 shows, lotus leaves are covered with tiny bumps called papillae. When the surface is wetted by water, the drop goes into a Cassie-Baxter wetting state. In a Cassie-Baxter wetting state, a composite solid–air–liquid interface forms, and the water drop sits atop pockets of air trapped between the papillae. The effect could be demonstrated on the microscopic level using an analogous liquid of Mercury in the SEM (Figure 1.1c). The roughness of the papillose leaves can also lead to a reduced contact area between particles and the solid underlying surface (Figure 1.1b), which makes the particles easy to remove from the leaves.

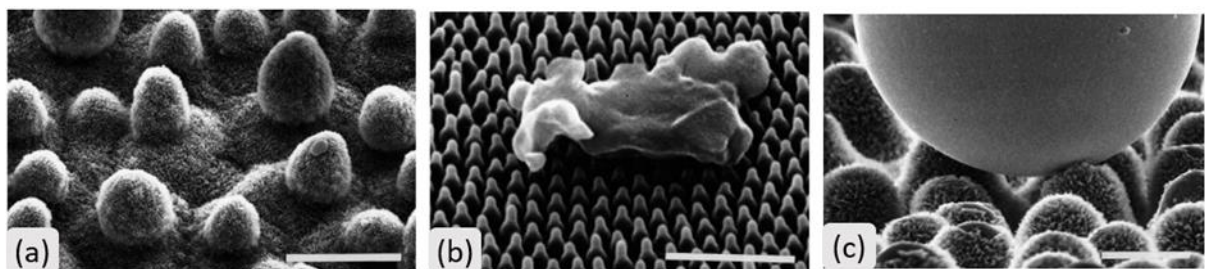


Figure 1.1. Scanning electron micrographs of the *Nelumbo nucifera* adaxial leaf surface (a), (b) contaminating particle on a regularly sculptured wing surface and (c) mercury droplet on the papillose adaxial epidermal surface.<sup>1</sup> (Scale bar = 1µm)

Inspired by lotus leaves, ‘superhydrophobic’ surfaces have been widely studied to achieve water repellent surfaces. However, the lotus leaf structures have some limitations due to the fact that they rely on trapped air pockets, which can be penetrated by the liquid when the ambient pressure is greater than capillary pressure.<sup>2</sup> Once liquid penetrates inside the air pockets, a transition from the Cassie-Baxter state to the Wenzel state (Figure 1.2) occurs.<sup>3</sup> The Wenzel state is not advantageous for achieving liquid-repellent properties due to the larger contact area between the liquid and surface; this increases the adhesion force between them. Moreover, humidity and temperature can damage these lotus leaf structures, thus leading to the loss of the desired water-repellent property. Another limitation of traditional lotus-inspired surfaces is that they are not able to repel low surface tension liquids, such as silicone oil, hexadecane and heptane,<sup>2,4</sup> unless specific topographical features exist on the surface, and the surface is coated with special hydrophobic chemicals<sup>5–7</sup>.

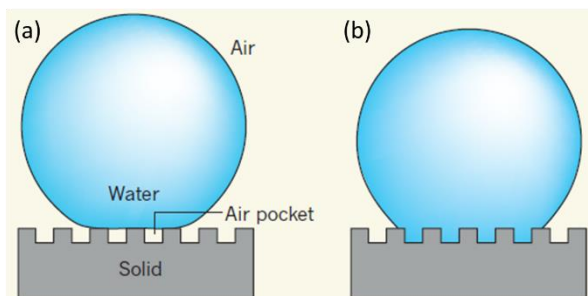


Figure 1.2. Wetting status on lotus-effect surfaces. (a) The Cassie–Baxter model and (b) the Wenzel model wetting status.<sup>3</sup>

### 1.1.2 Slippery liquid-infused porous surfaces (SLIPS)

In order to overcome many of the challenges associated with lotus-inspired surfaces, lubricant-infused, porous materials have been designed; these surfaces are inspired by the insect-eating pitcher plant. This type of surface is also commonly known as a slippery, lubricant-infused porous surface (SLIPS).<sup>8,9</sup> As shown in Figure 1.3a, when a liquid drop is placed on the material, a solid–lubricant–liquid interface is formed. The lubricant has a similar function to the air pockets in the lotus effect, but it can also form a continuous film, which prevents the liquid drop from being able to penetrate the solid porous texture. SLIPS can be used to achieve a self-cleaning<sup>10</sup>, anti-fouling<sup>11,12</sup> and anti-icing<sup>13</sup> properties, or used to decrease drag for increasing liquid transportation efficiency.<sup>12,14</sup> Nearly any liquid can easily be repelled as long as there is a stable lubricant layer on the surface and as long as the two liquids are not miscible (Figure 1.3b)<sup>9</sup>. However, for SLIPS, it is challenging to maintain a lubricant layer because the lubricant depletes as drops slide off them; the loss of lubricant over time can be caused by the shear stress of flowing fluids during use. Anand et al<sup>15</sup> reported that ice formation and water droplets can accelerate lubricant depletion. SLIPS lose their exceptional liquid-repellent properties when the lubricant layer does not fully cover the structured surface (Figure 1.4).<sup>16</sup>

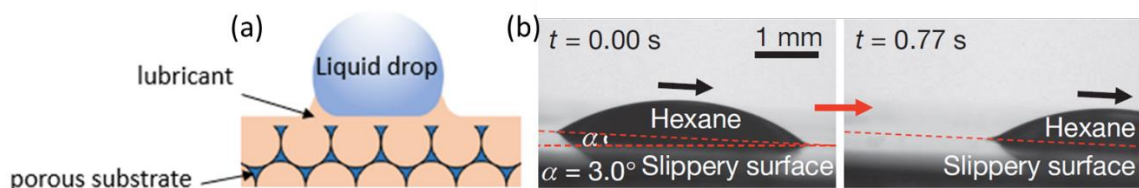


Figure 1.3. Slippery lubricant-infused porous substrate (SLIPS) (a) Scheme of SLIPS<sup>8</sup> (b) optical micrographs demonstrating the mobility of a low-surface-tension liquid sliding off from SLIPS.<sup>9</sup>

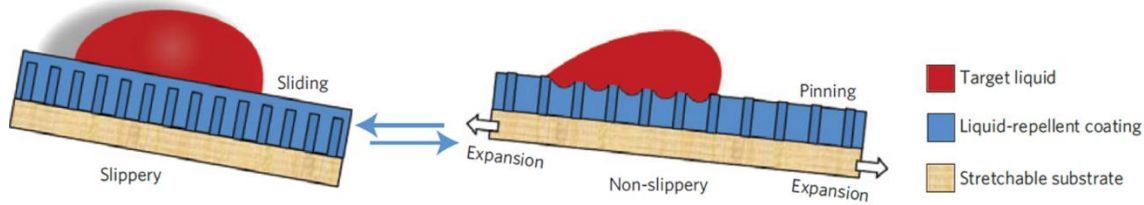


Figure 1.4. Schematic showing under a mechanical stretch, a droplet of test liquid changes from sliding to pinning when lubricant layer cannot overcoat the substrate.<sup>16</sup>

### 1.1.3 Lubricant-infused gels (swollen elastomers)

SLIPS have attracted great interest, as discussed above, and wetting behaviors of SLIPS have been widely studied from both fundamental and applied perspectives<sup>8,9,14,17–21</sup>. However, the most challenging point for SLIPS is their durability towards long-lasting use. Moreover, their porous structures are often fragile. To overcome these limitations, lubricant-infused gels (LIG) have been investigated. LIGs are crosslinked polymer networks, infused with a compatible lubricant. Hence, this effectively offers molecular scale “pores” that may help trap lubricant within the polymer surface. However, even though LIGs have attractive properties for potential application as slippery surfaces, the mechanisms of how the polymer network, the lubricant, and the target liquid drop interact with each other is still not well understood and is at the core of this dissertation.

## 1.2 Wetting on soft surfaces

When a liquid drop is deposited on a soft surface, like crosslinked polydimethylsiloxane (PDMS), surface tension from liquid drop generates a small deformation of the soft surface, forming a “ridge” around the liquid drop. There are a couple of ways to directly observe the small deformation caused by liquid surface tension. Deformation of soft surfaces highly depends on stress and modulus.<sup>22–25</sup> The existence of “ridge” can affect droplets moving dynamic as S. Karpitschka. et al reported.<sup>26</sup> They provide a mechanism for stick-slip motion when a drop is forced to move on a viscoelastic substrates, they found the water-PDMS contact line depins and slides down the wetting ridge, forming a new one after a transient, which is not as straightforward as water drop moving dynamic on SLIPS.

### 1.2.1 Force balance on the contact line of soft surface

The wetting behavior of drops on a rigid surface is well understood. The droplet has a certain contact angle and can be described by Young’s equation  $\gamma_S = \gamma_{SL} + \gamma_L \cos\theta$ , where  $\gamma_S$  is solid surface energy,  $\gamma_L$  is liquid surface energy and  $\gamma_{SL}$  is interfacial energy between solid surface and liquid (Figure 1.5a). However, wetting on a soft surface is different from a rigid surface. When an immiscible liquid drop is deposited on a soft surface, like soft PDMS, surface tension from the liquid drop generates a deformation of the surface, forming a “ridge” around the drop (Figure 1.5b). In this case, the force

balance should satisfy Neumann's triangle (Figure 1.5c), which requires that surfaces must intersect at fixed orientations determined by the interfacial tensions.

When considering the deformation of soft interfaces in Figure 1.5b, we need to pay attention to the so called surface stress,  $\Upsilon$ , which has a conceptual difference from liquid surface tension  $\gamma$ :  $\gamma$  is the force required to create a unit area by bringing new molecules to the surface, while  $\Upsilon$  is defined as the force required to create a unit surface by stretching a constant number of molecules on the surface.<sup>27,28</sup> It was argued recently that soft substrate deformations can be taken into account by substituting the surface stresses instead of surface tensions (surface free energies) to account for the local balance of capillary and elastic forces at the triple-phase contact line, as illustrated in Figure 1.6a.<sup>29</sup> For liquids,  $\gamma = \Upsilon$  when no elastic force contributes to the substrate deformation, while for solids,  $\gamma \neq \Upsilon$ . This is because at the surface, there is limited movement of molecules in a solid, which alters the intermolecular distance.  $\gamma$  and  $\Upsilon$  are related by the Shuttleworth equation and  $\Upsilon(\lambda) = \partial\gamma(\lambda) + \gamma/\partial\lambda$ , where  $\lambda$  is a two-dimensional strain tensor in the plane of the interface<sup>30</sup>

Recently, Heyi, et al.<sup>29</sup> reported the forces that balance at the triple-phase contact line can also be treated as a quartet of forces: three surface tensions (free energies) and an elastic force (Figure 1.6b). The elastic force is balanced by the sum of surfaces tensions acting at the triple-phase contract line. If one considers only three line forces acting at the triple-phase contact line and accounts for the elastic force as a part of the surface stresses, the surface stress values appear to be unphysically large. While the above studies have made

significant progress on microscale soft contact, more physical details at the triple-phase contact line on soft gels is still under investigation.

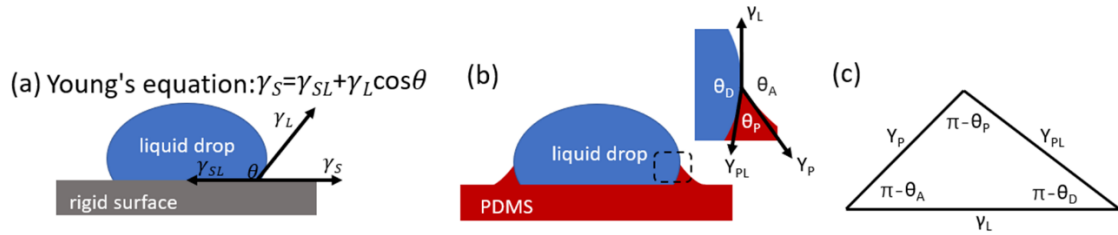


Figure 1.5. Schematics illustrating a liquid drop on a rigid surface (a) and (b) on a soft deformable polymer (PDMS), (c) Neumann's triangle relating the surface tensions and contact angles of (b) in static equilibrium

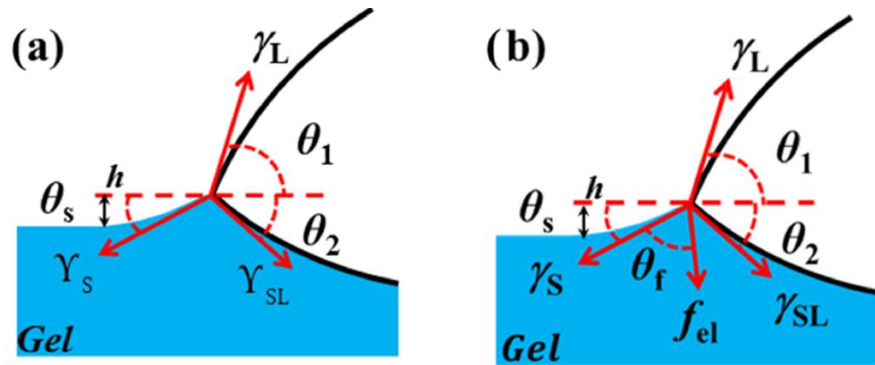


Figure 1.6. Droplet on soft (gel-like) substrate. (a) Line force balance conditions for surface stresses. (b) Line force balance conditions with elastic force.<sup>29</sup>

To investigate contact zones of soft deformed interfaces, the first step usually starts with small scale contact zone visualization. There are a couple of approaches to directly observe small deformations caused by liquid surface tension. In 2013, Style et al.<sup>31</sup> reported a way to observe deformation of a soft PDMS ( $E \sim 1$  kPa) by putting fluorescent nanoparticles at the PDMS surface and then imaging it with confocal microscopy (Figure

1.7b). Park et al.<sup>32</sup> developed a method to visualize deformation by X-ray microscopy (Figure 1.7a). In both cases, deformation of the soft surfaces highly depends on modulus<sup>22,25</sup>. However, these materials were fabricated by curing polymer chains into a network, and not all polymer chains were attached to the network. They contain a significant fraction of free polymer chains, which acts as liquid and makes these materials two-phase systems. This modifies the physical picture of how drops interact with soft surfaces, which is commonly assumed to be homogeneous. Therefore, one must consider both how the crosslinked polymer network and the liquid phase of the material governs the physics of soft wetting.

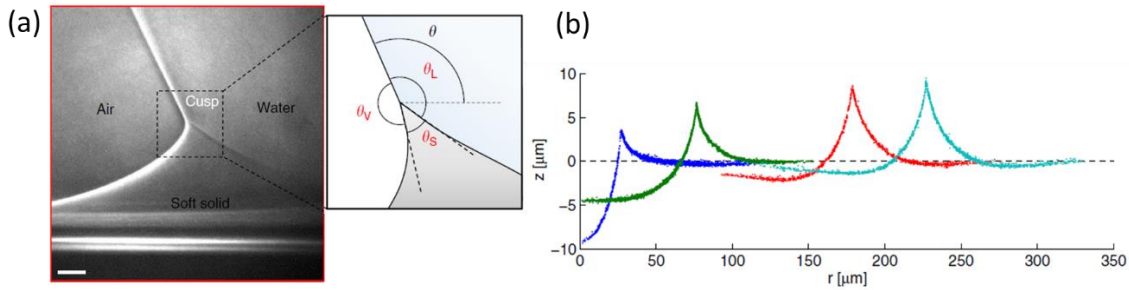


Figure 1.7. Deformation of PDMS after water drop deposited: (a) via X-ray microscopy.<sup>32</sup> and (b) PDMS contact line via confocal microscopy.<sup>31</sup>

### 1.2.2 Lubricant layer formation on infused elastomer gels

When a water drop is placed on a surface, the drop typically can slide when there is a layer of lubricant on surface. This is obvious on SLIPS, where a lubricant layer covers the porous surface. However, when gels are infused with lubricant, it is not obvious if and how a lubricant layer forms. By mixing lubricant in a PDMS mixture (base unit and

curing agent) and then curing, Urata. et al<sup>33</sup> found that the lubricant will leech out from the network to the surface after gelation, because of demixing due to an increase in Gibbs energy (Figure 1.8a). Yeong et al<sup>34</sup> used a similar method to show lubricant (silicone oil) leaching to the surface after three months aging at room temperature (Figure 1.8b), which is mainly because  $\Delta G$  changes during aging. However, the lubricant layer formation is hard to control and it affects how drops interact with the surface. For example, Urata showed that the formation of a lubricant layer can contribute to enhanced liquid sliding<sup>33</sup>. On the other hand, Yeong showed that the formation of a lubricant layer can decrease the slippery property because it alters the microtexture, transforming drops from the Cassie-Baxter state to the semi-Cassie/ Wenzel state.

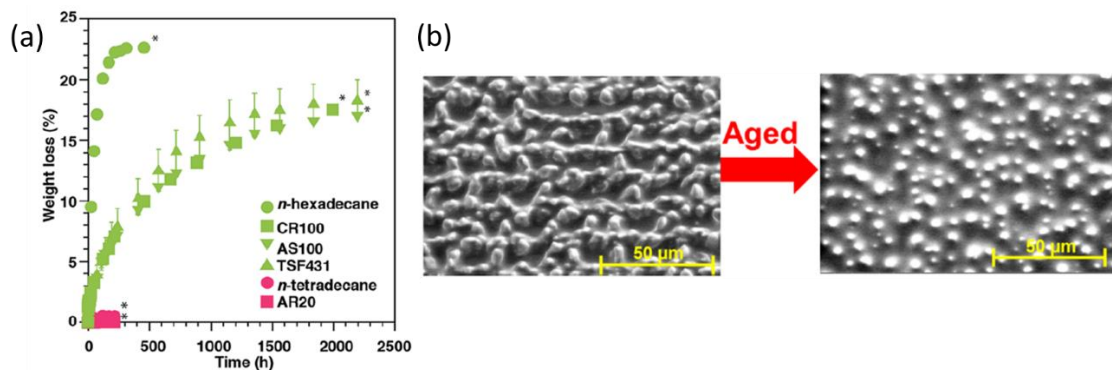


Figure 1.8 (a) Weight loss of a PDMS gel with different lubricants, green singles lubricant in graph with positive  $\Delta G$  and pink lubricant with negative  $\Delta G$ .<sup>33</sup> (b) SEM images showing the surface microtexture morphology of PDMS material infused with 15% 1000 cSt oil after aging for three months at room temperature.<sup>34</sup>

### 1.2.3 Phase separation at the contact line

In recent soft wetting theories, surface energy drives deformation to increase contact area while bulk elasticity opposes it. However, Jensen et al.<sup>35</sup> found that to satisfy this wetting condition while avoiding divergent elastic stress, the gel and its solvent phase separate near the contact line of a microparticle(Figure 1.9a). By combining confocal microscopy and the colloidal probe technique, Pham et al.<sup>25</sup> developed an approach to capture a cross-sectional image of the contact and measure the force between an indenting rigid microsphere and a soft PDMS at the same time. The total force is the combination of contributions from elastic deformation and adhesion, interfacial stretching within the contact zone, and the capillary forces due to the solvent phase (Figure 1.9b):<sup>25</sup>

$$F_{total} = \frac{8Ea\delta}{3} - \frac{8Ea^3}{9R} + 2\pi Y(\delta + c(\delta)) - 2\pi\gamma a \sin\beta \quad 1.1$$

Equation 1.1 suggests that the interfacial physics must include elastic forces, surface tension, surface stress, and geometric parameters. While in these studies, the authors made a hypothesis about the shape of liquid and solid phases, the real phase shape at contact zone is unknown. Moreover, these studies are based on contact between solid particles and soft materials, and little is known about phase separation during liquid drop wetting. These studies on solvent phase separation at a contact zone provides motivation for investigating how lubricant is pulled out from the polymer network at the contact zone of a liquid drop on a soft surface, and how the liquid phase contributes to liquid-repellency.

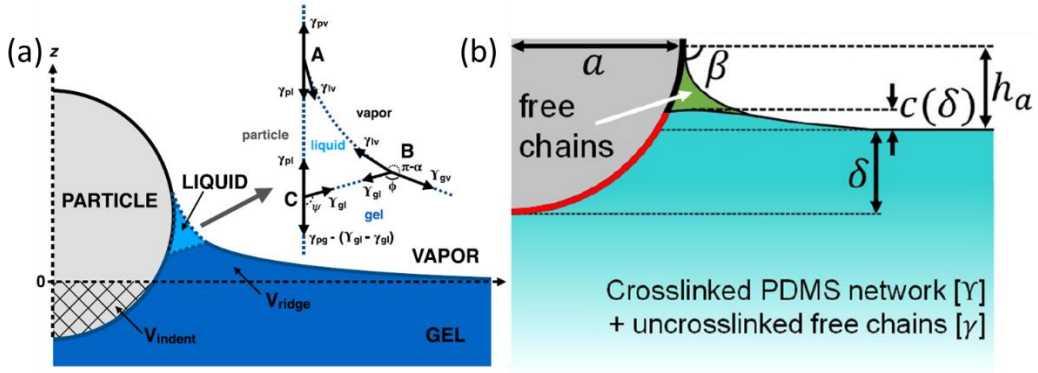


Figure 1.9 Schematic of the four-phase contact zone. (a) (Inset) Schematic of the surface tension balance at each of the contact lines A, B, and C.<sup>35</sup> (b) Schematic of force balance based on Equation 1.1<sup>25</sup>

### 1.3 Dissertation organization

To understand the fluid separation at the contact line area in wetting on soft, swollen elastomers, we break up this dissertation into three core sections: 1. Choosing and fabricating an appropriate material system for fundamental wetting studies, as well as characterizing and controlling the mechanical properties of the material system; 2. Developing a method to visualize the fluid separation at the contact zone and investigating the factors that affect the fluid separation during static wetting; and 3. Expanding the investigation into dynamic wetting cases, including the effects of surface properties on drop sliding as well as investigating the velocity dependence. Overall, the work in this dissertation includes development of special sample preparation methods, dye selection and confocal microscopy for imaging, and customizing setups for measuring friction force and velocity dependence of wetting ridges.

## CHAPTER 2. SWOLLEN ELASTOMER PREPARATION

### 2.1 Background

To study wetting on swollen elastomers, silicone elastomers (e.g. crosslinked polydimethylsiloxane, PDMS) with modulus on the order of a few kPa are often employed<sup>31,32,35–38</sup>. The mechanical properties are obtained by macroscopic rheological measurements and the material is assumed to behave as a homogenous solid<sup>39,40</sup>. However, this may not be sufficient for describing the wetting of swollen networks. PDMS elastomers typically possess uncrosslinked molecules inside the crosslinked network, which are effectively fluid silicone oil that swells the network. This oily fluid is left over after crosslinking, and is likely a mix of linear, cyclic and branched chains of unknown molecular weight<sup>41</sup>. Recently, Hourlier-Fargette et al. deposited water drops on vertical surfaces of stiff PDMS and measured their downward sliding velocity<sup>42</sup>. They found that the velocity drastically increases after a certain distance, and suggest that trace amounts of oily fluid inside the elastomer are pulled from the surface and encapsulate the drop; this effectively lubricates the drop. Others have also demonstrated that upon removing a water drop from a soft silicone surface, the wetting ridge relaxes and the dynamics appear to be affected by this oily fluid<sup>43,44</sup>. Moreover, the contact mechanics of soft silicone elastomers are also complicated by oily fluids in the material<sup>25,35,45</sup>. Despite progress in characterizing how drops interact with soft surfaces, a quantitative understanding of how crosslinking and swelling govern the wetting behavior is lacking.

Therefore, it is important to be able to prepare well-defined elastomers with known swelling ratios and mechanical properties, which will be described in this Chapter.

## 2.2 Experimental plan

As described above, a swollen silicone elastomer material system should be well designed and controlled before any fundamental wetting experiments can be conducted. Throughout this entire dissertation, we choose to use a crosslinked PDMS-silicone oil gel system unless otherwise stated, due to the relatively simple ability to control both the degree of swelling and the mechanical properties. The PDMS network is prepared from a commercially available elastomer kit, Sylgard 184, which is then infused with a silicone oil of known molecular weight. In commercially available PDMS elastomers, uncrosslinked (free) chains remain in the sample after curing, which may affect the general wetting behavior. Therefore, we first extract uncrosslinked chains from the as-prepared material. We fabricate PDMS with different network densities by controlling the mixing ratio of the PDMS base and crosslinker from the Sylgard 184 kit. After curing the mixture, PDMS samples are then washed in hexane to exclude the influence of free chains initially inside of the network. After washing and drying, silicone oil is infused into the washed PDMS samples. To investigate how network density affects the degree of swelling, the dry PDMS networks are infused with lubricant by immersing the sample into a lubricant batch until equilibrium swelling is reached. Using these bulk samples will allow for characterization of the material system with different mechanical and swelling properties. This information is important for future chapters, which will utilize these materials for wetting studies.

### 2.3 Preparation of bulk, as-prepared PDMS

Polydimethylsiloxane (PDMS) elastomers are one of the most utilized soft surfaces for wetting studies<sup>34,44,46-49</sup>. Here, we use the commercially available Sylgard 184 PDMS kit, which comes as a two-part system that includes a base and a curing agent. The mechanical properties of as-prepared PDMS can be controlled by varying the base/crosslinker mixing ratio. The recommended mixing ratio from the manufacturer is 10:1. In our studies, the base/crosslinker are mixed with weight ratio of 5:1, 10:1, 20:1, 30:1, 40:1, 50:1 and 60:1 to control the polymer network density and modulus. As the base/crosslinker mixing ratio increases, the polymer network density decreases, which leads to softer samples. The base and crosslinker are mixed and stirred well with a steel bar in a 20 ml glass vial, and then pour into a plastic petri-dish, followed by a degassing process in a vacuum desiccator. The PDMS mixture is then put into an oven at 65°C for curing. After curing for 2 days, samples are taken from the oven and quenched to room temperature. These PDMS samples are called “as-prepared” PDMS.

The as-prepared PDMS contains uncrosslinked polymer chains inside the network. The amount of uncrosslinked polymer chains is dependent on the mixing ratio. At high base/crosslinker ratio (e.g. 60:1), the base is in excess relative to the crosslinker; this results in more uncrosslinked polymer chains existing in the as-prepared samples compared to lower base/crosslinker ratio (e.g. 10:1). The molecular weights of these uncrosslinked chains are unknown and hard to control because they are from a commercial product. Consequences of the presence of uncrosslinked chains (also called

as free chains) in silicone elastomers have been recently investigated in the context of adhesion,<sup>35</sup> osmocapillary phase-separation,<sup>50</sup> swelling of composite structures,<sup>51</sup> surface tension<sup>52</sup> and droplet dynamics.<sup>42</sup> These studies reveal that the existence of free chains at the scale of the polymer network can lead to significant macroscopic effects of the material and of soft surfaces for wetting. Therefore, free chains need to be removed to exclude the undesirable and uncontrolled effects.

### 2.3.1 Extraction of uncrosslinked (free) PDMS chains

As described above, uncrosslinked polymer chains exist in as-prepared PDMS, which may affect the materials properties. In order to exclude the influence of uncrosslinked free chains, we wash the as-prepared samples with hexane until no more free chains can be extracted. We choose hexane as our washing solvent due to its good compatibility with PDMS.<sup>53</sup> To prevent the samples from damage during washing, and to retain the appropriate sample geometry for wetting experiments, the washing process is conducted on a bath of water with hexanes on top, as described elsewhere.<sup>54</sup> Briefly, as-prepared PDMS samples are released onto a bath of water, and then submerged in excess hexane to allow for the free chains to migrate out of the network. During this procedure, the samples float at the hexane–water interface. To minimize the concentration of free silicone chains in the surrounding hexane environment, the hexane is exchanged every two days. After multiple washing steps, most hexane is removed by syringe and a little bit residual hexane is left to evaporate, leaving extracted PDMS samples on the water surface. Therefore, we define the extracted PDMS film as the dry network.

After extraction, the mass of samples decreases due to the removal of free chains (i.e. there is a volume loss). To quantify the amount of free chains in the as-prepared material as a function of different base/crosslinker mixing ratios, our group previously measured the mass loss of samples after several washing cycles<sup>54</sup>. As shown in Figure 2.1, the measured mass loss first increases with washing time, and then reaches a constant. For different PDMS base/crosslinker mixing ratios, the mass loss does not change after ~80 hours of washing, which means all free chains that can be extracted by a solvent washing process have been removed. Therefore, to make sure that effectively all free chains are extracted by this process, we use a washing time that is longer than 80 hours.

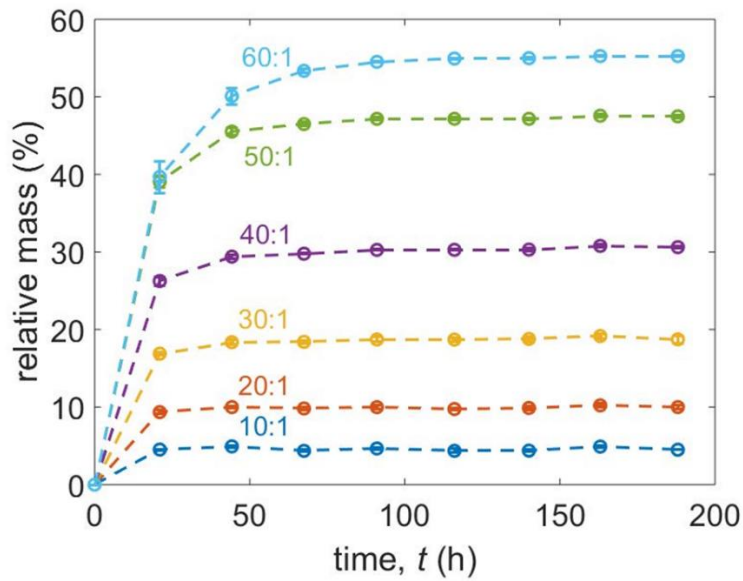


Figure 2.1. PDMS mass loss as a function of washing time.<sup>54</sup>

### 2.3.2 Swelling of extracted (dry) PDMS network with silicone oil

Unless otherwise stated, Trimethylsiloxy-terminated linear silicone oil (Mw: 770g/mol) is used for swelling the dry PDMS network throughout this dissertation. There are several reasons for using this fluid to swell the crosslinked PDMS network. First, the network can be highly swollen in this fluid, due to its chemical compatibility. Second, the low molecular weight (and low viscosity) allows the system to reach an effective equilibrium more quickly than higher molecular weight oils. Third, silicone oil does not readily evaporate compared to other good solvents for PDMS (e.g. toluene). The silicone oil is put on the dry samples' surface and the oil spontaneously infuses into the PDMS network. The infusion of silicone oil into the PDMS network is analogous to elastomer swelling, where oils expand the polymer network. Figure 2.2 shows an example of a 20:1 PDMS sample being swollen in silicone oil; a significant increase of the sample volume is observed as it is swollen to its saturated swelling state (i.e. the maximum amount of oil that can be infused).

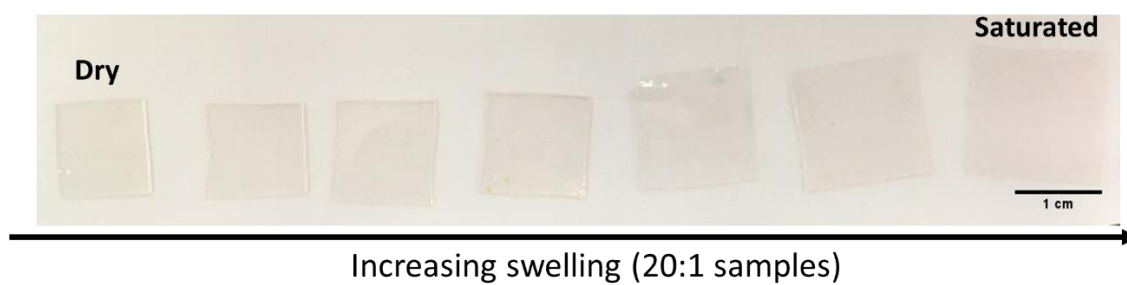


Figure 2.2. A 20:1 example showing sample volume increases with increasing silicone oil swelling.

The saturated degree of swelling changes with the as-prepared network density. Compared with a high network density, a polymer network with lower network density (i.e., lower crosslinking) contains more oil when it is swollen to saturated. When a polymer network is swollen, the total free energy of swelling of the network is given by<sup>55</sup>

$$\Delta G = \Delta G_m + \Delta G_e \quad 2.1$$

where  $\Delta G_m$  is the free energy of the mixing, given by the Flory-Huggins expression for the mixing, and  $\Delta G_e$  is the free energy change upon expanding the elastomer network, which can be obtained from the isothermal reversible work per unit volume  $w$ . The work is given by

$$w = \frac{3\rho RT}{2M_c} \left( \varphi_2^{-\frac{2}{3}} - 1 \right) \quad 2.2$$

where  $\varphi_2$  is the volume fraction of polymer,  $M_c$  is the number-average molar mass of the chains between crosslinks,  $\rho$  is the density,  $R$  is the universal gas constant, and  $T$  is the temperature. The free energy change upon expanding the network can be obtained by the number of moles of silicone oil expanding network,  $n_1$ . The relationship between  $\varphi_2$  and  $n_1$  is given by

$$\frac{1}{\varphi_2} = 1 + n_1 V_1 \quad 2.3$$

where  $V_1$  is the molar volume of the silicone oil. Hence, the total free energy of swelling in Equation 2.1 becomes

$$\Delta G = RT \left[ \ln(1 - \varphi_2) + \left(1 - \frac{1}{\chi}\right) \varphi_2 + \chi \varphi_2^2 + \frac{\rho V_1}{M_c} \varphi_2^{-\frac{1}{3}} \right] \quad 2.4$$

where  $\chi$  is the Flory interaction parameter that describes the interaction energy between the polymer network and the silicone oil. Assuming that the degree of polymerization  $x$  is infinitely high, and  $\Delta G = 0$  at equilibrium (saturated) swelling, this then leads to the Flory-Rehner equation

$$\ln(1 - \varphi_2) + \varphi_2 + \chi \varphi_2^2 + \frac{\rho V_1}{M_c} \varphi_2^{-\frac{1}{3}} = 0 \quad 2.5$$

Expanding the logarithmic term up to terms in  $\varphi_2^2$  to give

$$\left(\chi - \frac{1}{2}\right) \varphi_2^2 + \frac{\rho V_1}{M_c} \varphi_2^{-\frac{1}{3}} \approx 0 \text{ or } \frac{\rho V_1}{M_c} \approx \left(\frac{1}{2} - \chi\right) \varphi_2^{\frac{5}{3}} \quad 2.6$$

Therefore, at saturated swelling condition, the value of  $\varphi_2$  decreases with increasing  $M_c$ . We assume that  $\chi$  and  $V_1$  do not change, since we use the same silicone oil and PDMS network. The saturated degree of swelling is related to  $1/\varphi_2$ ; that is, a large  $1/\varphi_2$  indicates a large saturated degree of swelling, and hence more oil can swell the network. According to Equation 2.6,  $1/\varphi_2$  decreases with increasing network density  $1/M_c$ . Therefore, a less crosslinked material with a lower network density should be able to contain more silicone oil at saturated swelling, and is thus expected to have a larger maximum degree of swelling (Figure 2.3). To confirm that the degree of swelling is related to the degree of crosslinking, we measure the degree of swelling for different PDMS elastomers with various network density, as described in the next section.

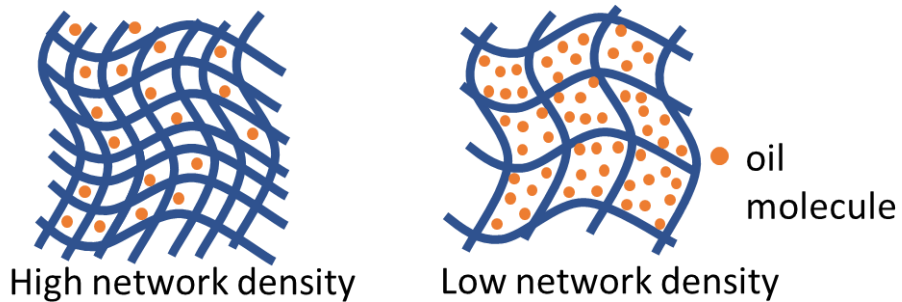


Figure 2.3. Schematic of oil-swollen PDMS with high and low network density. The PDMS with a lower network density can be swollen with more oil than the one with higher network density.

## 2.4 Characterization of oil-swollen PDMS elastomer

As discussed above, crosslinked PDMS networks swollen with silicone oil are utilized as the swollen elastomer for wetting studies in future chapters. Hence, characterization of the materials is necessary. We first quantify the maximum degree of swelling for different mixing ratios. We then investigate how the base/crosslinker mixing ratio and the degree of swelling affect the mechanical properties.

### 2.4.1 The degree of swelling measurement

When oil swells the PDMS network, the volume and weight of the samples change. To characterize the amount of oil infused into each network, the degree of swelling is

quantified and defined as  $Q = V_s/V_d$ , where  $V_d$  is the volume of the dry sample and  $V_s$  is the volume of the sample after swelling. The degree of swelling  $Q$  will reach to a maximum ( $Q_{max}$ ) when samples are swollen to saturation. As discussed in the last section 2.3.2, when the base/crosslinker ratio is increased from 5:1 to 60:1, the saturated degrees of swelling  $Q_{max}$  increased. To experimentally investigate how the saturated swelling changes with different network density, we immerse dry PDMS samples with various network density in a batch of silicone oil, and then weighed samples with different immersing time. Figure 2.4 shows the 5:1 (stiff sample), 30:1 and 60:1 (soft sample) samples mass as a function of immersing time. The samples mass first increases with immersion time, indicating the oil goes into the network and swells samples. After 5 days of immersing, the sample mass does not change, which indicates that all samples have reached the saturated swelling condition. Using the same method, we find the maximum weight increase of 5:1, 10:1, 20:1, 30:1, 40:1, 50:1 and 60:1 base/crosslinker mix ratio PDMS when they reach to saturated swelling condition. The maximum weight increases with the base/crosslinker ratio as shown in Figure 2.5. Overall, the experimental result confirms our hypothesis in section 2.3.2: the saturated swelling highly depends on network density, and the lower network density can contain more oil.

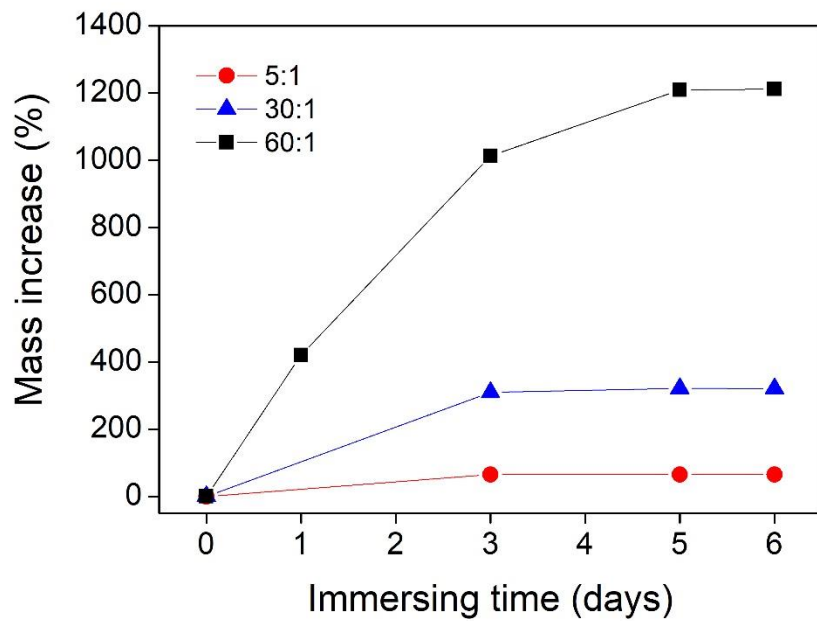


Figure 2.4. Examples of 5:1, 30:1, and 60:1 PDMS mass increasing with lubricant immersing time.

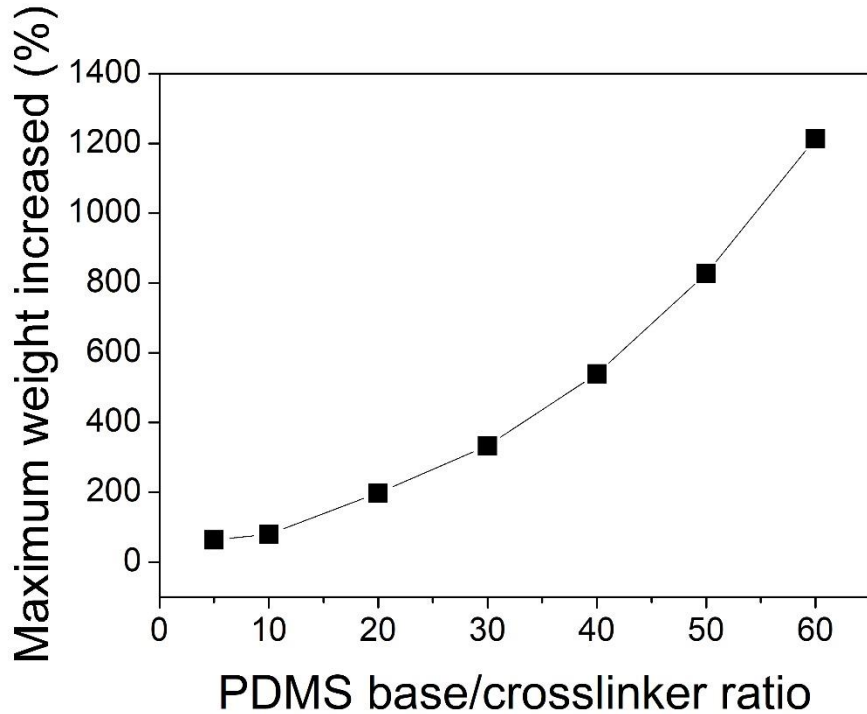


Figure 2.5. Saturated oil swelling/infusing weight as a function of PDMS base/crosslinker ratio.

#### 2.4.2 Rheological measurements

To characterize the mechanical properties of the materials, rheological measurements on samples are taken for the different degrees of crosslinking and swelling. For samples with lower base/crosslinker mixing ratio, like 30:1 samples, the network density is higher than samples with higher base/crosslinker mixing ratio, like 60:1. Thus, the modulus of dry 30:1 samples should be higher than 60:1 dry samples. However, the degree of swelling can also affect the modulus. A higher degree of swelling leads to a lower modulus.

To conduct rheological measurements, samples are produced with as-prepared mixtures

of 30:1, 40:1, 50:1 and 60:1 by weight of the Sylgard 184 base and curing agent. These mixing ratios are chosen because they will be used for wetting studies in following chapters; it is difficult to observe large wetting ridges for materials with higher modulus than 30:1. After mixing and degassing, the mixtures are then poured into a 35 mm diameter plastic Petri dish and cured in a 65°C pre-heated oven for 48 hours. A rheometer (TA Instruments Discovery HR-2) equipped with 8 mm aluminum parallel plates is used to measure the shear modulus of dry and swollen elastomers. The plates are scratched to help with mitigating slip at the boundaries. Figure 2.6 shows results for frequency sweep experiments for samples with different degrees of crosslinking and swelling. The storage modulus of dry and slightly swollen samples are highly dependent on test frequency; this shows that the dry and slightly swollen samples have a more viscoelastic nature compared to highly swollen elastomers. For simplicity, we define the modulus as ones taken at low frequency, where the rate-dependence is negligible: the shear storage modulus of highly swollen samples are taken with a strain of 1% at a frequency of 0.1 Hz and the dry and slightly swollen samples are taken with a strain of 1% at a frequency of 0.01 Hz.

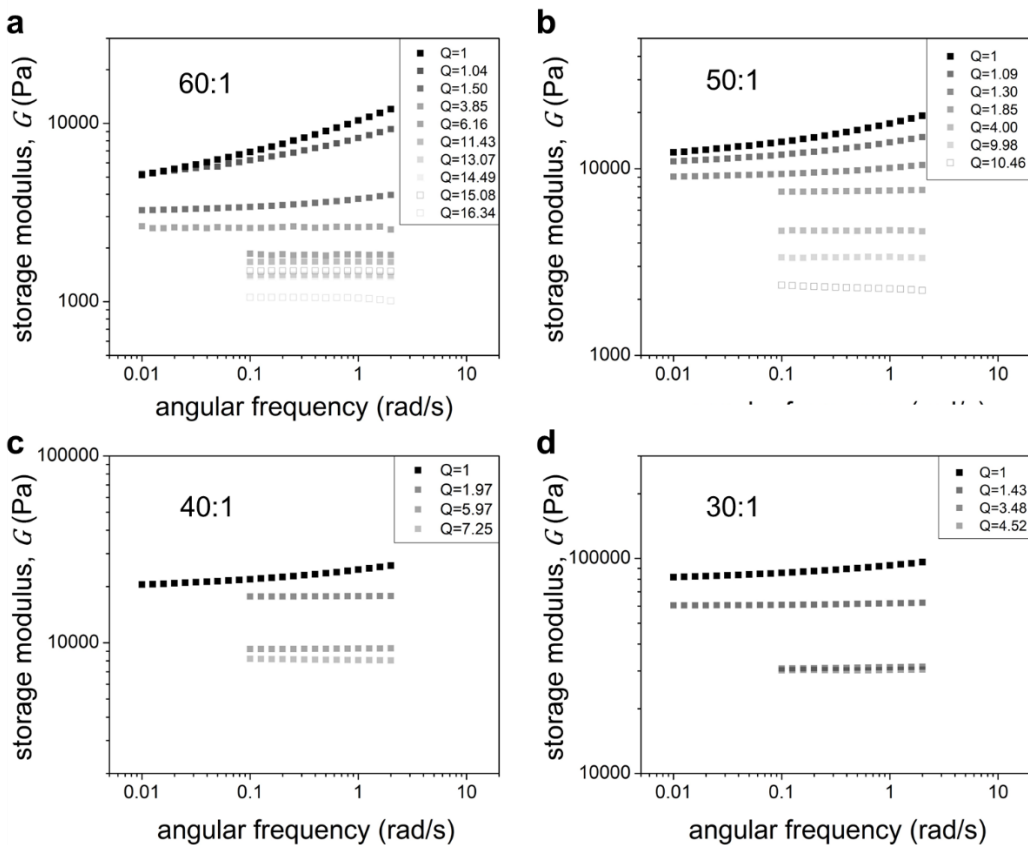


Figure 2.6. Storage modulus vs. frequency. Plots of shear storage modulus ( $G$ ) vs. frequency for the different degrees of swelling  $Q$  with as-prepared mixing ratios of (a) 60:1, (b) 50:1, (c) 40:1 and (d) 30:1.

For all the degrees of crosslinking, the measured moduli decrease with increasing swelling (Figure 2.7). The measured moduli are also compared with theoretical moduli calculated with the equation  $G = G_{\text{dry}}\phi^{0.56}$ , where  $G_{\text{dry}}$  is the shear storage modulus of the dry sample with a certain base/crosslinker mixing ratio, and  $\phi$  is the polymer volume fraction. This equation has the assumption that the swelling solvent is a good solvent for the polymer network, that the swollen concentration is always lower than the preparation concentration, and that it is larger than crossover concentration<sup>56</sup>. Shown in the Figure 2.7,

the measured moduli follows the trend of the calculated data reasonably well (shown as the red dashed line). This makes sense as the increased swelling leads to a decrease in the polymer network density. The strains used for these rheological measurements were confirmed to be in the linear region of a stress-strain curve, by conducting a strain sweep up to 10% (Figure 2.8). Note that we use Young's modulus  $E$  to describe the modulus throughout the majority of this study. This is calculated from the shear storage modulus ( $G$ ) by assuming a Poisson's ratio of  $\nu=0.5$  for incompressibility, which is common for gels and elastomers.<sup>54,57–59</sup>

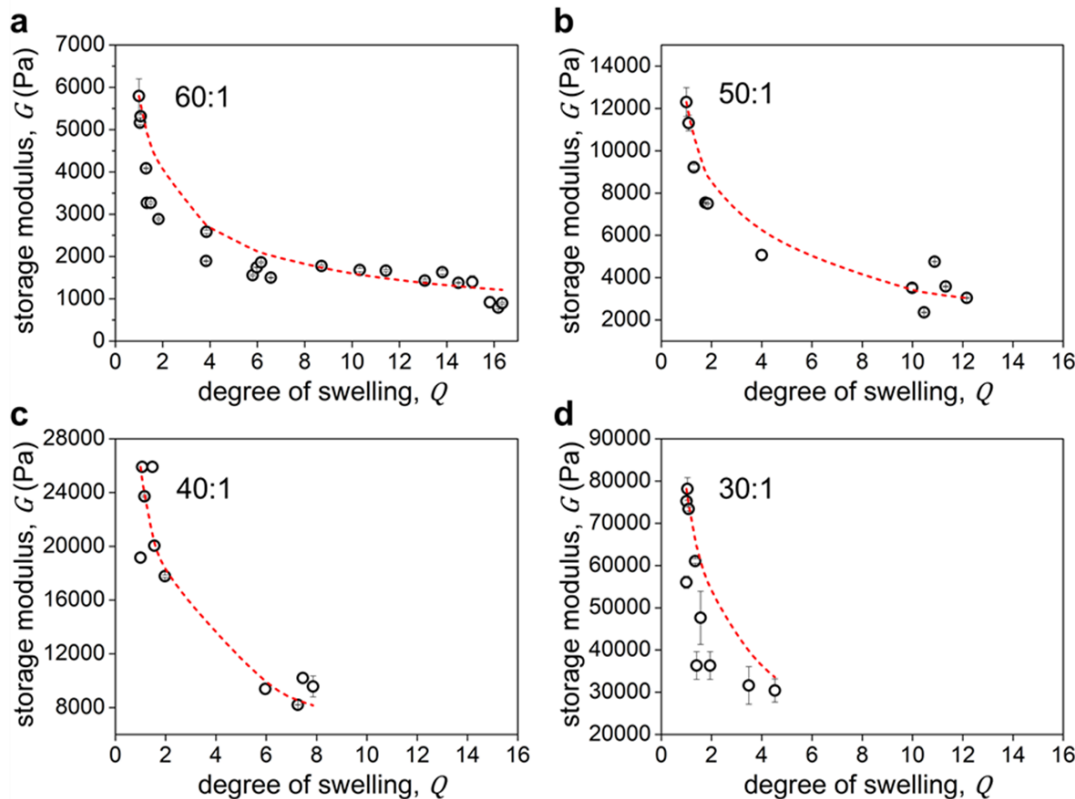


Figure 2.7. Shear storage modulus. Plots of shear modulus vs. swelling ratio of (a) 60:1, (b) 50:1, (c) 40:1 and (d) 30:1 base/crosslinker mixing ratios. The dashed lines are calculated values given by  $G = G_{\text{dry}} \phi^{0.56}$ .

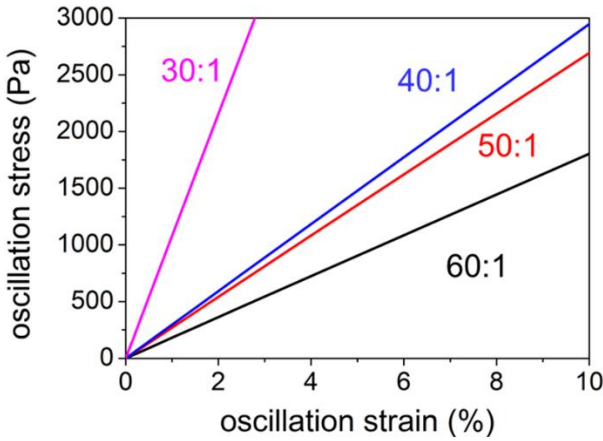


Figure 2.8. Stress vs. strain. A plot of stress vs. strain for dry 60:1, 50:1, 40:1, and 30:1 samples with a frequency of 10 Hz. The samples remain in the linear region up to 10% strain, which is used for the frequency sweeps to quantify modulus values.

## 2.5 Summary

In this chapter, we have characterized silicone oil-swollen PDMS elastomers as our soft, swollen elastomers for wetting investigations conducted in future chapters. We chose a commercial PDMS and qualitatively control the network density by controlling the base/crosslinker ratio. For preparing the swollen PDMS elastomer, we first wash the as-prepared PDMS to extract uncrosslinked polymer chains, and then re-swell the extracted network with silicone oil of a known molecular weight. Meanwhile, we control the degree of swelling during the re-swelling process. We find that the samples with higher base/crosslinker ratio (lower degree of crosslinking) can be swollen with more oil due to the lower network density. A rheometer is used to characterize the mechanical properties

of dry and swollen elastomers. Experimental results show that the modulus of samples increase with decreasing either the base/crosslinker ratio or the degree of swelling.

## CHAPTER 3. STATIC WETTING ON SOFT, SWOLLEN ELASTOMERS

### 3.1 Background and introduction

As previously discussed, the surface tension of a water drop can induce deformation of a substrate if the substrate is sufficiently soft, which means the deformation depends on the substrate modulus. In general, an elastocapillary deformation cannot be ignored when the characteristic length scale of deformation is on the order of the elastocapillary length,  $L_{EC}$ , given by the ratio of the surface stress  $\gamma$ , to Young's modulus  $E$  ( $L_{EC} = \gamma/E$ ). For elastocapillary deformation, the geometry of the contact line between a water drop and a soft substrate should be determined by a balance of surface stresses, elastic forces, and interfacial tensions. The wetting behavior on soft gels is more complex because it is a multi-phase material system that also includes thermodynamic interactions between the lubricant and polymer. A couple of important questions arise: How does the degree of crosslinking and the amount of lubricant infused into the network affect soft wetting? What parameters govern whether the lubricant separates from the polymer network at the contact zone? These questions in wetting of soft gels have not been clearly and systematically explored experimentally.

As described in Chapter 1, when a water drop is placed onto a soft crosslinked solid, a wetting ridge develops around the drop periphery (Figure 3.1). The surface tension of the drop drives the formation of the wetting ridge while the elasticity of the crosslinked

network resists it. However, if the soft solid is replaced by an immiscible fluid (e.g. oil), both liquids deform until they adopt the appropriate contact angles, defined by their interfacial tensions<sup>60,61</sup>. This liquid-liquid contact is commonly observed in slippery, lubricant-infused porous surfaces (SLIPS)<sup>9,62,63</sup>, which are traditionally textured surfaces infiltrated with an oil. The wetting of soft crosslinked solids and SLIPS has received a lot of attention, but swollen networks, often referred to as gels or infused elastomers, have received less attention. Swollen elastomers are crosslinked polymers network swollen with a compatible fluid. When a drop is placed onto a swollen network, it is unclear if the surface creates a homogeneous wetting ridge, like for soft solids (Figure 3.1a), or if the fluid interfacial tensions define the contact line, like for SLIPS (Figure 3.2b). Given the fact that swollen networks are commonly used for soft (bio)materials applications, this highlights an important knowledge gap in our understanding of soft wetting. Additionally, the development of slippery surfaces<sup>9,64–66</sup>, anti-icing surfaces<sup>34</sup>, self-lubricating surfaces<sup>33,67</sup>, surfaces for cell<sup>68,69</sup> or drop<sup>40</sup> patterning, and surfaces for regulating drop dynamics or coalescence<sup>36,37</sup> all require the understanding of wetting on soft swollen/infused surfaces.

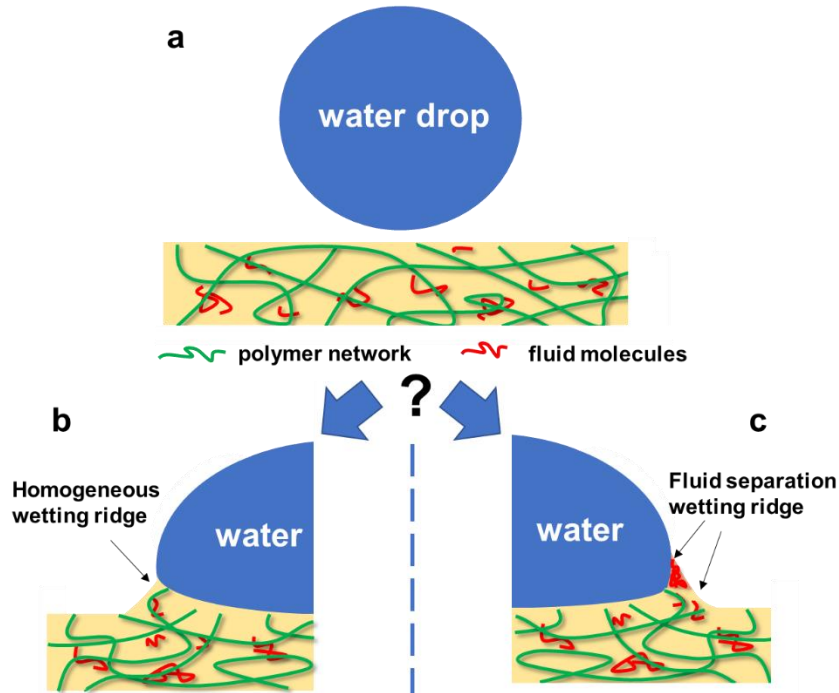


Figure 3.1 Schematic illustration of possible outcomes for soft wetting on a swollen network. (a) Prior to drop deposition, the surface is homogeneous and flat. (b-c) Schematic of two possible wetting ridges upon placing a water drop on the surface: (b) a homogeneous ridge and (c) a fluid separating ridge.

Understanding wetting on soft, swollen elastomers requires knowledge of both the materials factors and the ability to measure the shape of the wetting ridges that is generated by the water drop. To visualize wetting ridges, several microscopy techniques have been used, including high speed optical imaging<sup>70</sup>, schlieren optics<sup>71</sup>, x-ray microscopy<sup>32</sup>, and confocal microscopy<sup>31,38</sup>. However, visualizing the crosslinked network and the imbibed fluid separately is a difficult process, because they usually have similar chemical makeup. Furthermore, there have not been any reports of wetting experiments with in-situ viewing combined with control over the degrees of crosslinking

and swelling, which is likely due to the challenges in both imaging and sample preparation.

In this Chapter, the influence of both the degrees of crosslinking and swelling on the static wetting ridge of a soft and swollen network is investigated. The research focuses on PDMS networks that are swollen with low molecular weight fluid silicone oil or with hexadecane. By using confocal microscopy and fluorescent dyes, we show conclusively that fluid silicone oil can separate near the contact line of a water drop and a swollen network, while the network is also pulled up. This generates a pure liquid tip at a three-phase contact line of the drop, fluid, and air. We call the fluid separation phenomenon at the wetting ridge as “fluid separation”. The fluid separation helps reduce the elastic energy penalty associated with pulling up the network, while still accommodating the surface tension of the water drop. Theoretically, the fluid separation is driven by the spreading parameter (interfacial tensions), balanced by network elasticity and osmotic pressure. A simplified model that is developed in the chapter suggests that fluid separation happens in all PDMS networks that are swollen with fluid silicone oil, even at moderate levels of swelling. However, fluid separation is not observed when the network is swollen with hexadecane. Using hexadecane instead of silicone oil changes the drop-elastomer system to have a negative spreading parameter.

### 3.2 Visualizing the fluid separation

To understand if and when infused oil separates from the PDMS network at the contact zone, confocal microscopy is used to visualize the cross-sectional contact line of a water

drop on silicone oil infused PDMS elastomers, where the network and oil are dyed with two separate colors. As-prepared Sylgard 184 PDMS with mixing ratios of 30:1, 40:1, 50:1 and 60:1 are first washed and then reswelled with silicone oil ( $M_w=770\text{g/mol}$ ). The degree of swelling of samples is controlled from 1 (no swelling) to saturated swelling.

### 3.2.1 Special sample preparation of thin samples

As described in Chapter 2, after curing, the as-prepared PDMS contains a significant amount of uncrosslinked polymer chains. Therefore, the as-prepared samples need to undergo an extraction process and an oil-reswelling procedure to obtain the final swollen samples. However, in order to clearly visualize the wetting ridge with the confocal microscopy, the test sample should be sufficiently thin of the order  $\sim 100\ \mu\text{m}$ ) to keep it within a reasonable working range of the confocal microscope. Therefore, a special sample preparation is developed to retain the thin geometry required for wetting experiments (Figure 3.2). To do this, the base and crosslinker are mixed and spin-coated onto a glass slide, which has already been coated with a water-soluble sacrificial polymer layer (polyacrylic acid). After curing, the PDMS film is released onto a bath of water, and then submerged in excess hexane to allow for the oily, uncrosslinked free chains to migrate out of the network. After multiple washing steps, the hexanes are left to evaporate, leaving a thin, extracted, PDMS film. We define the extracted PDMS film as the “dry” network. The dry network is then swollen with a nonfunctional, low molecular weight (770 g/mol) trimethylsiloxy-terminated linear silicone oil. The degree of swelling is controlled by adjusting the amount of oil swollen into the dry samples when it is still

floating on the water surface. It is then sealed with aluminum foil for 1 week to allow the swelling to reach an equilibrium state. The volumetric swelling ratio is defined as the swollen volume over the dry volume  $Q = V_{\text{swell}}/V_{\text{dry}}$ . The volume of the thin films is determined by capturing top-view images while they are still floating on water. The area of the film before and after swelling and extraction are then measured and the area ratio is calculated; the area ratio  $A$  is equal to area of the swollen sample divided by dry (extracted) area,  $A = a_s/a_d$ . Assuming the samples swell isotropically, the volumetric swelling ratio  $Q$  is then calculated as  $Q = A^{3/2}$ . This volume calculation determined by measuring the area ratio is confirmed to be consistent with swelling experiments on thicker, macroscopic samples.

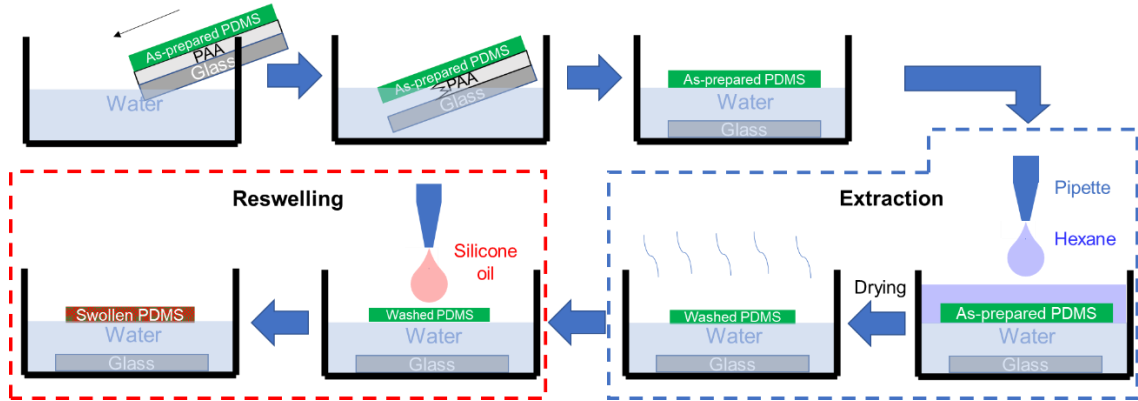


Figure 3.2. Schematic of interfacial extraction and swelling method. The as-prepared PDMS films are released on a water surface by dissolving the sacrificial PAA underlayer. For extraction, hexane was then carefully added to the petri dishes to swell the network and allow uncrosslinked molecules to migrate into the surrounding media. During this procedure, the film remains at the hexane–water interface. To swell the sample with the desired silicone oil fluid, drops of dyed silicone oil are added directly onto the extracted film when it is still floating on the water surface.

### 3.2.2 Visualizing the wetting ridge with confocal microscopy

Different from a traditional optical microscope, a confocal microscope uses a laser to provide the excitation, after which the emission fluorescence response of a dyed sample is recorded within a desired wavelength range. By moving the objective vertically, enabled by a piezo-driven objective, the microscope focuses on one line at a time and scans an  $xz$  planar slice directly (where  $z$  is the vertical direction through the sample thickness), which allows viewing of the surfaces from the side in a cross-sectional image. To visualize the swelling fluid (i.e. silicone oil) and the crosslinked network (i.e. PDMS elastomer) at the wetting ridge, fluorescent dyes are incorporated into the material. Confocal microscopy uses a laser with a particular wavelength to excite fluorophores and subsequently collects the emission by a photodetector within a specified wavelength range; this allows for precise control over which fluorophores are being excited and captured by the detectors. In order to visually separate the infused silicone oil from the PDMS network on confocal images, two dyes with distinct emission spectra and no overlap are used to dye the polymer network and the silicone oil. Two high sensitivity photodetectors are used to collect the emission of the two different dyes in two separate channels. Therefore, it is important that the two dyes do not have any overlap in the emission wavelength range, such that only one fluorophore is captured in each channel. Moreover, the dye for the PDMS network should be chemically connected into the network to make sure the dye does not disperse in oil when swelled. To satisfy this requirement, a commercial fluorescein diacrylate is used as a green fluorophore (emission

wavelength:  $\lambda_{em} \sim 520$  nm in PDMS) to dye the PDMS network. A small amount of fluorescein diacrylate is added to the PDMS base and crosslinking agent, and then cured in an oven; the fluorescein diacrylate incorporates into the PDMS network during curing/crosslinking<sup>72</sup>. Perylene monoimide (PMI) dye is used to dye silicone oil because it is chemically modified to have a strong red shift in its absorption and emission ( $\lambda_{em} \sim 700$  nm in silicone oil), which does not overlap with fluorescein diacrylate. Emission spectra of these two dyes are obtained directly on the microscope (Figure 3.3), confirming the emission ranges of the fluorescein and PMI dyes in the actual PDMS swollen elastomer environment of our experiment.

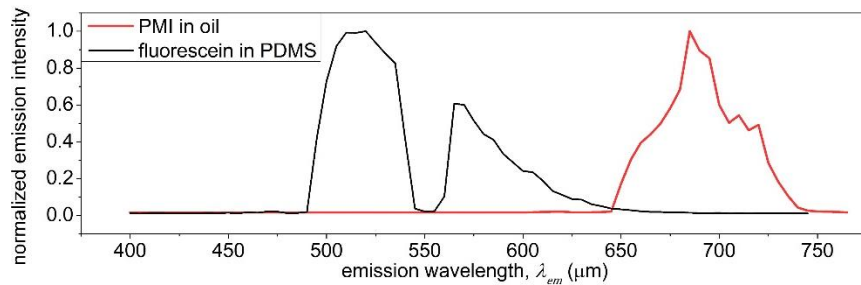


Figure 3.3. Emission spectrum. Fluorescein in PDMS is excited with a 488 nm laser (black line) and Perylene monoimide in silicone oil is excited with 638 nm laser (red line). This shows a non-overlapping emission of the two dyes.

Moreover, in order to minimize the pixel distortion when taking cross-session images with a confocal microscopy, an objective with a correction ring is used to correct z-axis distortion. To verify that confocal microscopy images can be quantitative in the thickness direction, we compare thickness measurements from confocal microscopy to those taken by optical profilometry as a second technique (Figure 3.4).

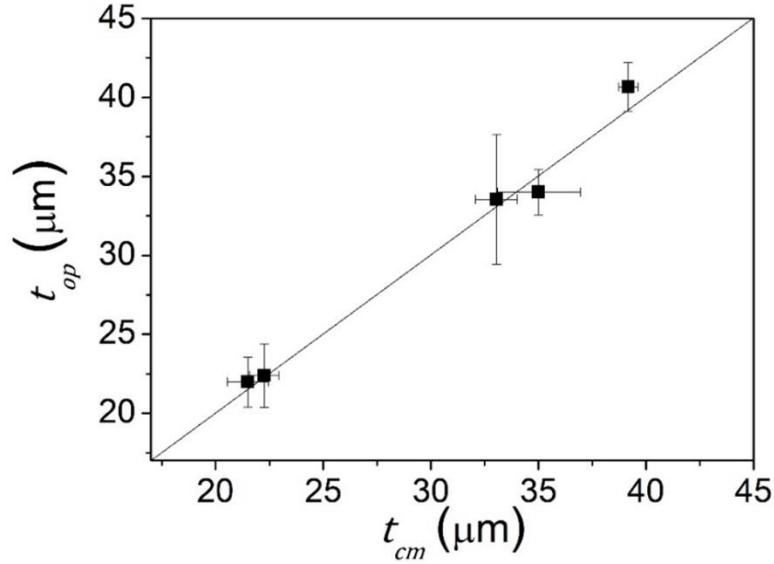


Figure 3.4. Thickness measurements by optical profilometry and confocal microscopy. A plot of the comparison of the thickness measurements from confocal microscopy to optical profilometry.  $t_{op}$ : the thickness measured by the optical profilometry, and  $t_{cm}$ : the thickness measured by the confocal microscopy. Optical profilometry measurements were taken on a Filmetrics Profilm 3D.

By using this specific dye combination (Figure 3.5a, b), we are able to simultaneously visualize the PDMS network and silicone oil separately by confocal microscopy at the contact line. Cross-sectional confocal images show the PDMS network (channel 1, Figure 3.5c, d) and the silicone oil (channel 2, Figure 3.5e, f) with two colors at the water-elastomer contact line—green color is tagged as the network and red color is tagged as the oil. In the combined channel, which includes both channel 1 and channel 2 (Figure 3.5g, h), the network appears yellow since the red and green colors are mixed. For the specific example in Figure 2, the surface is a 60:1 material near its saturated swelling ratio and the macroscopic Young's modulus is  $E \approx 3$  kPa (See data from Chapter 2).

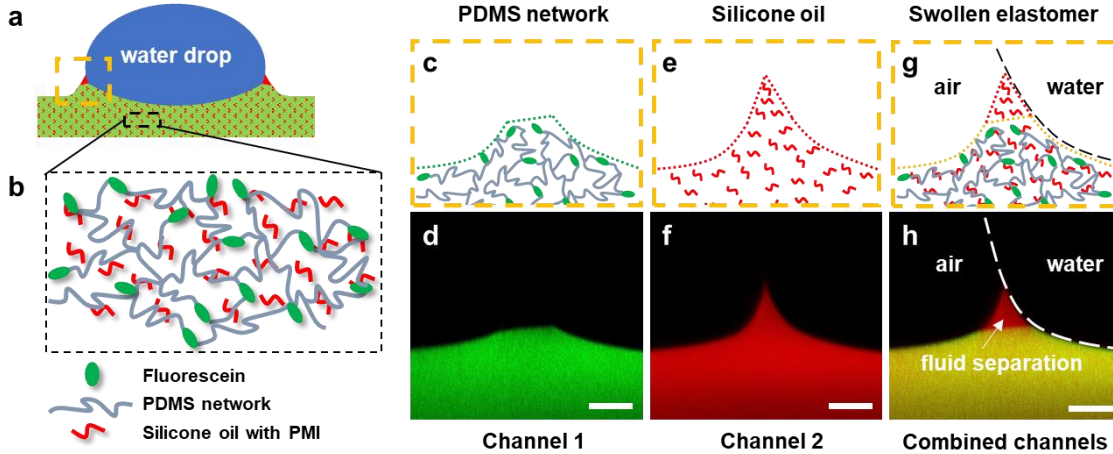


Figure 3.5. Visualizing the network and fluid parts separately at the contact line. (a) Schematics of a water drop on a swollen surface, and (b) the PDMS elastomer, where the network is dyed with fluorescein and the silicone oil is dyed with PMI. (c)-(h) Schematics and corresponding confocal images of a wetting ridge for swollen network with a water drop deposited on the surface. (c), (d) Channel 1 shows the PDMS network (green), (e), (f) channel 2 shows the silicone oil (red), and (g), (h) the combination of channels 1 and 2 show both parts (yellow). Scale bars: 20  $\mu\text{m}$ .

### 3.2.3 Modulus and degree of swelling variation

To study the modulus and degree of swelling effects on wetting ridges, the degree of swelling is varied from  $Q=1$  (dry) to saturation (maximum swelling) for the four base/crosslinker mixing ratios. Examples of wetting ridges for varying degrees of crosslinking and swelling are presented as a qualitative map in Figure 3.6. Column A displays the dry samples that have been fully extracted. Images in the columns moving

rightward display wetting ridges with increasing degrees of swelling. Column B displays wetting ridges for the maximum swelling cases. The rows show the different degrees of crosslinking from the lowest (60:1) in the top row to the highest (30:1) in the bottom row. Let us first consider the dry cases, where fluid separation is not possible. Since the surface tension of the water drop  $\gamma_w$  remains constant, the amount of network deformation is expected to be larger for softer networks. This is confirmed in column A of Figure 3.6, illustrating that the largest wetting ridge appears for the 60:1 samples, which decreases as the degree of crosslinking increases toward 30:1. To describe the effect of swelling, consider the 60:1 samples as a first example (Figure 3.6, top row). Upon swelling the network to lower swelling ratios, the height of the wetting ridge increases ( $Q \approx 2.8$  and 7.9). This is not surprising because  $E$  decreases with increasing  $Q$  (Chapter 2). As  $Q$  is increased further however, fluid clearly separates from the network ( $Q \approx 13.4$ ). By continuing to increase the degree of swelling towards saturation (column B), the amount of fluid separation increases. Qualitatively, the general trend of an initially increasing wetting ridge height followed by fluid separation is universal, regardless of the degree of crosslinking; this is illustrated in the 50:1, 40:1 and 30:1 rows of Figure 3.6.

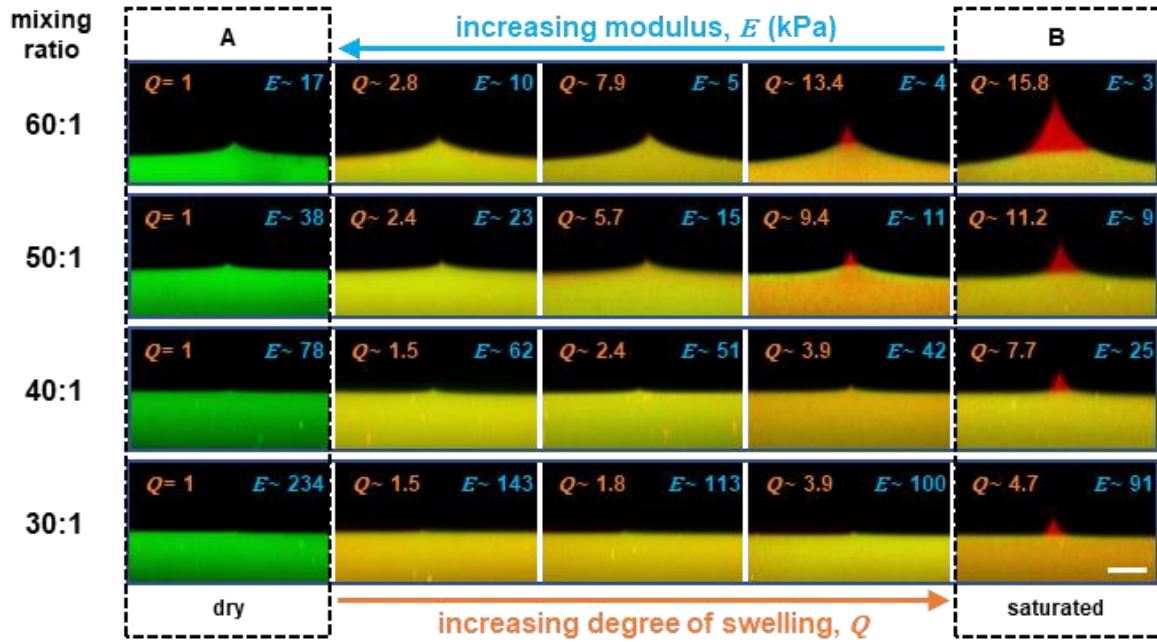


Figure 3.6. Qualitative map of cross-sectional confocal images of contact line with varying degrees of crosslinking and swelling. Each row of pictures from top to bottom corresponds to samples with a dry modulus ranging from 17 kPa to 234 kPa, and a base/crosslinker ratio from 60:1 to 30:1, respectively. Orange numbers inside each image indicate the degree of swelling and blue numbers indicate the macroscopic modulus. Column A and B display the dry and saturated conditions, respectively. Scale bar: 20  $\mu\text{m}$ .

### 3.3 Characterization of contact angles and fluid separation

#### 3.3.1 Contact angles

Here we measure the macroscopic apparent contact angle ( $\theta_{\text{app}}$ ) using a traditional goniometer (Figure 3.7a) and the wetting ridge tip angle ( $\theta_{\text{tip}}$ ) that can be extracted by confocal microscopy images. The contact angle in the dry state ( $Q = 1$ ) shows the apparent contact angle is constant at  $\theta_{\text{app}(\text{dry})} = 111.9 \pm 0.8^\circ$  for all the degrees of crosslinking (Figure 3.7b); this illustrates that contact angle is not strongly influenced by the degree of crosslinking/modulus in the dry state. In the range of the lower swelling ratios  $Q = 1$  to  $Q \approx 2$ , the contact angle precipitously decreases (Figure 3.7b), while above  $Q \approx 2$ , the contact angle remains nearly constant at  $\theta_{\text{app}(\text{swell})} \approx 101.2 \pm 1.1^\circ$ , regardless of the degree of crosslinking, and hence the modulus. This suggests that at  $Q \gtrsim 2$ , a sufficient amount of fluid separates, which may play a governing role in defining the apparent contact angle. To see if the tip angle changes for different swelling cases, several xz profiles are overlaid with aligned tips. As shown in Figure 3.7c, which includes 50:1 and 60:1 samples for situations with and without clear fluid separation, the tip angles  $\theta_{\text{tip}}$  of wetting ridge is constant at around  $71.5 \pm 6.5^\circ$ , at least to our level of precision. This is more clearly displayed in Figure 3.7d, where the red data is for no clear fluid separation, purple is for a small amount of fluid separation, and green is for significant fluid separation (note that the network part of the green is out of view). Since  $\theta_{\text{tip}}$  appears constant, regardless of the wetting ridge height and phase, the angle at the tip is most likely governed by a constant interfacial tension. However, more experiments

with higher resolution would be useful to better interpret this finding. In particular, the angles could be interpreted as not constant, if the angles were measured by extending the vertical length of the measurement zone (in which  $\theta_{\text{tip}}$  would increase as red>purple>green). To attempt to focus on the very tip, we limit the angle measurement to a 1  $\mu\text{m}$  zone at the tip. In general, the apparent contact angles (above  $Q \approx 2$ ) and the tip angles appear constant for the different degrees of crosslinking, pointing to the swelling fluid playing an important role in the wetting.

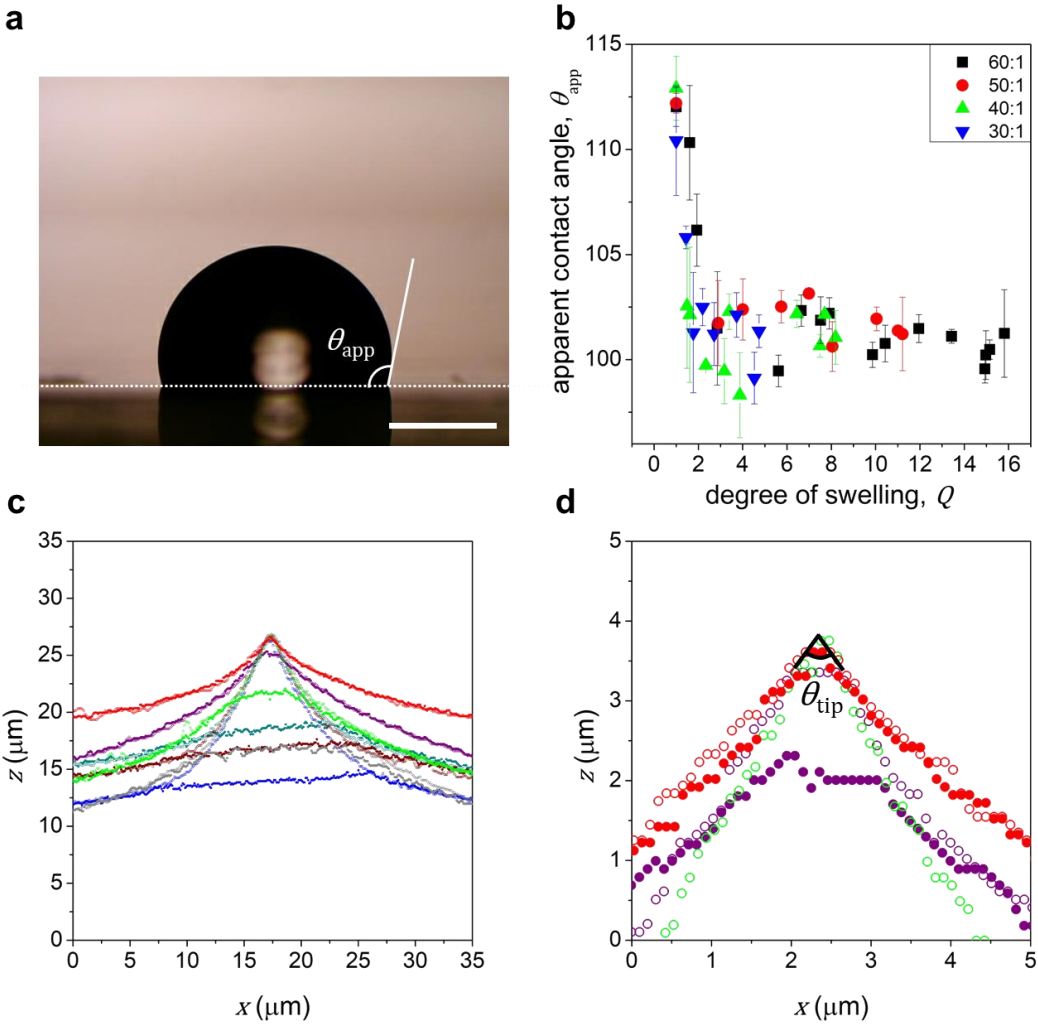


Figure 3.7. Apparent contact angle ( $\theta_{app}$ ) and wetting ridge tip angle ( $\theta_{tip}$ ). (a)-(b) The apparent contact angle for substrates with different degrees of swelling and base/crosslinker mixing ratios. Scale bar: 1 mm. (c) Examples of tip-aligned xz profiles for 50:1 and 60:1 samples, both with and without clear fluid separation. (d) Zoomed-in xz profiles for three samples with no fluid separation (red), a small amount of fluid separation (purple), and a significant amount of fluid separation (green). The open data points are for the fluid profile and the filled data points are for the network profile.

### 3.3.2 Wetting ridge quantification

To quantify the wetting ridge, we measure the heights of both the network ( $h_n$ ) and the fluid ( $h_f$ ) relative to the unperturbed surface, as illustrated in Figure 3.8a. To simplify the wetting heights, the network height  $h_n$  is taken as the right side network height (i.e. the maximum network height). In Figure 3.8b-d, both heights  $h_n$  and  $h_f$  are plotted as a function of swelling for the different degrees of crosslinking. For the 60:1 material (Fig. 5b),  $h_n$  (filled data points) and  $h_f$  (open data points) remain nearly identical from  $Q = 1$  to  $Q \lesssim 7$ . In this lower swelling regime, the  $h_n$  and  $h_f$  both continue to increase as the swelling ratio is increased, and it is difficult to discern a difference between them if one exists. At  $Q \approx 7$ ,  $h_f$  starts to clearly deviate from  $h_n$ . As the swelling is increased even further,  $h_n$  reaches a peak at  $\sim 15 \mu\text{m}$  and then starts to decrease, while  $h_f$  continues to climb. Notably, this illustrates that at higher  $Q$ , the material expels fluid to allow the network to relax while accommodating the water drop. For the 50, 40, and 30:1 materials,

the qualitative trends are similar, consistent with the images in Figure 3.6. However, the quantitative values for both  $h_n$  and  $h_f$  differ for the different degrees of crosslinking. As the degree of crosslinking is increased, the overall magnitudes of both  $h_f$  and  $h_n$  decrease. For example, the peak network heights are  $\sim 15$ ,  $7$ ,  $3$ , and  $1 \mu\text{m}$  for the 60:1 to 30:1 mixing ratios, respectively. Additionally, the apparent transition of where clear fluid separation occurs is also shifted to lower swelling ratios.

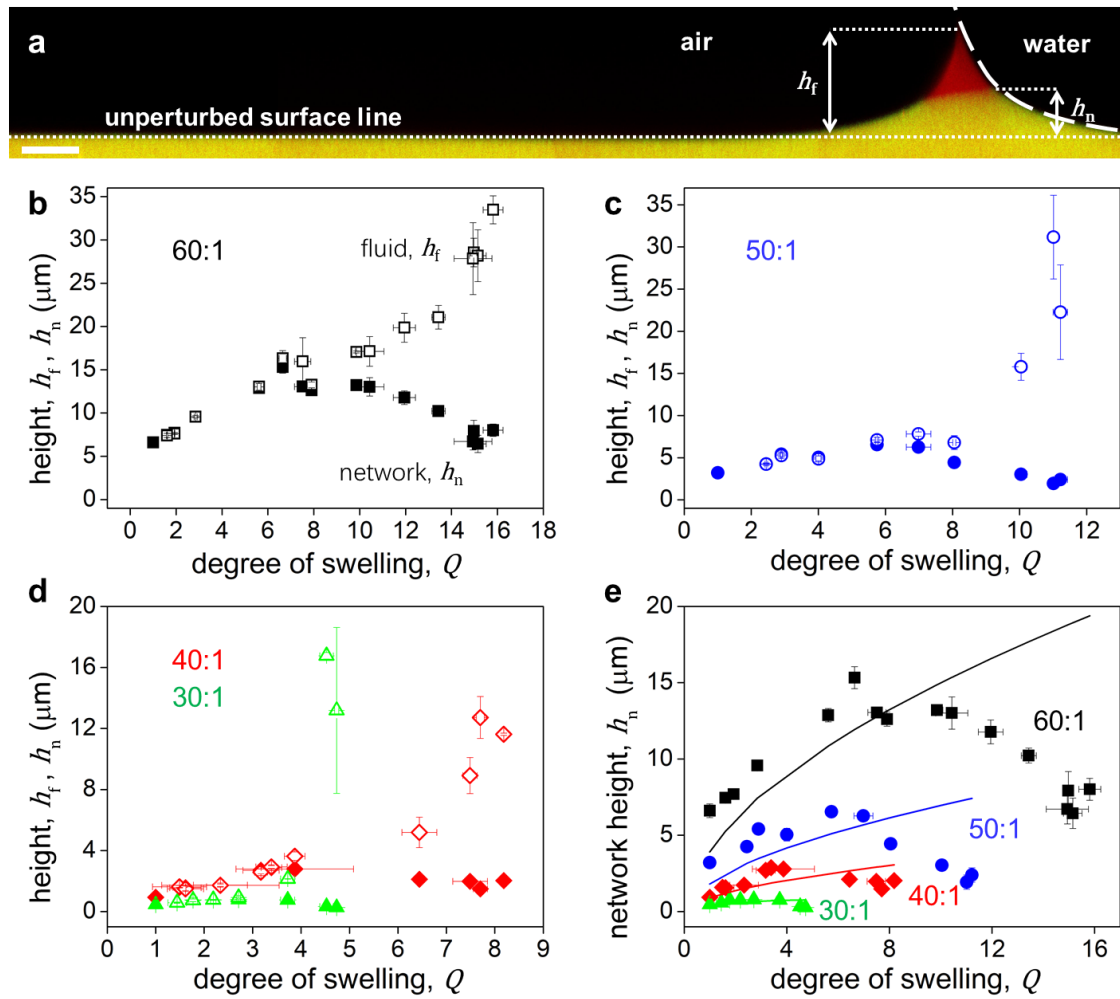


Figure 3.8. Quantifying the wetting ridge heights. (a) Example of a cross-sectional confocal image of a water drop on swollen 60:1 PDMS ( $h_f$  and  $h_n$  are the fluid and network tip heights relative to the unperturbed surface). Note that several images are stitched together to obtain a larger field of view. Scale bar: 20  $\mu\text{m}$ . (b)-(d) Graphs of fluid height ( $h_f$ , open data points) and network height ( $h_n$ , filled data points) as a function of the degree of swelling ( $Q$ ) with mixing ratios of (b) 60:1, (c) 50:1, (d) 40:1, and 30:1. (e) The network height for different degrees of swelling and crosslinking, where the solid curves are predictions given by  $\approx \gamma_w \sin \theta / E$ . Error bars denote standard deviations.

In addition, using this method for imaging, we also conducted a set of control experiments to investigate the effect of sample thickness. We measured the wetting ridge height on 50:1 and 60:1 dry samples with varying thicknesses (Figure 3.10). We find that there is no change in the wetting ridge geometry above a certain thickness, which is consistent with our choice of  $\sim 100 \mu\text{m}$  sample thickness.

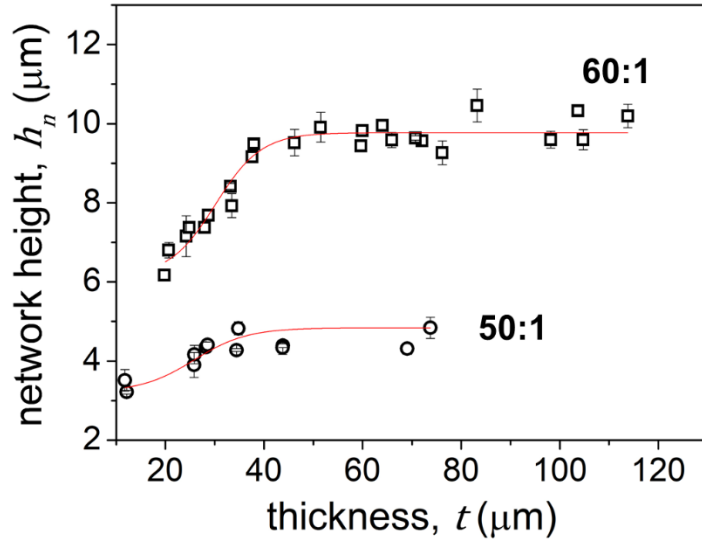


Figure 3.9. Height of wetting ridge as a function of substrate thickness. Examples of wetting ridge heights for 60:1 and 50:1 as-prepared samples. The red line shows that the height of the wetting ridge is first increasing with thickness and then remains constant at thickness values larger than ~50  $\mu\text{m}$  for 60:1 and ~40  $\mu\text{m}$  for 50:1.

### 3.3.3 Network wetting ridge height

Commonly, the wetting ridge heights for soft solids are described in the literature by  $h_n \approx \gamma_w \sin \theta / E$ , where  $\theta$  is the contact angle<sup>32</sup>. Using measured values for the apparent contact angle (Figure 3.7b) and modulus (Chapter 2, Figure 2.7), we overlay this calculated  $h_n$  as a solid line with our experimental results in Figure 3.8e. The modulus is assumed to follow  $E = E_{\text{dry}}\phi^{0.56}$ , which is consistent for a material system where the fluid likes to swell the network (Figure 2.7)<sup>73</sup>. Here  $E_{\text{dry}}$  is the measured modulus for dry samples and  $\phi = 1/Q$  is the volume fraction of the polymer network. The calculated wetting ridge height values reasonably predict the observed network height at lower swelling ratios. However, it cannot capture the network height for the cases where larger amounts of fluid separation are observed. This is also evident when plotting  $h_n$  vs.  $E$  (Figure 3.10). In this figure, one can see that many of the data points line up on the solid lines, which are cases with little to no fluid separation. Hence, this common relationship may be able to capture the wetting ridge heights at lower swelling ratios, as has been suggested by prior studies<sup>32,74,75</sup>, but cannot capture  $h_n$  when significant fluid separation occurs.

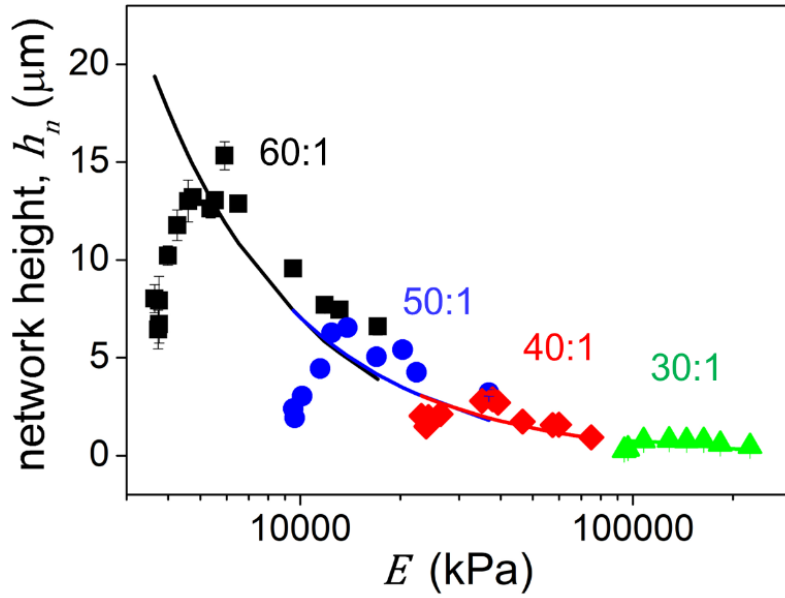


Figure 3.10. Network height vs. modulus. A plot of the network height ( $h_n$ ) vs. modulus ( $E$ ) for 60:1 (black squares), 50:1 (blue circles), 40:1 (red diamonds), and 30:1 (green triangles) samples. The solid lines are calculated values given by  $h_n = \gamma_w \sin\theta/E$ .

We propose two possible reasons for the peak in  $h_n$  as a function of  $Q$ . First consider that when fluid separation does not occur (e.g.  $Q = 1$ ), the network is being pulled up as a point load at the three-phase contact line of water, network, and air (Figure 3.11a). Upon swelling the network,  $E$  decreases, such that one should expect a higher  $h_n$ . However, if fluid is expelled, then two separate forces exist pulling up on either side, which are the fluid-air surface tension ( $\gamma_f$ , left) and the water-fluid interfacial tension ( $\gamma_{wf}$ , right) (Figure 3.11b, c). Hence, the two forces are separated by a distance, leading to two weaker forces pulling on the network. At lower swelling ratios, a very small amount of fluid separates, if at all. Therefore, the two forces from  $\gamma_f$  and  $\gamma_{wf}$  are close and may act together; this will lead to a  $h_n$  that is higher than the dry case because of the lower

modulus. Whereas at higher swelling ratios, the distance between the two forces becomes larger, and the two weaker forces may act at two points (Figure 3.11c).

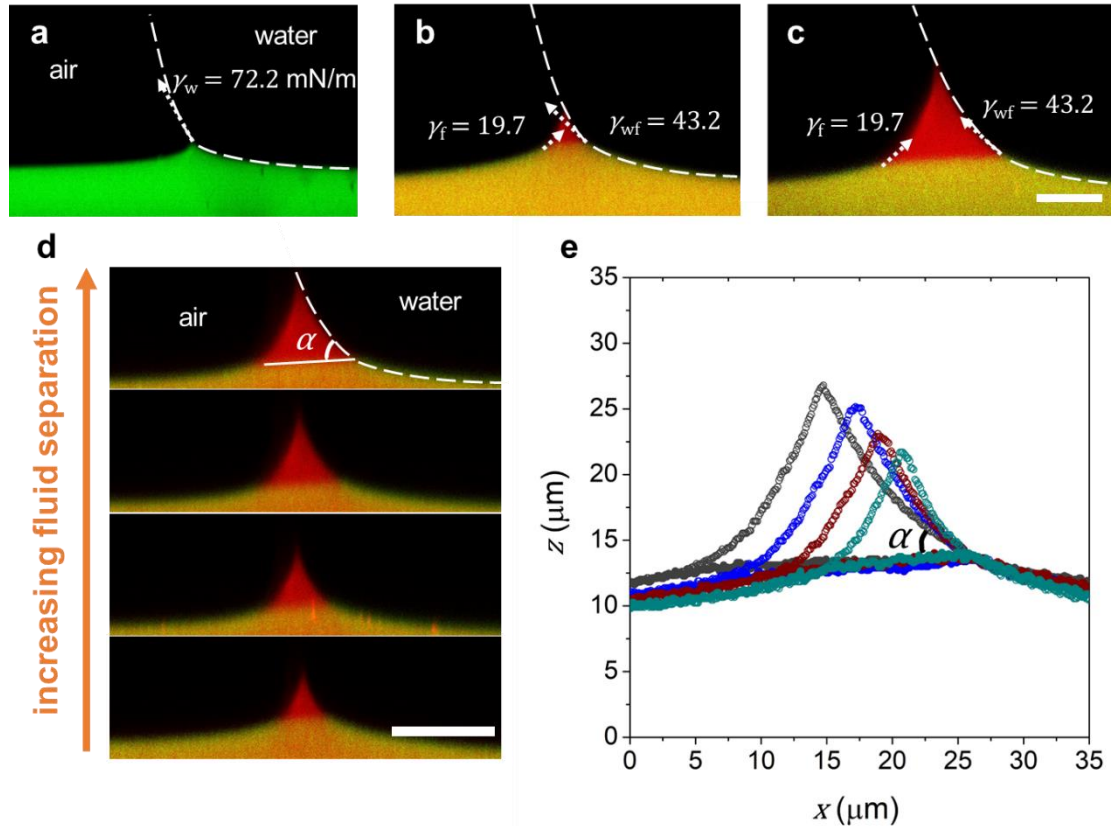


Figure 3.11. Possible wetting ridge height mechanisms. Confocal images show the surface/interfacial tensions pulling up the network for (a) dry, (b) low swelling ratio, and (c) high swelling ratio 60:1 samples. (d) Cross-sectional confocal images of four 50:1 samples with different levels of swelling and fluid separation, and (e) the corresponding profiles aligned at the network-fluid-water contact line on the right side. Interfacial tensions are shown as vectors with magnitude given in mN/m. Scale bar: 20  $\mu\text{m}$ .

A second possible reason for the peak in  $h_n$  as a function of  $Q$  is due to a decrease in the network-fluid-water angle on the bottom right of the fluid separation zone (Figure 3.11d,

e). In order to compare the angles, which we are defining as  $\alpha$ , several xz profiles are overlaid for 50:1 samples with the point aligned. When the degree of swelling increases (and more fluid separates),  $\alpha$  decreases. The vertical force that pulls on the network is related to  $\gamma_{wf} \sin \alpha$ . Since  $\alpha$  decreases with increasing fluid separation, the vertical force would also decrease. Therefore,  $h_n$  first increases with  $Q$  due to a decreasing modulus, but then  $h_n$  would decrease with  $Q$  when large fluid separation occurs due to a decreasing vertical force.

### 3.3.4 Proposed fluid separation mechanism

Here we seek out a simple, semi-quantitative model in attempt to understand what drives fluid separation. First consider the case where a water drop is placed on a layer of immiscible oil, as often observed in SLIPS. Typically, the spreading parameter  $S = \gamma_w - (\gamma_{wf} + \gamma_f)$  defines the “spreading power” (i.e. total vs. partial wetting). The oil lubricant cloaks the drop when the spreading parameter is positive<sup>18,76,77</sup>. To measure the spreading parameter  $S$  when water is placed on the oil, we first use the pendant drop method to measure the surface tension of water and the silicone oil, as well as the interfacial tension between the silicone oil and water. In addition, we measure the interfacial tension between hexadecane and water. Hexadecane is another liquid that we use to swell the PDMS network, for the purpose of comparison with silicone oil swollen PDMS. We will describe the differences of these two swelling fluids later in this section. The results are presented in Figure 3.12. Notably, the surface and interfacial tension values from these pendant drop measurements are consistent with literature<sup>78,79</sup>. Additionally, we note that

there is no difference of interfacial tension between water-oil and water – dyed oil, which indicates the introduction of dye into the oil does not change the surface property of the silicone oil.

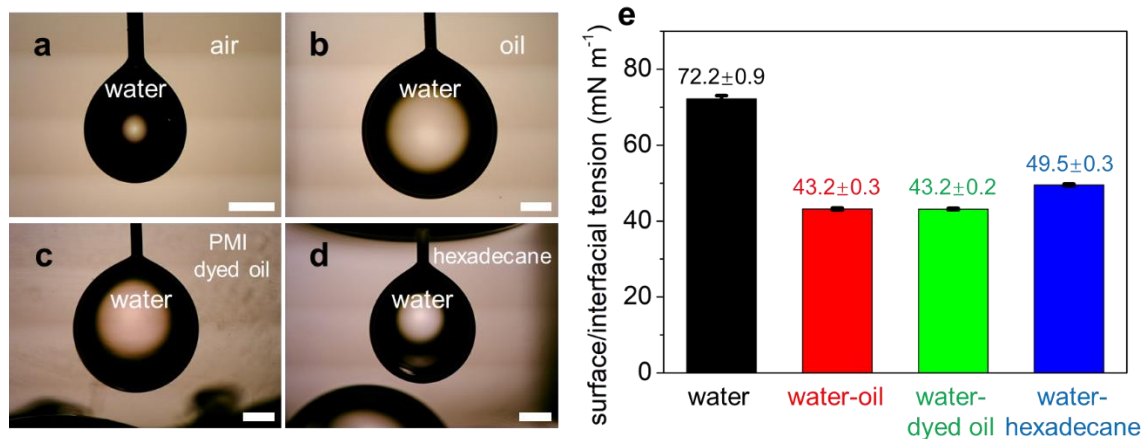


Figure 3.12. Surface/interfacial tensions. A pendant water drop in (a) air, (b) silicone oil, (c) PMI dyed silicone oil and (d) n-hexadecane. Scale bars: 1mm. (e) A bar plot showing the surface/interfacial tensions of water-air, water-oil, water-PMI dyed oil, and water-hexadecane.

In the situation where a water drop wets on an oil-swollen elastomer, the spreading parameter  $S = 72.2 - (43.2 + 19.7) > 0$ ; this means that in the absence of competing forces, the swelling fluid (silicone oil) should cloak the drop. Since cloaking is not observed in our experiments, additional energies must be considered. Moreover, recent experiments from others also suggest that cloaking does not occur in static wetting on soft PDMS materials, probed by other means<sup>48,80</sup>. To rationalize this behavior, we hypothesize that while the interfacial tension of the drop pulls the network up and the fluid out, elastic energy and the energy of mixing between the network and fluid lead to a

finite fluid height,  $h_f$ , as illustrated in Figure 3.13a. To describe fluid separation in a simplified manner, the interfacial energy is balanced by the elastic and mixing energies in equilibrium as  $U_{\text{interfacial}} = U_{\text{elastic}} + U_{\text{mix}}$ . The elastic energy per unit volume for a deforming solid is given by integration of stress ( $\sigma$ ) and strain ( $\varepsilon$ ),  $U_{\text{elastic}} \approx \int \sigma \varepsilon$ . Assuming Hooke's law is valid, this gives  $U_{\text{elastic}} = E\varepsilon^2/2$ . Strain is defined as  $\varepsilon = h_n/t$ , where  $t$  is the unperturbed sample thickness, such that the strain is defined in the vertical direction. This is an approximate global strain through the entire thickness and not the true local strain around the tip, since there is a complex relationship of the local and global stress and strain states that are not easily written analytically. The energy of mixing per unit volume  $U_{\text{mix}}$  is related to the network volume fraction  $\phi$  and the interaction parameter  $\chi$  between the network and the swelling fluid. For simplicity, this is taken as the effective osmotic pressure derived from a Flory-Huggins energy of mixing,  $U_{\text{mix}} = (k_B T / b^3) (\ln(1 - \phi) + \phi + \chi \phi^2)$ , where  $k_B$  is the Boltzmann constant,  $T$  is the temperature, and  $b$  is the Kuhn length<sup>81</sup>. Note that an exact value for  $\chi$  is difficult to obtain. In addition to the enthalpic interactions,  $\chi$  has also been shown to be a function of molecular weight, crosslinking density, and other factors<sup>82,83</sup>. Because of these complexities, an effective parameter  $\chi_{\text{eff}}$  is used, which is expected to be in the range of 0.3-0.5<sup>84</sup>. For  $U_{\text{interfacial}}$ , we consider the spreading coefficient  $S$  as the driving force. From dimensional analysis, a length scale  $\Delta h$  arises as  $U_{\text{interfacial}} \sim S/\Delta h$ , which is assumed to describe the height of the fluid separation,  $\Delta h = h_f - h_n$  (Figure 3.13a). Thus  $\Delta h$  may provide an idea of the fluid separation by rearranging the energy balance as:

$$\Delta h \approx \frac{\gamma_w - (\gamma_{wf} + \gamma_f)}{\frac{E\varepsilon^2}{2} + \frac{k_B T}{b^3} (\ln(1 - \phi) + \phi + \chi_{\text{eff}} \phi^2)} \quad 3.1$$

To compare the equation to our experiments, we calculate the fluid separation height  $\Delta h$  using a Kuhn length of  $b = 1.4 \text{ nm}^{85,86}$  and fitting an effective interaction parameter  $\chi_{\text{eff}}$ , combined with measured values for the strain  $\varepsilon$ , moduli  $E$ , volume fractions  $\phi$ , and surface/interfacial tensions  $\gamma_w$ ,  $\gamma_{wf}$  and  $\gamma_f$ . The calculated values of  $\Delta h$  from Equation 3.1 are overlaid with measured values for  $h_f - h_n$  from our confocal data in Figure 3.13b-e. The data can be well fit to the equation except at very high swelling ratios, with  $\chi_{\text{eff}} = 0.44 \pm 0.04$  for the different degrees of crosslinking. We suspect that the main reason for discrepancy at high swelling is associated with challenges in sample preparation of highly swollen thin films (which is also seen by the large error bars for  $h_f$  at higher  $Q$ ). At swelling ratios near saturation, there is likely small amount of extra fluid on the surface, which would shift  $h_f$  higher than expected. Additionally, as we will show later, it is possible that oil migrates toward the surface at very high swelling ratios. However, this does not affect measurements at swelling ratios below saturation, since the size of the films is directly measured. Nevertheless, the general trends of increasing  $\Delta h$  with increasing  $Q$  between our experiments and Equation 3.1 are in agreement. This suggests that the fluid separation occurs due to a balance of the network elasticity, osmotic swelling pressure, and interfacial tensions. At very high swelling ratios, however, it is possible that a different, more sophisticated model is required.

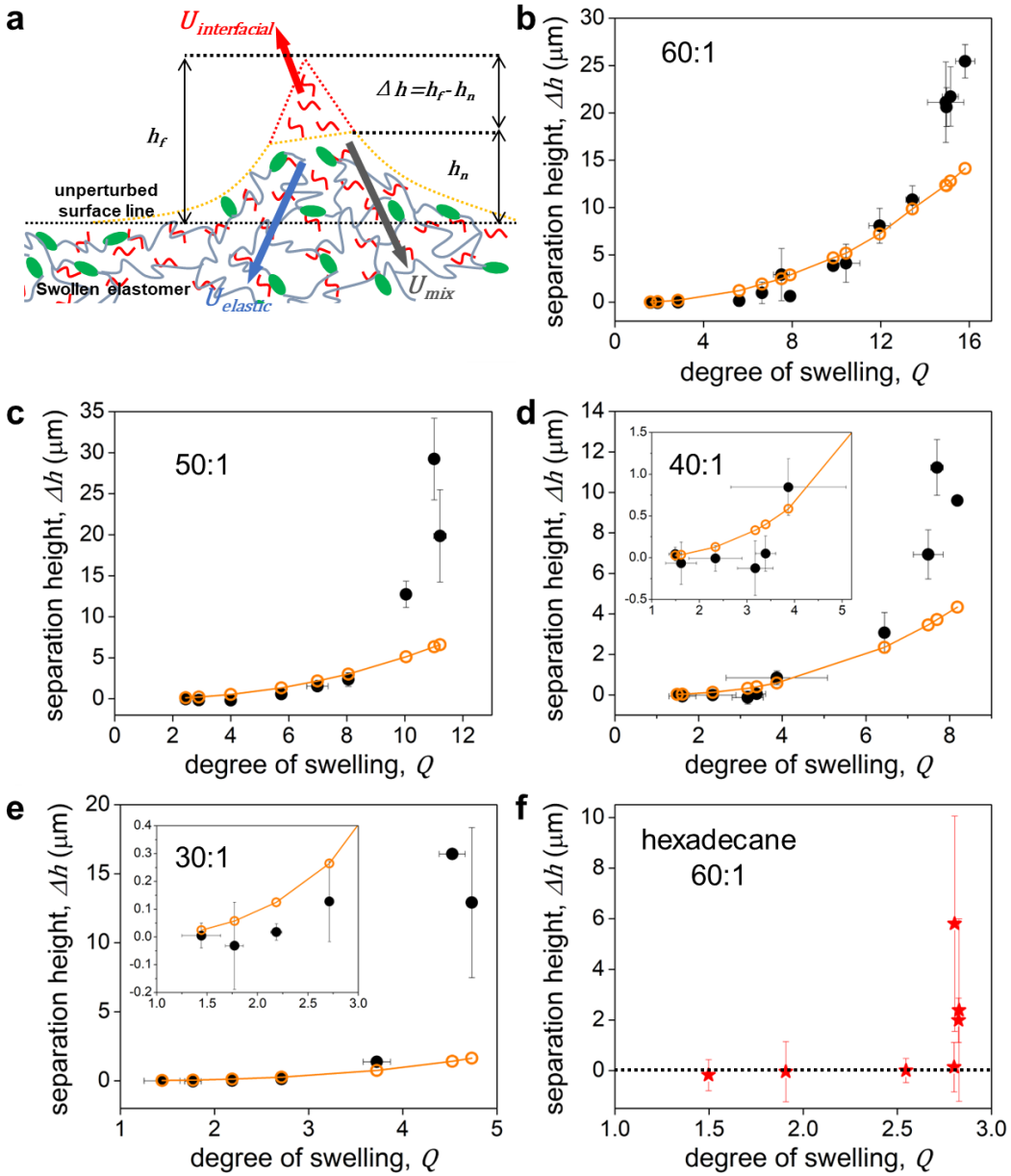


Figure 3.13. Comparison of experiment to approximate theory. (a) Schematic describing the balance of elastic, mixing, and interfacial energy.  $h_n$ ,  $h_f$ , and  $\Delta h$  are also described in the schematic. (b)-(e) Plots of the experimental (filled black points) and theoretical (Equation 1, orange open points and lines) separation heights as a function of degree of swelling with mixing ratios of b 60:1, c 50:1, d 40:1 and e 30:1. Insets show zoomed-in data of lower swelling for clarity. (f) Separation height as a function of degree of swelling for hexadecane (60:1).

of hexadecane swollen 60:1 PDMS. The dotted line is at  $\Delta h = 0$ . Error bars denote standard deviations.

Thus far, we have focused on PDMS networks swollen with a fluid silicone oil having nearly identical chemistry. To test whether the underlying concept of Equation 3.1 works for a different system, we performed a set of experiments using the 60:1 mixing ratio PDMS with hexadecane as the swelling fluid. Hexadecane is used because it swells PDMS (albeit with a much lower maximum swelling ratio), it does not readily evaporate, and it has a significantly different spreading power. For hexadecane, the spreading parameter  $S = 72.2 - (27.5 + 49.5)$ , noting that our measured hexadecane-water interfacial tension of  $49.5 \pm 0.3$  (Figure 3.12) is similar to literature<sup>87</sup>. Since  $S < 0$ , no fluid separation is expected to occur. Indeed, no fluid separation is observed below the saturated swelling ratio, as illustrated in Figure 3.13f; the dotted line denotes zero fluid separation (also see Figure 3.14a). Near the saturated swelling ratio, excess hexadecane droplets can be seen at the surface since it does not completely spread like fluid silicone oil (Figure 3.14b, c). This supports our hypothesis that the large discrepancy between experiments and Equation 3.1 near saturation is likely due to small amounts of excess fluid. The lack of fluid separation with the hexadecane swollen PDMS is consistent with Equation 3.1, illustrating its generality.

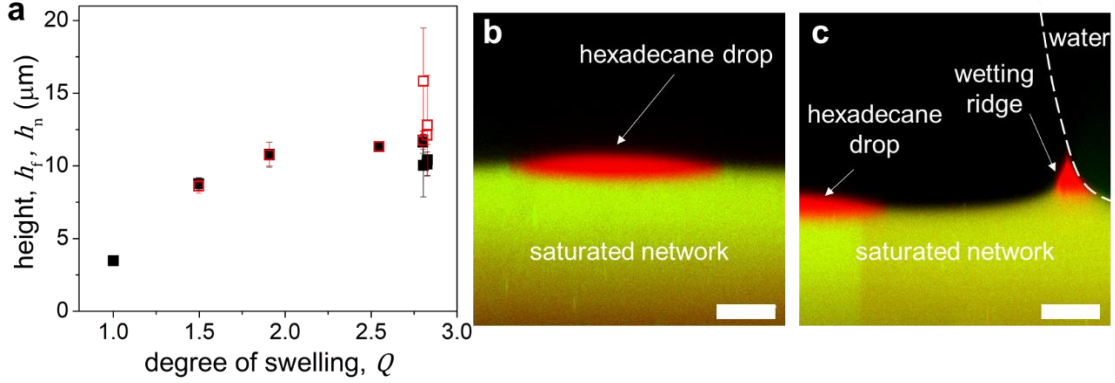


Figure 3.14. Hexadecane swollen samples. (a) A plot of network height  $h_n$  and fluid height  $h_f$  as a function of the degree of swelling ( $Q$ ) of hexadecane swollen samples. (b) Confocal image showing a small excess hexadecane droplet on a saturated network. (c) The hexadecane droplets can be found near a wetting ridge. The fluid zone of the wetting ridge likely comes from the excess droplets. Scale bars: 20  $\mu\text{m}$ .

### 3.3.5 Discussion

Here we call out our experimental results in Figure 3.8, which suggested an abrupt transition of where fluid separation occurs. However, our proposed mechanism suggests that fluid separation should occur for all PDMS networks swollen with fluid silicone oil, even at lower swelling ratios. This inconsistency likely originates from the spatial resolution of confocal microscopy, which is on the order of several hundreds of nm, making it difficult to clearly visualize any separation at lower  $Q$ . For example, for the 60:1 samples at  $Q \approx 3$ , Equation 3.1 gives  $\Delta h \approx 200 \text{ nm}$ , which is not easily observed, whereas for  $Q \approx 7$ , Equation 3.1 predicts  $\Delta h \approx 2.5 \mu\text{m}$ , which is clearly visible. The apparent abrupt transition of fluid separation observed in the experiments should actually

be a smooth transition governed by a balance of forces. This can be understood as follows: Because the network and fluid have favorable interactions, the network wants to retain the fluid. At low  $Q$ , the substrate imposes a high swelling pressure to keep the fluid inside the network, and the wetting ridge is dominated by the deformation of the overall gel (swollen network). At high  $Q$ , the drive for the network to retain fluid decreases because it already has a significant amount of oil inside it. This allows for the network to expel fluid at the contact line to mitigate the energy penalty of deforming the crosslinked network.

Our study is motivated by ongoing efforts in understanding how drops wet soft solids, as well as how drops behave on engineered slippery surfaces. Therefore, it is instructive to consider how our work fits into the framework of soft wetting and coatings development. For many studies, the wetting ridge is assumed to be described only by bulk mechanics while neglecting oils within the network<sup>26,29,88–90</sup>. However we suggest here that fluid can come out at the tip of the contact line for swollen PDMS networks, even at moderate levels of swelling. Recently, Zhao et al. showed numerically that for a drop on a poroelastic substrate, the concentration of swelling fluid diverges near the contact line<sup>44</sup>. This is not inconsistent with our experiments, which show that fluid separation occurs to mitigate the elastic penalty at the contact line.

Aside from drop wetting, our study is relevant for the adhesion of soft materials. For example, Berman et al. studied high-rate adhesive detachment of soft silicone elastomers from a small rigid sphere. They suggest that fluid inside the network generates a poroelastic behavior that needs to be considered in order to describe the detachment dynamics<sup>91</sup>. Elastowetting has also been considered for hydrogel materials and not

limited to silicones. When a soft hydrogel sphere is placed onto a rigid surface, the sphere deforms and creates a foot near the contact line, analogous to a wetting ridge<sup>92,93</sup>. However, whether this foot is made up of mostly water or polymer is not well described. In these cases, we expect similar physics to our wetting results, except that one of the phases is non-deformable (i.e. the rigid underlying surface); this may also lead to more complex stress distributions that may need to be considered.

From an engineering perspective, swollen networks have been considered for slippery and repellent coatings (e.g. soft SLIPS). By crosslinking a PDMS network in the presence of a solvent, Urata et al. showed that the solvent can continuously leech out if the mixing energies are unfavorable; this lubricates the surface and enables easy sliding of drops<sup>33</sup>. In addition, Golovin and Tuteja developed a range of silicone elastomers for anti-icing, and demonstrated that the performance is enabled by oily plasticizers (e.g. a swelling fluid)<sup>94</sup>. Although it was not explicitly studied, network deformation and fluid separation are likely important for both of these applications. Aside from soft surfaces, it has been shown for stiff, lubricant infused surfaces that the size of a lubricant wetting ridge is a function of the initial oil layer thickness<sup>8,21</sup>. Superficially, this may be analogous to the amount of fluid in a swollen network. However, these lubricant-infused, microporous surfaces do not possess a mixing energy associated with the fluid-network interactions (e.g.  $\chi$ ) or a degree of crosslinking, which is needed to describe the wetting of soft and swollen surfaces.

### 3.4 Summery and conclusion

In summary, we present an approach to visualize a crosslinked network and its swelling fluid separately by employing fluorescent molecules and confocal microscopy. Our experiments reveal that the static wetting ridge of a soft and swollen network can comprise both a region of network pull-up and a region of pure fluid. Our calculation suggests that fluid separation occurs in all PDMS networks swollen with fluid silicone oil, although the size can be small at lower swelling ratios. The wetting ridge height of the crosslinked network increases initially with increasing swelling, but then decreases upon further swelling because more fluid is separated from the network; this allows the overall material system to mitigate the elastic energy penalty by balancing it with osmotic pressure. Using a PDMS network swollen with hexadecane, we also show that fluid separation does not occur when the swelling fluid has a negative spreading parameter. Our results clearly demonstrate the importance of considering the fluid inside of gels when investigating the wetting of soft surfaces, which are likely even more critical for dynamic cases. Overall, the work in this Chapter offers fundamental insight into soft wetting, and poses many outstanding questions on how molecular architecture, chemical interactions, and nonlinear and complex strain states may all affect the wetting behavior of soft and swollen materials. The majority of the work described in this Chapter has been published<sup>95</sup>.

## CHAPTER 4. DYNAMIC WETTING ON SOFT, SWOLLEN ELASTOMERS

### 4.1 Background and introduction

Water-repellent surfaces have attracted significant attention due to their diverse range of applications, from self-cleaning to anti-fouling. One route to achieve water repellency is by infusing lubricant into a crosslinked polymer network. In this case, the polymer network is infused with a lubricant, creating a swollen elastomer, which has been described in detail in the last chapters of this dissertation. Lubricant-swollen elastomers can have excellent liquid-repellent properties, which are generally afforded by a lubricant layer that persists on the polymer surface<sup>33,67,96</sup>. In contrast to traditional slippery lubricant-infused porous substrates (SLIPS), which are usually micro- or nano-structured surfaces infiltrated with a lubricant<sup>9,19,62</sup>, the lubricant layer on swollen elastomers can display syneresis, dramatically minimizing lubricant-depletion and increasing the slippery function of the surfaces. Aside from liquid repellency, soft substrates offer flexibility, stretchability, and biocompatibility, making them potential candidates for applications in cell culture and biomedical devices<sup>68,97,98</sup>, soft robotics,<sup>99</sup> and electronic skins<sup>100,101</sup>. Although many lubricant-swollen elastomers rely on a lubricant layer at the topmost surface to maintain the slippery properties, recent studies suggest that swollen elastomers can also maintain slippery behavior even when no lubricant layer is clearly observable on the surface<sup>48,102</sup>. This is likely the result of lubricant being pulled out from the polymer network at the contact line of a water drop or a solid contact<sup>25,35,42,95</sup>, known

as the fluid separation we have shown in Chapter 3. Although crosslinking effects have been considered for the wetting of infused elastomers in literature, they are usually relatively stiff and swollen to saturation (equilibrium)<sup>69,103–105</sup>. Hence, it is not well known how the degree of crosslinking of the polymer network, together with the swelling ratio, govern the ability for water drops to slide on low modulus, swollen elastomers. Moreover, there is no current knowledge of how the fluid-separation occurs on moving water drops. Therefore, a systematic analysis that examines dynamic wetting on soft, lubricant-swollen, low modulus elastomers would be beneficial for developing water-repellent soft coatings.

In a real application, like water-repellent surfaces, water usually moves and slides on the surfaces; this indicates that the wetting occurs in a dynamic situation. This is different from the static wetting situation discussed in Chapter 3, where a drop is placed on a horizontal surface and left stationary. In dynamic wetting conditions, the shape of the wetting ridge plays an important role as it likely controls how the drop can move. In this Chapter, we investigate two perspectives of dynamic wetting. At first, we investigate how the degree of crosslinking and the degree of swelling controls when a drop is pinned or slides on a soft silicone elastomer. In this study, we focus on softer materials with dry shear moduli ( $G$ ) ranging from ~5 to 82 kPa, and swollen shear moduli ranging from ~1 to 27 kPa (base/crosslinker ratio 60:1, 50:1, 40:1 and 30:1). With gravity as the driving force, we quantify the critical volume required for a drop to slide on these surfaces when held vertically. Secondly, we investigate wetting ridges on soft and swollen polydimethylsiloxane (PDMS) substrates, formed during steady-state sliding of water drops. We develop a cantilever-based approach to measure lateral friction forces between

drops and soft surfaces moving at different velocities, while observing the water-elastomer contact line with confocal microscopy. Cross-sectional views of the moving wetting ridge yield their shape and the spatial distribution of network and oil phases in the ridge.

#### 4.2 Drop pinning and sliding on soft swollen elastomers

Before investigating how a drop sticks on a swollen elastomer, we first study the pinning of water drops on dry surfaces with different degrees of crosslinking. Different than the thin samples in Chapter 3, the soft swollen elastomers in the drop pinning/sliding investigation are all bulk samples (thickness > 1mm).

##### 4.2.1 Experimental set up

To study drop pinning, the samples are vertically placed in a chamber with a relative humidity of 70% to 75%. Water drops of different volumes are then placed on the surface by micropipette, and a side-view camera is used to record drop motion (Figure 4.1). Drop-surface interactions (related to adhesion) drive the drop to stick, while gravity (related to drop size) drives the drop to slide. Hence, two main outcomes exist: A water drop can either stick (Figure 4.1b) or slide (Figure 4.1c) on the surface. We note that a third case can also be observed, where the water drop initially slides slowly and then sticks on the surface. One reason for this mixed case may be that initial sliding occurs

due to the kinetic energy introduced when the drop is placed; once the kinetic energy is consumed by friction, the drop sticks on the surface. For simplicity, we describe drop behaviors as either a sliding case or a sticking case, and recognize the third case (sliding first followed by sticking) as the sticking state.

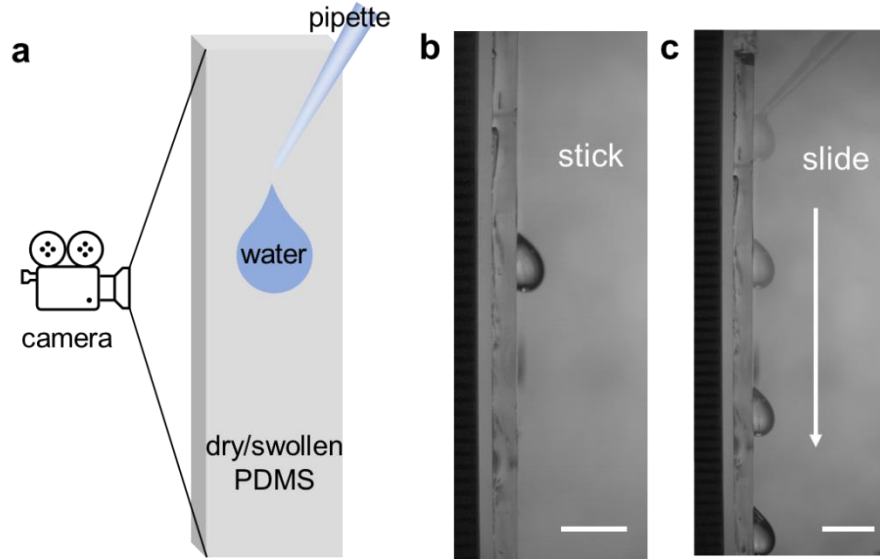


Figure 4.1. A water drop is deposited on a vertical PDMS elastomer. (a) A schematic of the experimental setup. (b) An image of a water drop sticking to a surface and (c) of a water drop sliding on the surface. Note that four images are overlaid in (c) to illustrate drop sliding. Scale bars: 5 mm.

#### 4.2.2 Pinning/sliding on dry elastomers

For dry surfaces with different crosslinking, we plot the percentage of drops that slide as a function of drop volume (Figure 4.2). This approach is used to present the data because we find that even on the same samples, some drops of the same volume slide while others

stick. For example, each data point includes at least 5 drops at that particular volume. If 4 out of 5 drops slide, this equates to an 80% sliding percentage. Hence, by plotting the percentage of drops that slide, we incorporate both potential error as well as the sensitivity to how drop volume controls drop sliding. As illustrated in Figure 4.2a and b for the four crosslinking ratios, all drops stick (0%) below a certain volume while all drops slide (100%) above a certain volume, with a transition region that exists in between. To quantify a critical volume ( $V_c$ ), we define it as when 50% of the deposited drops slide down the surface. Critical volumes are obtained by fitting the sliding percentage data with a Boltzmann function,  $y = \frac{A_1 - A_2}{1 + e^{(x-x_0)/dx}} + A_2$ , where the 50% threshold of  $y$  is obtained at the  $x, y$  point  $(x_0, (A_1 + A_2)/2)$ . In our case,  $y$  represents the sliding percentage and  $x$  represents the water volume, and  $A_1$  and  $A_2$  are set to 0% and 100%, respectively; after fitting,  $x_0$  represents the critical volume. This 50% point is noted as a star in Figure 4.2. As shown in Figure 4.2c,  $V_c$  for 30:1 substrates (dry shear modulus  $G_{\text{dry}} \sim 82$  kPa) is around  $\sim 30.5$   $\mu\text{L}$ , while  $V_c$  for the 40:1 ( $G_{\text{dry}} \sim 21$  kPa), 50:1 ( $G_{\text{dry}} \sim 12$  kPa), and 60:1 ( $G_{\text{dry}} \sim 5$  kPa) (modulus values taken from Chapter 2) mixing ratios are around  $\sim 31.5$   $\mu\text{L}$ . It appears that  $V_c$  is independent of crosslinking for the 40, 50, and 60:1 dry samples. The 40, 50, and 60:1 samples display a similar plot shape in the transition region, while the 30:1 substrates have a steeper transition. This may suggest that the 30:1 substrates are sufficiently stiff, such that their drop-surface behaviors are different than the softer mixing ratios. In addition, we initially hypothesized that softer samples (e.g. 60:1) require a higher  $V_c$  because they have larger wetting ridges. Recall that the wetting ridge is an out-of-plane substrate deformation that occurs at the drop periphery due to the water drop surface tension <sup>31,32,106</sup>. In general, softer substrates have a weaker elastic

restoring force, leading to larger wetting ridges that would hinder drop motion<sup>90</sup>. In Chapter 3, we found that the wetting ridge heights for a static water drop range from  $\sim 6.5 \mu\text{m}$  for a 60:1 dry PDMS surface down to  $\sim 0.5 \mu\text{m}$  for a dry 30:1 surface. However, one possible reason that  $V_c$  is not related to the degree of crosslinking may be due to the introduction of the different modulus. If we consider that a drop slides down a surface by moving a solid wetting ridge<sup>26,71</sup>, then the wetting ridge height and wetting ridge stiffness (i.e. modulus) both play a role. Since the wetting ridge height is inversely proportional to modulus<sup>24</sup>, this may lead to similar  $V_c$  on soft samples.

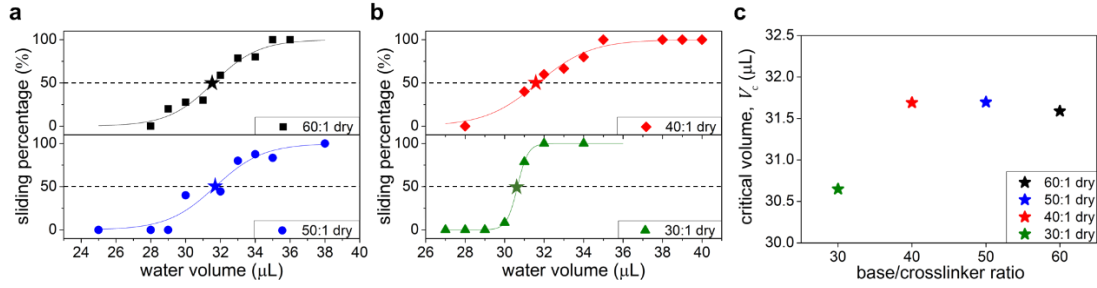


Figure 4.2. Water drop sliding percentage on dry surfaces with base/crosslinker ratios of (a) 60:1 and 50:1, and (b) 40:1 and 30:1. The horizontal dashed line represents the sliding percentage of 50%. The star shows the 50% point of our fit, which is taken as  $V_c$ . Each data point includes at least 5 drops. (c) The critical volume  $V_c$  as function of base/crosslinker ratio for dry samples.

#### 4.2.3 Sliding on swollen elastomers

We now turn our attention to water drop pinning/sliding on oil-infused (swollen) elastomers. We continue to use a low molecular weight trimethylsiloxy-terminated linear silicone oil ( $M_w$ : 770 g/mol) as our swelling fluid. To characterize the amount of oil infused into each network, the degree of swelling is quantified here by weight and defined as  $Q = w_s/w_d$ , where  $w_d$  is the weight of the dry sample and  $w_s$  is the weight of the sample after swelling. For our following studies, we prepare samples that are near their saturated swelling ratio, as well as one at an intermediate swelling ratio, in addition to the dry sample tested above.

In the same approach used for dry elastomers, we measure  $V_c$  on swollen substrates with the four base/crosslinker mixing ratios at different  $Q$ . Since an oily layer at the surface can play a role in drop wetting<sup>33,67,96,103</sup>, it is important have a consistent testing surface. In the literature, this can be done by wiping the surface prior to placing drops<sup>33,107</sup>; however, for our very soft, and sometimes sticky samples, it is challenging to wipe without damage. Therefore, all swollen samples are rinsed with excess water to remove residual oil that may be on the surface, just before drop pinning experiments. In general, we find that  $V_c$  decreases with increasing  $Q$ , regardless of the degree of crosslinking (Figure 4.3a-b). For example,  $V_c$  on the 30:1 samples are ~31.5, 6.0, and 1.5  $\mu\text{L}$  for  $Q = 1$  (dry), 3.2 and  $Q_{\max}=4.1$  (saturated), respectively. This demonstrates that surfaces become more slippery when more oil is swollen into the network. For the 40, 50, and 60:1 samples, the same trend of decreasing  $V_c$  with increasing  $Q$  is observed, but with

quantitatively different values (Figure 4.3c). In particular, we can compare the cases at  $Q_{\max}$  for the different mixing ratios; the  $V_c$  are 1.5, 5.7, 6.1, 5.6  $\mu\text{L}$  for the saturated 30:1, 40:1, 50:1 and 60:1 substrates, respectively. This implies that for saturated networks,  $V_c$  is not strongly correlated to crosslinking at a 40:1 mixing ratio and softer. In a consistent fashion to the dry samples in Figure 4.3c, the 30:1 sample has a slightly lower  $V_c$  than the 40, 50, and 60:1 samples.

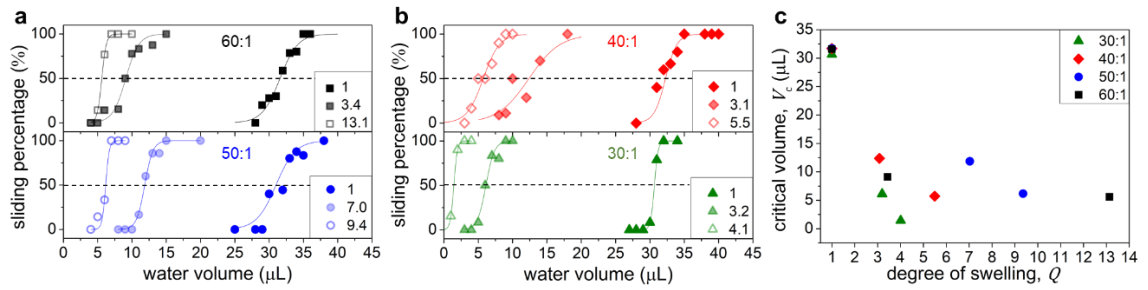


Figure 4.3. Water drop sliding percentage on surfaces with various degrees of swelling for (a) 60:1 and 50:1 samples and for (b) 40:1 and 30:1 samples. The horizontal dashed line represents the sliding percentage of 50%. (c) The critical volume  $V_c$  as a function of degree of swelling  $Q$  for the 30:1, 40:1, 50:1 and 60:1 samples.

#### 4.2.4 Calculation of critical drop volume

Water drop pinning on a vertical surface usually results from a competition between the drop interaction with the substrate balanced by the gravitational force acting on the drop. For a water drop with volume  $V$ , the gravitational force is:

$$F_g = \rho V g \quad 4.1$$

where  $\rho$  is the density of water and  $g$  is the gravitational acceleration. Gravity drives the water drop to slide while adhesion and capillarity pin the drop in place. The maximum/critical pinning force of a water drop with the contact diameter  $D$  can be calculated as<sup>108,109</sup>:

$$F_p = k\gamma D(\cos\theta_R - \cos\theta_A) \quad 4.2$$

where the  $k$  is a constant related to the shape of the drop,  $\gamma$  is the water surface tension, and  $\theta_R$  and  $\theta_A$  are the receding and advancing contact angles, respectively. When a small drop sticks on the surface, gravity cannot overcome the critical pinning force (i.e.,  $F_g < F_p$ ). As the volume of the drop is increased, it eventually reaches a critical volume  $V_c$ , at which point gravity is sufficiently high to overcome the pinning force. Theoretically,  $V_c$  occurs when  $F_g = F_p$ . Thus,  $V_c$  can be approximated by combining Equations 4.1 and 4.2 as:

$$V_c = \frac{k\gamma D(\cos\theta_R - \cos\theta_A)}{\rho g} \quad 4.3$$

The contact diameter  $D$  varies with the drop volume, with larger drops having larger  $D$ . To simplify the relationship between  $V$  and  $D$ , we assume the two factors follow the function:

$$V = aD^3 \quad 4.4$$

where  $a$  is a constant. By combining and rearranging Equations 4.3 and 4.4, a prediction for  $V_c$  becomes:

$$V_c = \left[ \frac{k\gamma(\cos\theta_R - \cos\theta_A)}{a^{\frac{1}{3}}\rho g} \right]^{\frac{3}{2}} \quad 4.5$$

Since the drop is not a spherical cap due to gravity, we use  $a$  as an empirical constant. To determine  $a$  for our material systems, we test a range of drops with different  $V$  ( $1 \mu\text{L}$  to  $40 \mu\text{L}$ ) when they stick on either dry or swollen surfaces and measure  $D$ . Figure 4.4 shows a plot of  $V$  as a function of  $D^3$ . The volume  $V$  follows a linear function with  $D^3$ , consistent with Equation 4.4, regardless of the degrees of crosslinking and swelling; an  $a$  value of 0.17 is obtained by fitting a line and taking the slope

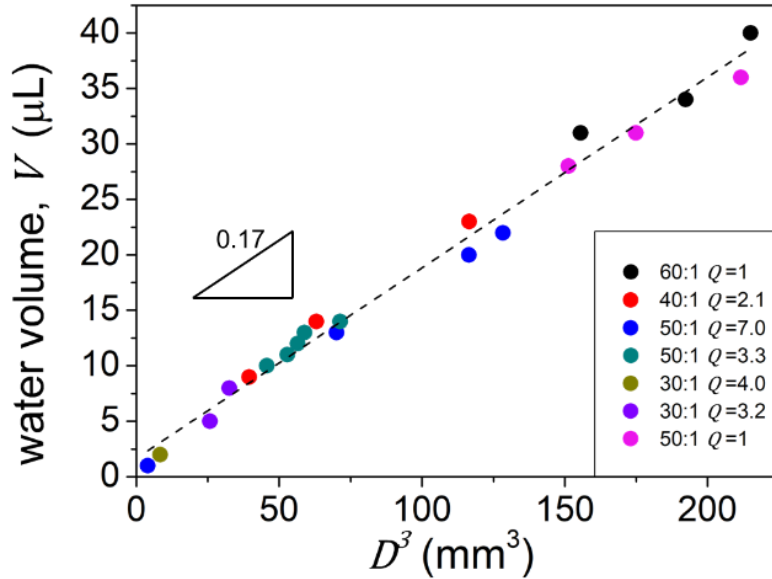


Figure 4.4. Water volume  $V$  as a function of contact diameter cubed  $D^3$  on different elastomers. The dashed line is a linear fit of all data points with a resulting slope of 0.17.

The advancing ( $\theta_A$ ) and receding ( $\theta_R$ ) contact angles are measured by using an automatic dispensing system. The dispensing system outputs and inputs water on the sample surface with a constant inject/withdraw speed (0.05  $\mu\text{L}/\text{s}$ ). The advancing angles are taken as the apparent contact angle when the contact line depins and expands during water injection, while the receding angles are obtained when the water contact line depins and starts moving backwards during water withdrawal<sup>18,48,110</sup>. Figure 4.5 shows plots of advancing and receding contact angles on samples with different degrees of crosslinking and different  $Q$ . As suggested in Figure 4.3, the surfaces are more slippery with higher  $Q$ ; that is,  $V_c$  is smaller for surfaces with higher  $Q$ . Hence, the contact angle hysteresis ( $CAH = \theta_A - \theta_R$ ), which offers information on drop-surface adhesion, is also expected to be smaller for higher  $Q$ . This is confirmed in Figure 4.5, where the smallest  $CAH$  for a given base/mixing ratio is observed at  $Q_{\max}$ . The  $CAH$  increases with decreasing  $Q$ , and are largest when samples are dry. Moreover, we point out that the 30:1 substrates (Figure 4.5a) display the smallest  $CAH$  at  $Q_{\max}$ , while  $CAH$  for saturated 40:1, 50:1 and 60:1 are larger. This is consistent with the  $V_c$  results in Figure 4.3, suggesting that 30:1 samples have slightly different properties.

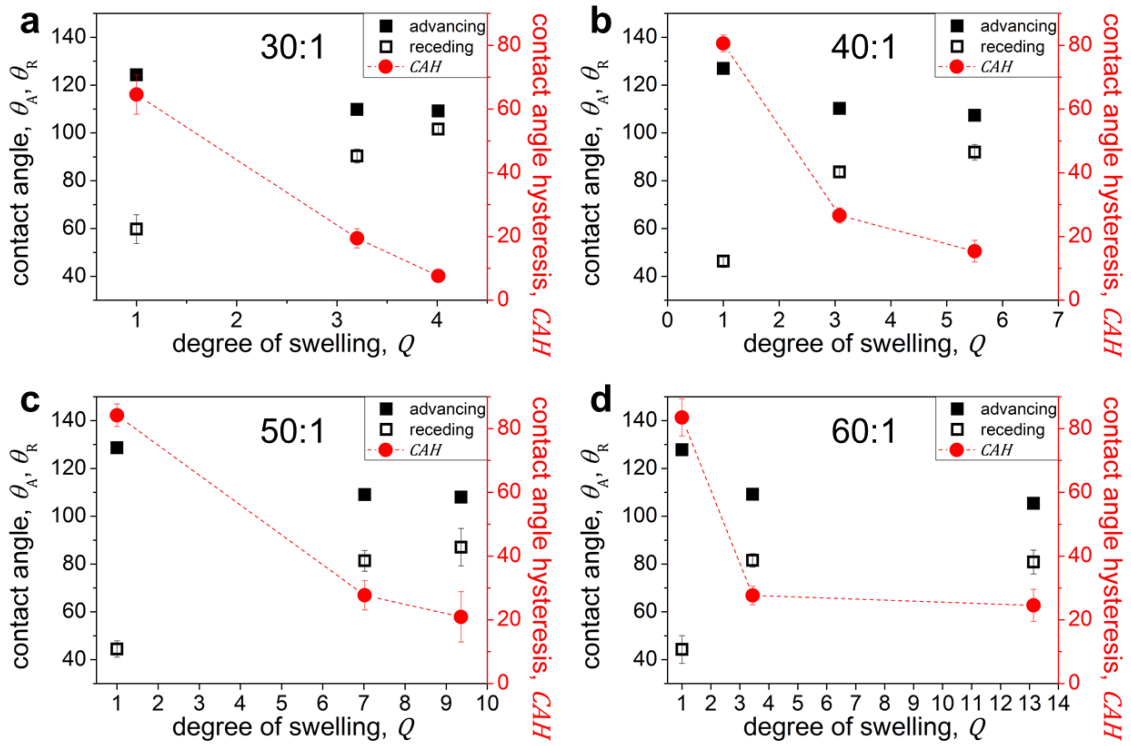


Figure 4.5. Advancing and receding contact angles, as well as the contact angle hysteresis of water on (a) 30:1, (b) 40:1, (c) 50:1 and (d) 60:1 samples with different degrees of swelling from dry to saturated.

To compare Equation 4.5 to our experiments, we calculate the critical volume  $V_c$  by using measured  $\theta_R$  and  $\theta_A$ , a value of  $a = 0.17$ , and known values for  $\rho$ ,  $g$  and  $\gamma$  for water. This leaves the parameter  $k$ , which depends on the geometry of the drop and can be difficult to determine. In literature,  $k$  has been reported to be in a range of 0.5 to  $\pi/2$  (1.57)<sup>111–113</sup>. Since we do not have a way to determine  $k$ , and because it is not yet consistent in literature, we assume that  $0.5 \leq k \leq \frac{\pi}{2}$ . In Figure 4.6, the experimental data for  $V_c$  is plotted alongside calculated values from Equation 4.5 for  $k = 0.5$  (red dashed line) and for  $k = 1.57$  (black dashed line). Our results are close to  $k = \pi/2$  but lie within

these two regions, indicating that Equation 4.5 is consistent with experimental  $V_c$  for our substrates, including both dry and swollen elastomers.

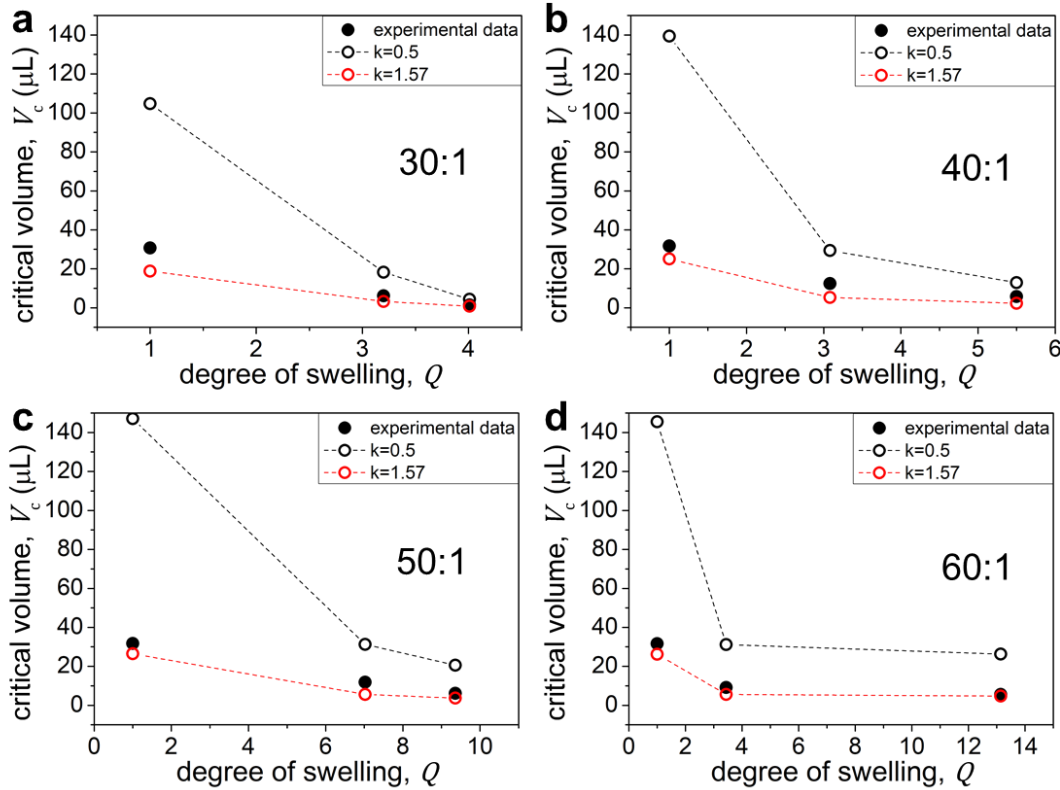


Figure 4.6. Plots of the experimental data for  $V_c$  vs.  $Q$  (filled black data points) overlaid with calculated values from Equation 4.5 for (a) 30:1, (b) 40:1, (c) 50:1 and (d) 60:1 swollen elastomers. The open black circles and dashed lines are the calculated from Equation 4.5 with  $k = 0.5$ , and the open red circles and dashed lines for  $k = 1.57$ .

#### 4.2.5 Rinsing, aging and re-lubrication

Maintaining slippery properties is a challenge for lubricant-infused surfaces<sup>17,20,21,114</sup>, because lubricant can be depleted by rinsing. In this section, we investigate the rinsing, aging, and re-lubrication behavior of our swollen samples. To rinse a surface, 500 mL of deionized water is steadily poured onto the surface. During this rinsing cycle, extra oil on the surface is removed. Directly afterwards, water drops are then deposited onto the surface to determine  $V_c$ . Moreover, we continue to measure  $V_c$  for several days after the rinsing process to examine the effects of aging and re-lubrication. For aging, samples are left in an ambient environment (closed petri dish) without applying any external energy. This rinsing and aging process is conducted over multiple rinsing cycles on the same surface, which allows us to investigate drop pinning/sliding before and after rinsing. In Figure 4.7, we plot  $V_c$  during such an experiment for a saturated 40:1 sample ( $Q_{\max} = 5.5$ ). The original starting  $V_c$  directly after rinsing is  $\sim 8 \mu\text{L}$ . However, over the course of a week in an ambient environment, the  $V_c$  decreases significantly. For example,  $V_c$  decreases to  $\sim 5 \mu\text{L}$  and  $1 \mu\text{L}$  after 1 day and 7 days, respectively (Figure 4.7, first box). During aging, oil likely leaches out from the network and lubricates the surface, which manifests itself by decreasing  $V_c$ . This extra oil near the surface can be rinsed off with water in a second rinse cycle, reverting  $V_c$  close to its original value ( $\sim 7 \mu\text{L}$ ). Again over the course of several days,  $V_c$  decreases. This oil leaching behavior is consistent over at least 5 rinsing cycles (Figure 4.7), with only a small change in the starting  $V_c$ . The same slippery property recovery is observed with a highly swollen ( $Q = 7.0$ ) 50:1 substrate, where  $Q_{\max} = 9.4$  (Figure 4.8a).

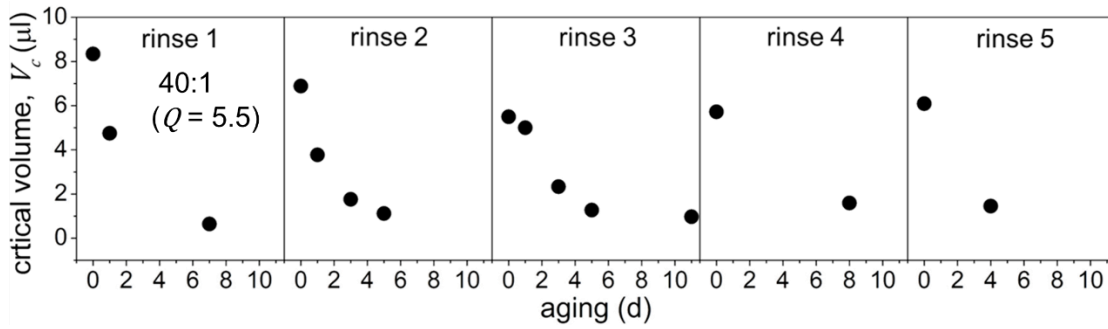


Figure 4.7. The critical water volume as a function of aging days for a swollen 40:1 ( $Q = 5.5$ ) elastomer. Each box represents one rinse and aging cycle using the same sample.

To consider if such behavior is limited to Sylgard 184, we also test a PDMS elastomer prepared from Gelest starting materials as a comparison. Gelest elastomers are produced by mixing hydride terminated polydimethylsiloxane (Gelest, DMS-H25) with a chemical crosslinker (Gelest, VDT-5035) and a catalyst (Platinum(0)-1,3-divinyl-1,1,3,3-tetramethyldisiloxane complex solution, Sigma-Aldrich). After mixing and degassing, the mixture is poured into a 35 mm diameter plastic Petri dish and cured in a 65°C pre-heated oven for 48 hours. The extraction and reswelling procedures are same as those for Sylgard 184 sample preparation. Since the starting materials are controlled, we know there are no additional fillers, which may exist in the proprietary Sylgard 184 kit. Our Gelest silicone has a saturated swelling ratio of  $Q_{\max} = 4.5$ , which is between the 30:1 and 40:1 Sylgard 184. By measuring  $V_c$  for a saturated Gelest elastomer, we observe the same slippery property recovery after aging for 6 days (Figure 4.8b). These results demonstrate that highly swollen, soft PDMS elastomers have the ability to maintain slipperiness over time and use.

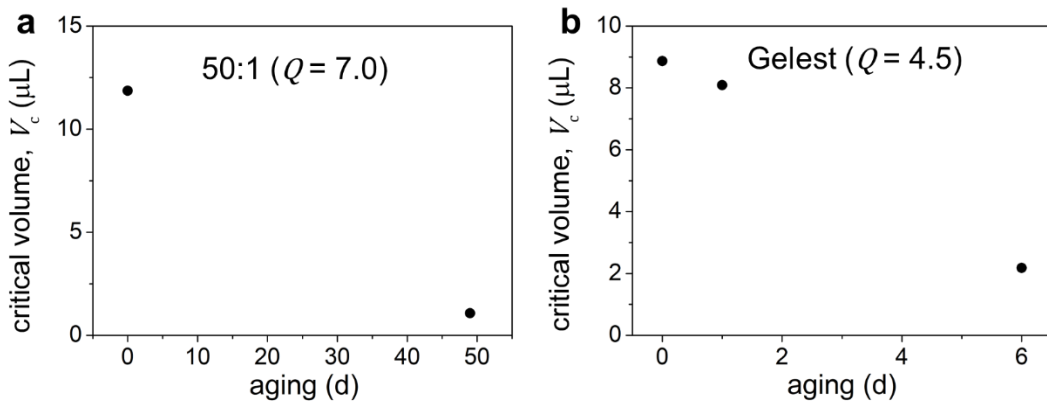


Figure 4.8. The critical water drop volume as a function of aging days for a 50:1 ( $Q = 7.0$ ) elastomer (a) and a silicone elastomer prepared from Gelest starting materials (b). The highly swollen 50:1 sample shows a decrease in  $V_c$  with aging, consistent with the 40:1 tests in Figure 4.7.

We hypothesize that an oil layer leaches out to the surface during aging, which is removed during the rinsing process (Figure 4.9a). Prior literature has shown that oil replenishing can occur at the surface of higher modulus, lubricant infused PDMS substrates<sup>34,107</sup>. To experimentally test whether oil replenishes at the surface of softer, oil-infused materials, we place the PDMS substrate in contact with a piece of standard printer paper for 10 s, and then remove it to see if an oil stain remains. For a rinsed, highly swollen 40:1 sample, no oil stain is transferred to the paper (Figure 4.9b-c), this confirms that excess oil is removed during the rinsing process. After 7 days of aging in ambient environment, the substrate is again placed on the paper for 10 s. Upon removing the PDMS, an oil stain remains, indicating there is an extra oil layer on the aged sample (Figure 4.9d-e). Although others have utilized an AFM technique to quantify oil layer

thicknesses<sup>96,115</sup>, it can be challenging on very soft surfaces. Therefore, we use the oil stain test as an indirect route to observe whether an oil layer exists on the surface.

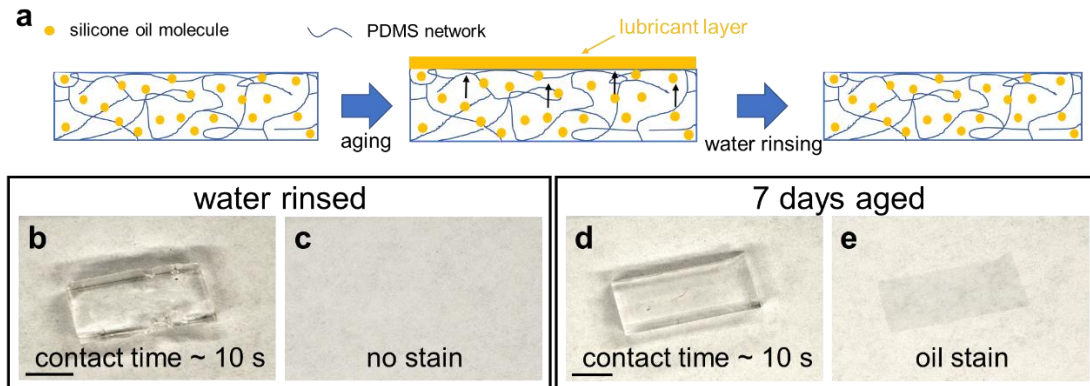


Figure 4.9. (a) A schematic of rinsing, aging, and re-lubrication of highly swollen PDMS. (b-e) Paper stain test with a highly swollen 40:1 ( $Q = 5.5$ ) sample. (b-c) A water-rinsed sample and (d-e) a sample aged for 7 days. No stain is left on the paper for water-rinsed samples (c), while an oil stain is observed on the paper for the 7-day aged sample (e). Scale bars: 5 mm.

#### 4.2.6 Oil leaching mechanism

The fact that imbibed oil migrates to the surface can be explained by the different surface tensions of the PDMS network compared with the low molecular weight silicone oil. The surface tension of PDMS in air is in the range of  $\sim 20$  to  $24$  mN/m<sup>115–117</sup>, while the surface tension of low molecular weight silicone oil is  $19.7$  mN/m (Gelest, Trimethylsiloxy-terminated,  $5$  cSt)<sup>118</sup>. Since the silicone oil has a lower surface tension, we expect it to migrate to surface to cover the elastomer and lower the overall energy. However, once the

surface is covered with a thin layer of oil, the oil layer should not continue to increase in thickness, based on a surface energy argument. Recently, Lavielle et al. suggested that further crosslinking of the PDMS network can explain a continuously increasing layer of lubricant in oil-infused silicones<sup>96</sup>. However, our as-prepared samples are first extracted, such that excess crosslinkers and excess uncrosslinked free chains are removed. Hence, the only obvious source of further crosslinking would come from unreacted dangling ends. Since these elastomers are highly swollen, such that the network chains are expanded, it may not be as likely that these dangling ends are able to react with each other to increase crosslinking, although we cannot exclude it as a possibility. Another possible reason for re-lubrication may be due to surface defects, leading to a “defects-driven” mechanism for lubricant separation on the surface of a swollen elastomer. As drawn in Figure 4.10, the surface of a swollen elastomer may not be perfectly smooth; microcavities may exist on the surface. Inside cavities, a high capillary pressure arises from the high curvatures; the capillary pressure can drive the imbibed oil to separate from the network and fill the cavities through osmo-capillary phase separation<sup>50</sup>. Moreover, an open environment could allow very small dust or contaminate particles to land on the surface. These small particulates may also drive oil out from the network through capillarity<sup>25,35</sup>. Driven by small defects or particulates, lubricant would gradually separate from the elastomer and accumulate on the surface. After several days, an apparent lubricant layer would then appear. Overall, it is possible that both continued crosslinking, as well as defect-driven oil separation, can aid in oil re-lubrication in highly swollen surfaces.

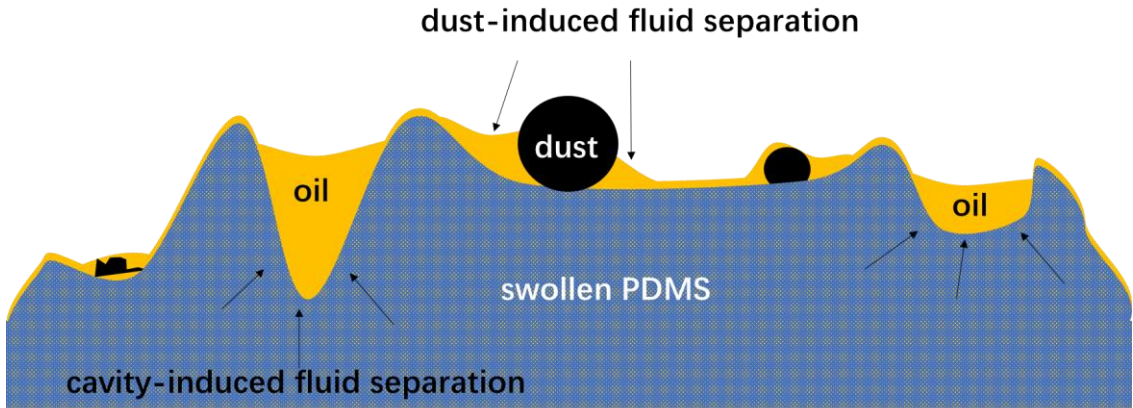


Figure 4.10. Schematic of a potential mechanism that drives the oil separates from the swollen PDMS

Although oil layer formation is observed in highly swollen samples during aging, such behavior is not observed for an intermediate swelling ratio. For example, we measured  $V_c$  on a 40:1 sample with a swelling ratio of  $Q = 2.1$  (maximum swelling is  $Q_{max} = 5.5$ , which is tested in Figure 4.9). As illustrated in Figure 4.11a, the critical volume remains unchanged after leaving it in an ambient environment for over 4 months (134 days) after an initial rinsing cycle. The same paper-staining experiment shows that no oil-stain is transferred to the paper from this sample (Figure 4.11b, c). In Chapter 3, we proposed that strong affinity between the network and the oil can hold the oil inside the network. When the PDMS network is only lightly swollen, the polymer network pressure dominates; this means that oil will remain swollen inside the network, rather than segregate to the interface. This idea is consistent with our findings in Figure 4.11, in which a layer of oil is not observed during aging.

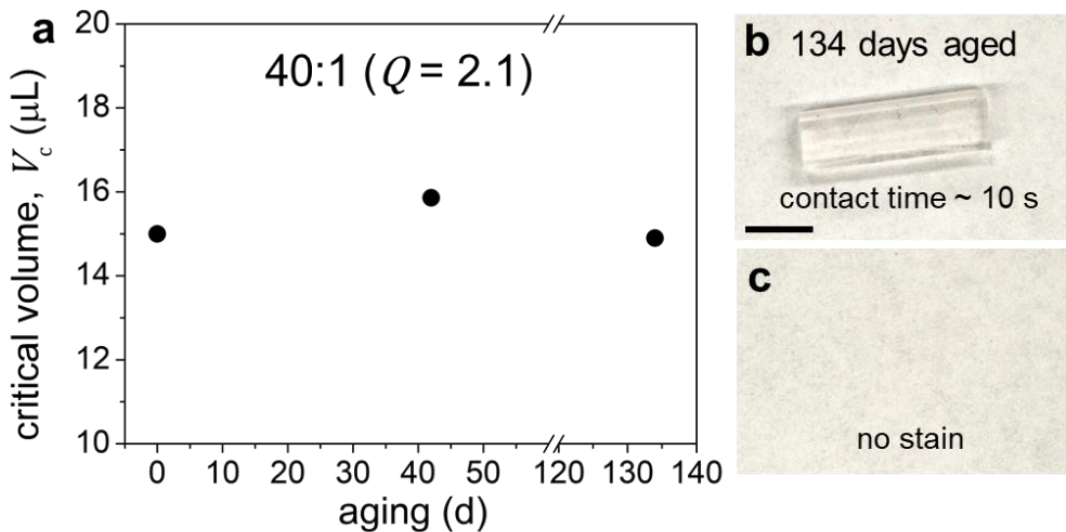


Figure 4.11. (a) Critical water volume as a function of aging days for 40:1 ( $Q = 2.1$ ) elastomers. For the substrate aged for 134 days, (b) it is put into contact with paper for 10 s, and (c) no stain is left on the paper. Scale bars: 5 mm.

#### 4.3 Effects of drop sliding velocity on wetting ridges

As discussed in Chapter 3, when a drop is placed on a soft surface, a “wetting ridge” emerges due to the normal component of the drop surface tension, which pulls on the substrate and deforms it upwards. We have shown above that ridges on swollen, crosslinked elastomers do not comprise a homogeneous phase. Swollen oil can phase-separate at the tip of the ridge, forming a region of pure liquid, these have been considered in static drops in Chapter 3.

In dynamic wetting conditions, where the drop is move along a surface, the ridge is highly relevant: Friction that builds up during drop sliding dissipates mostly in the

ridge<sup>71,119–121</sup>. Hence, the shape and material makeup of the wetting ridge are central components to determine drop movement. For soft, swollen elastomers, both the network and swollen liquid play a role in the wetting ridge. In Chapter 4, section 4.2, we investigated the effects of the degree of crosslinking and the degree of swelling on water drop pinning/sliding for soft PDMS elastomers swollen with silicone oil. Our experiments reveal that the critical water drop volume required to slide on a swollen elastomer is mainly controlled by the degree of swelling: Increasing the degree of swelling can dramatically decrease the water drop pinning force. However, it is still not understood how drop sliding speed affects phase separation, how the sliding induced separation is related to the swelling ratio of the underlying network, and what time scales govern the separation mechanism. In this section, we investigate the velocity-dependent drop sliding effects on the wetting ridges and fluid separation on soft swollen PDMS substrates. We develop a cantilever-based force measurement for single water drop sliding on the surface, and monitor the wetting ridge of sliding drops with laser scanning confocal microscopy at the same time.

#### 4.3.1 Experimental set up

60:1 PDMS oil-swollen thin films with different degree of swelling (i.e., swelling ratio  $Q = V_s/V_d$ ) were manufactured and placed on glass slides (preparation method is described in Chapter 3). The swollen PDMS networks are mounted on a motorized linear stage. A 8  $\mu\text{l}$  water drop (large enough to neglect evaporation but small enough to facilitate easy sliding) is then placed on the substrate. Upon deposition, there is an initial

drop dwell time, in which an annular wetting ridge forms at the three-phase contact line. An affixed metal ring (diameter  $\approx$  2.5 mm) hovers 1 mm above the substrate and holds the drop in position while the stage moves at constant speeds (5–800  $\mu\text{m/s}$ ), Figure 4.12. This generates a relative sliding motion between the drop and substrate, while holding the drop fixed within the laboratory frame for imaging. The setup is mounted on a laser scanning confocal microscope that enables microscopic visualization of the wetting ridge. The drop is positioned such that the advancing contact zone lies in the field of view, which spans  $250 \times 62 \mu\text{m}^2$ .

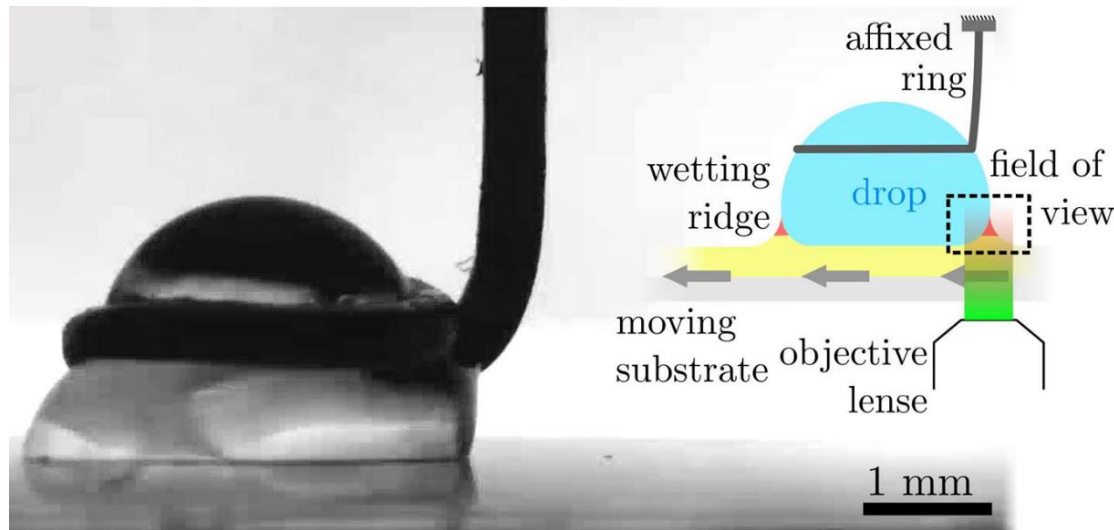


Figure 4.12. Drop sliding set-up and wetting ridge visualization. Macroscopic side view of affixed drop, substrate moves left while the drop is stationary. Inset, set-up schematic.

#### 4.3.2 Kinetic friction force of a sliding water drop

The friction of a single water drop sliding on the soft swollen surface is measured by measuring the displacement of a customized metal wire capillary. A long metal wire with a ring at the end to help hold the water drop while moving the underlying PDMS substrate with a constant speed. When the substrate moves, the drop is first deformed and then starts to slide on the substrate with the help of the metal wire. During sliding, the metal wire deflects due to the sliding friction force of the water drop, which induces a wire displacement corresponding to the original position (Figure 4.13a and b). The displacement of the wire relates to the force—the larger of the friction force, the larger of the displacement. Thus, the friction force can be calculated by the displacement and spring constant of the wire as  $F = k\Delta x$ , where  $k$  is the spring constant of the wire. In this set up, we have a spring constant of  $k = 0.19N/m$ .  $\Delta x$  is the wire displacement corresponding to the original position. Figure 4.13c shows the instantaneous friction force of a water drop during sliding. Before sliding, the force is 0 since the drop is static,. When the substrate starts moving, the drop needs to overcome a relatively large static friction, and before it starts to slide. After sliding starts, a constant kinetic friction force is observed (Figure 4.13c). The force reduces to 0 again when the substrate stops, and the drop is removed from the surface.

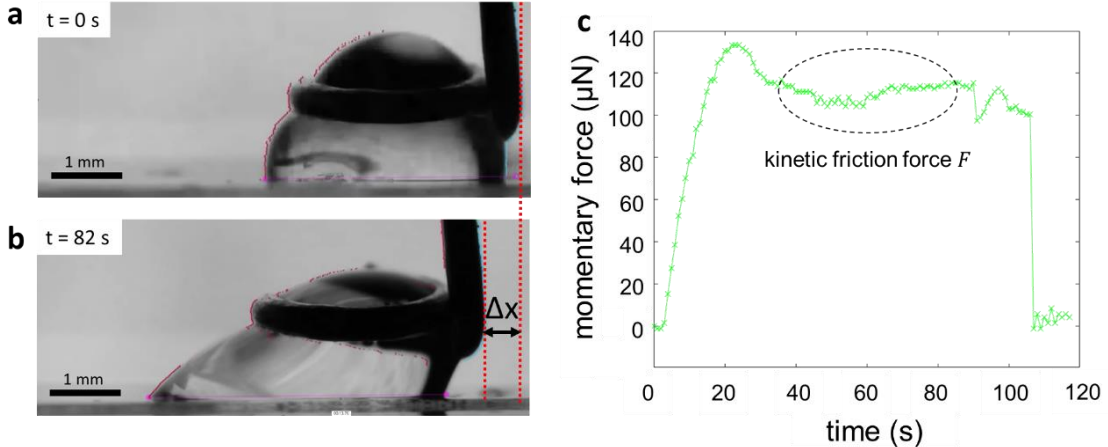


Figure 4.13. Force measurement by using a metal wire. The swollen PDMS substrate ( $Q = 14.5$ ) moves with a velocity of  $5 \mu\text{m/s}$ . The wire bends with a displacement  $\Delta x$  (b) from the original position (a) while the underneath substrate moves. (c) A plot of momentary friction force vs sliding time, the friction force is calculated with the equation  $F = k\Delta x$ .

Drop kinetic friction force is a function of sliding velocity. Generally, force increases with increasing sliding velocity, which is true for all samples with different degree of swelling (Figure 4.14). However, at a given velocity, samples with higher degree of swelling shows smaller friction than samples with lower degree of swelling. For example, when velocity is  $50 \mu\text{m/s}$ , a 60:1 sample with  $Q \sim 16$  shows a friction force around  $75 \mu\text{N}$ , while the 60:1 sample with  $Q \sim 7$  shows a larger force of  $100 \mu\text{N}$ . These results indicate a PDMS surface with a higher degree of swelling is more slippery (i.e., takes less force to slide). This is consistent with our previous results in Chapter 4, section 4.2, which shows the critical water drop volume required to slide on a swollen elastomer is

mainly controlled by the degree of swelling: Increasing the degree of swelling can dramatically decrease the water drop pinning force.

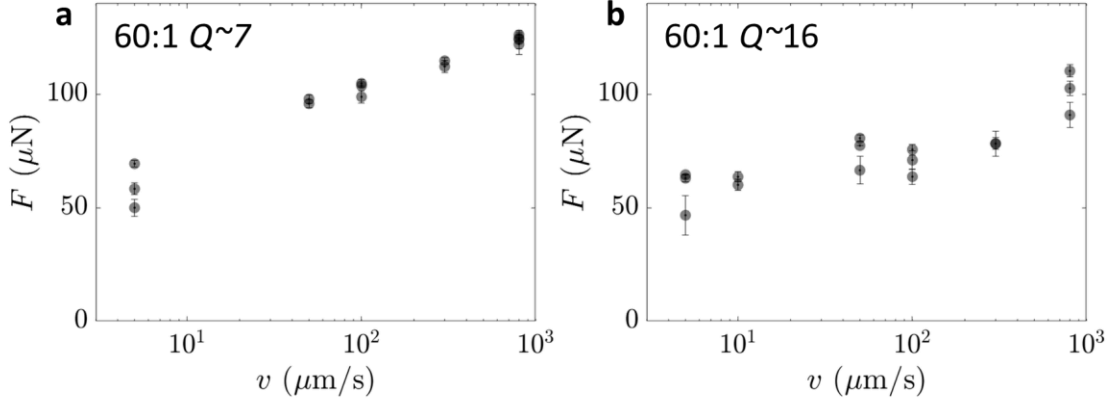


Figure 4.14. Kinetic friction force  $F$  as a function of sliding velocity  $v$  for swollen samples with degree of swelling  $Q$  of (a) 7 and (b) 16.

### 4.3.3 Fluid separation during sliding

A laser scanning confocal microscope is utilized to visualize the wetting ridge during drop sliding. As Figure 4.14a shows, the drop is positioned such that the advancing contact zone lies in the confocal microscope field of view. In steady-state motion, the wetting ridge assumes a near-constant shape at a stationary position within the field of view. We note that the dynamic wetting ridge shape does not depend on the dwell time of the drop prior to sliding. However on rare occasions, the ridge deviates from its stationary position due to contact line pinning, likely stemming from surface impurities or contamination<sup>122–124</sup>. Images are taken 1.6× per second, which enables resolving these

motions. This fast recording, however, brings higher signal noise with it - a drawback that we overcome by aligning each image by the tip of the ridge, followed by averaging. Extracting the interfaces of each phase reveals more quantifiable detail (Figure 4.15b).

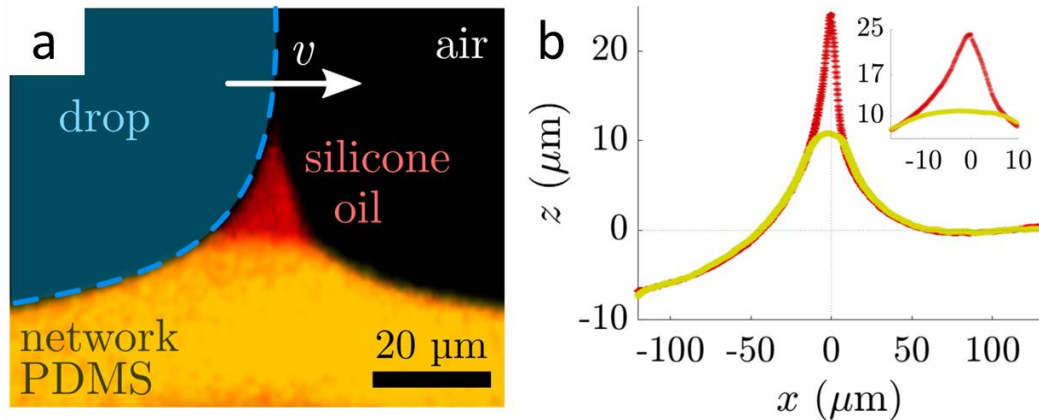


Figure 4.15. Wetting ridge visualization during drop sliding at  $5 \mu\text{m/s}$  on a swollen PDMS network ( $Q = 14.5$ ). Substrate moves left while the drop is stationary. (a) Temporal averaged ( $n = 158$ ) confocal microscopy image of a phase-separated wetting ridge. Red shows silicone oil and orange shows swollen PDMS network. (c) Extracted interfaces of silicone oil (red points) and PDMS network (yellow points). Inset, blown up section of the phase-separated zone in the wetting ridge. Standard errors are smaller than symbol size.

To investigate the sliding velocity on wetting ridges, we control the sliding speed and track the wetting ridge profile of both network and oil interfaces. The dynamic ridge profiles of silicone oil are shown in Figure 4.16a for  $Q = 16$  at various sliding speeds, together with the network profiles in the inset. The corresponding averaged confocal microscopy images at the slow and fast speeds are shown in the top row. The highest ridge ( $\approx 35 \mu\text{m}$ ) forms at low sliding speed (5  $\mu\text{m/s}$ , dark blue). Increasing  $v$  gradually

decreases the ridge height. The smallest recorded ridge is less than 20  $\mu\text{m}$  high at  $v = 800 \mu\text{m/s}$  (light yellow). This height-speed dependency is inverted for the network profile, i.e., the network rises with increasing speed. However, the sensitivity of the network height to  $v$  is not as pronounced as for the silicone oil tip height, Figure 4.16b. The max. oil height  $h_{oil,max}$  (red circles) decreases much steeper than the max. network height  $h_{net,max}$  (yellow circles) increases with faster speeds. For  $v > 100 \mu\text{m/s}$ , the height difference between  $h_{oil,max}$  and  $h_{net,max}$  is only 1 – 3  $\mu\text{m}$ . Additionally, the ridge becomes narrower with faster  $v$ . For substrates swollen to a lesser extent ( $Q = 14.5$ ), we observe smaller ridge heights ( $\approx 25 \mu\text{m}$  for  $v = 5 \mu\text{m/s}$ ) and narrower widths compared to the saturated ( $Q = 16$ ) substrate, Figure 4.16c-d. The less swollen substrate also has a less sensitive height-speed dependency. For  $v > 100 \mu\text{m/s}$ , the silicone oil does not clearly separate. When substrates are swollen even less to  $Q = 10$ , the ridges display no speed dependency and no visual phase separation; within experimental accuracy, all dynamic ridges collapse to the same shape, i.e.,  $h_{oil,max} \approx h_{net,max}$ , Figure 4.16e. The maximum ridge height reaches about 15  $\mu\text{m}$  for the entire speed spectrum. Thus, the drop sliding speed is a critical factor that governs phase separation in dynamic wetting.

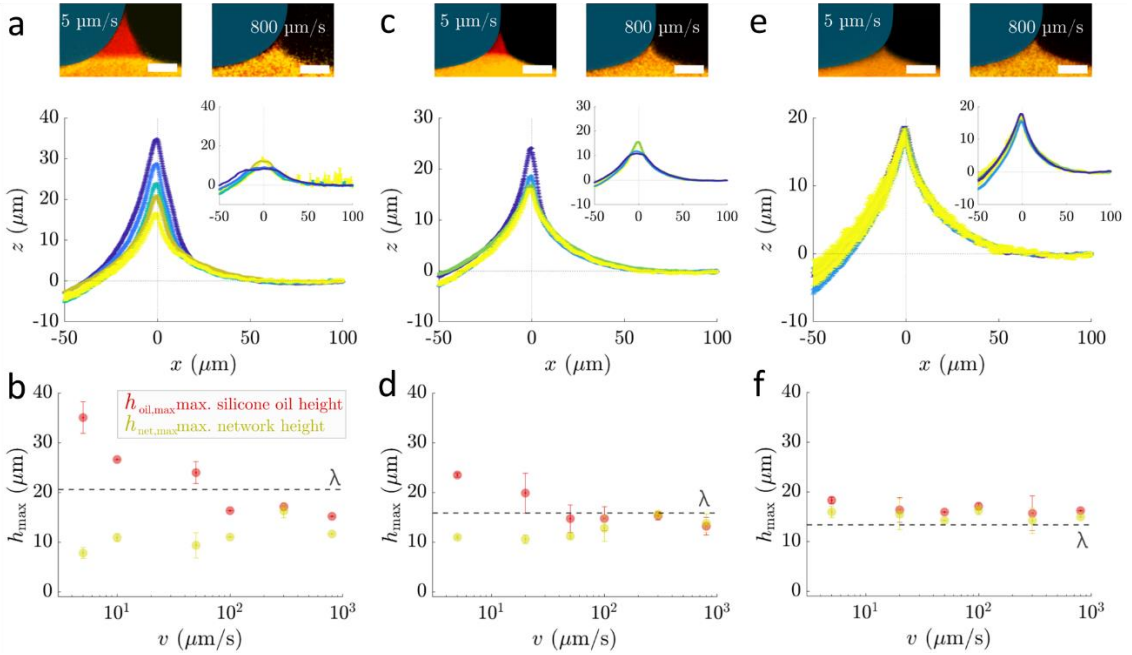


Figure 4.16. Dynamic wetting ridge shape for different sliding speeds and swelling ratios

(a), (b)  $Q = 16$ , (c), (d)  $Q = 14.5$ , (e), (f)  $Q = 10$ . (a), (c), (e) Dynamic ridge profiles of liquid silicone oil (and network PDMS as insets). (a), (c) For silicone oil, the ridge height gradually decreases for increasing drop speed,  $v = 5, 10, 50, 100, 300, 800 \mu\text{m/s}$ . Top row images are representative confocal microscopy images for  $v = 5 \mu\text{m/s}$  and  $v = 800 \mu\text{m/s}$  (scale bar 20  $\mu\text{m}$ ). (b), (d), (f) Maximum height of dynamic ridges of silicone oil (red) and network PDMS (yellow). Data shows average of min.  $n = 3$  repetitions together with standard deviations. Dashed lines mark dynamic elastocapillary height  $\lambda \sim \gamma \sin \theta_{adv}/E$ , which are (b) 21  $\mu\text{m}$  ( $E \approx 3 \text{ kPa}$ ) (d) 16  $\mu\text{m}$  ( $E \approx 3.9 \text{ kPa}$ ) (f) 13  $\mu\text{m}$  ( $E \approx 4.8 \text{ kPa}$ ).

#### 4.4 Summary and conclusion

In summary, we investigate the dynamic wetting behaviors on oil swollen PDMS elastomers. Firstly, we investigate the effects of the degree of crosslinking and the degree of swelling on water drop pinning/sliding for soft PDMS elastomers swollen with silicone oil. Our experiments reveal that the critical water drop volume required to slide on a swollen elastomer is mainly controlled by the degree of swelling: Increasing the degree of swelling can dramatically decrease the water drop pinning force. The degree of crosslinking does not strongly affect the critical drop volume when the PDMS base/crosslinker ratio is 40:1 or larger. Contact angle hysteresis decreases with increasing swelling, and is lowest when samples are saturated. Low contact angle hysteresis implies lower adhesion and a more slippery surface. Additionally, we show that highly swollen surfaces display a re-lubrication behavior after rinsing the surface with excess water. Highly swollen samples self-lubricate by generating extra oil on the surface over the course of days, leading to a decrease in the critical drop volume. This oil regeneration at the surface is consistent over multiple rinsing cycles. However, when the degree of swelling is lower, the oil leaching behavior does not occur; the oil remains inside the network rather than segregating to the network-air interface.

Secondly, we control the sliding velocity of a water drop and investigate the friction force of a single water drop, while observing the wetting ridge at the same time. We measure the kinetic friction force of a water drop sliding with a constant velocity on 60:1 swollen samples. Experimental results show that at the same sliding velocity, the friction force of the water drop on a sample with a higher degree of swelling is smaller than that on a

sample with a smaller degree of swelling, which indicates a surface with higher swelling is more slippery. Moreover, the sliding velocity can play an important role in the fluid separation at the three-phase contact line. For swollen samples, we showed in Chapter 3 that the fluid separation can be observed in static wetting; however we show here in Chapter 4 that the sliding of the water drop can suppress fluid separation. Results show that increasing sliding velocity can decrease the separation size  $\Delta h$ , and the fluid separation is fully suppressed ( $\Delta h \sim 0$ ) when the sliding speed is above a critical velocity. Overall, our study offers insight into the slippery properties of oil-swollen, low modulus silicone elastomers. Our findings on water drop pinning/sliding aims to offer guidelines on controlling drop dynamics and inform the design of the soft, water-repellent, surfaces. The majority of the work described in this Chapter has been published<sup>47,125</sup>.

## CHAPTER 5. CONCLUSION AND FUTURE WORK

### 5.1 Conclusions

In the dissertation, we have investigated both static wetting and dynamic wetting on oil-swollen, soft PDMS elastomers. We have seen that oil swollen into elastomers have a large contribution in surface properties, including slipperiness, pinning force, friction, and contact angles. In Chapter 2, we present a special sample preparation method to first extract uncrosslinked polymer chains and then reswelling with known silicone oil. We use rheology and a traditional goniometer to quantify the modulus for PDMS elastomers with: 1. different degrees of swelling from dry to saturated swelling and 2. various base/crosslinker mixing ratio from 30:1 to 60:1. We find that the modulus of elastomer is decreased by increasing the degree of swelling and base/crosslinker mixing ratio.

In Chapter 3, we have investigated static wetting on swollen elastomers, especially the fluid separation phenomenon when a water drop is placed on oil-swollen PDMS elastomers. By dying the PDMS network and oil separately and visualizing the microscale wetting ridge via confocal microscopy, we reveal that the static wetting ridge can comprise both a region of network pull-up and a region of pure fluid. The fluid separation size is mainly dependent on the degree of swelling. In general, the separation size increase with increasing the degree of swelling. The network wetting height increases initially with increasing the degree of swelling, but then decreases upon further swelling because more fluid separates from the network. We also show that fluid separation does not occur when the swelling fluid has a negative spreading parameter (i.e.,

hexadecane swollen PDMS elastomers). A model is developed that includes capillarity, osmotic pressure and elasticity that is able to capture the experimental results for the fluid separation size. Overall, the work in Chapter 3 offers fundamental insight into soft wetting, and provide in-depth information for drop dynamic wetting investigation in Chapter 4.

In Chapter 4, we expand the wetting investigation from static wetting cases to dynamic wetting cases by sliding water drops on the soft, swollen elastomers. At first, we investigate the effects of the degree of crosslinking and the degree of swelling on water drop pinning/sliding on vertical surfaces. The results reveals that the critical water drop volume required to slide on a swollen elastomer is mainly controlled by the degree of swelling. Additionally, an oil-leaching behavior is also observed after aging of high swollen samples over the course of days. The extra oil layer that leaches from the network can help to lubricate the surface, resulting a more slippery surface. Additionally, we introduce a unique approach that combines a customized force measurement with confocal microscopy; this allows us to experimentally measure the kinetic friction force of a single sliding water drop while simultaneously investigating the fluid separation as a function of sliding velocity. The measured friction force at a given sliding speed is smaller on a sample with higher degree of swelling compared to that on a sample with a smaller degree of swelling, suggesting that the amount of oil in bulk elastomer plays an important role on surface friction. Moreover, experimental results show the fluid separation size at water-elastomer contact zone is highly related to the drop sliding velocity. The fluid separation can be suppressed with a higher sliding speed. Our findings

on dynamic wetting aims to offer guidelines to inform the design the soft, water-repellent surfaces.

## 5.2 Future work

Our work on wetting of soft, swollen elastomers has demonstrated several unique methods and findings that may open the way for many future studies. In Chapter 3, we report a unique method to visualize the swollen liquid and network phases at the wetting ridge separately this may help provide foundational knowledge about separation for any two different phases on the microscale. However, the fluid separation studies in this dissertation are mainly based on oil swollen PDMS elastomers this is good material system to start, but is also a limitation. Although the hexadecane-swollen PDMS elastomer helps to reinforce the fluid separation model in Chapter 3, experiments with other material systems should be conducted to confirm the proposed model. Moreover, our static wetting studies are conducted with the assumption that the wetting ridge has reached an equilibrium state, which may need to be confirmed in the future. Meanwhile, it also brings out an interesting question of when the equilibrium state can be reached. .In particular, it would be interesting to consider how the material properties, such as the viscosity of the oil, the spreading coefficient, and the modulus can affect the time that is required to reach an equilibrium wetting state. Additionally, even though we do not observe an oil cloaking layer on the water drop in static wetting, this does not mean the oil will not cloak the drop after a long time (e.g. weeks or months); from the surface energy perspective, oil prefers to cover the water drop to minimize the total surface

energy. However, due to evaporation of water and the working distance limitations of confocal microscopy, we are not able to see the oil cloaking. Moreover, oil cloaking may be an important topic in the dynamic wetting investigation in Chapter4, since the oil can cloak the water drop easier when it is sliding. Future efforts may consider addressing the following questions: When does oil cloak? How does sliding velocity affect oil cloaking? How do material properties affect oil cloaking? What is the drop sliding behavior before and after oil cloaking? These would be beneficial scientific questions for the development of soft surfaces.

## REFERENCES

- (1) Barthlott, W.; Neinhuis, C. Purity of the Sacred Lotus, or Escape from Contamination in Biological Surfaces. *Planta* **1997**, *202* (1), 1–8. <https://doi.org/10.1007/s004250050096>.
- (2) Bocquet, L.; Lauga, E. A Smooth Future? *Nat. Mater.* **2011**, *10* (5), 334–337. <https://doi.org/10.1038/nmat2994>.
- (3) Nosonovsky, M. Slippery When Wetted. *Nature* **2011**, *477* (7365), 412–413. <https://doi.org/10.1038/477412a>.
- (4) Tuteja, A.; Choi, W.; Mabry, J. M.; McKinley, G. H.; Cohen, R. E. Robust Omniprophobic Surfaces. *Proc. Natl. Acad. Sci. U. S. A.* **2008**, *105* (47), 18200–18205. <https://doi.org/10.1073/pnas.0804872105>.
- (5) Pan, S.; Guo, R.; Björnalm, M.; Richardson, J. J.; Li, L.; Peng, C.; Bertleff-Zieschang, N.; Xu, W.; Jiang, J.; Caruso, F. Coatings Super-Repellent to Ultralow Surface Tension Liquids. *Nat. Mater.* **2018**, *17* (11), 1040–1047. <https://doi.org/10.1038/s41563-018-0178-2>.
- (6) Peng, J.; Zhao, X.; Wang, W.; Gong, X. Durable Self-Cleaning Surfaces with Superhydrophobic and Highly Oleophobic Properties. *Langmuir* **2019**. <https://doi.org/10.1021/acs.langmuir.9b01507>.
- (7) Liu, M.; Wang, Z.; Liu, P.; Wang, Z.; Yao, H.; Yao, X. Supramolecular Silicone Coating Capable of Strong Substrate Bonding, Readily Damage Healing, and Easy Oil Sliding. *Sci. Adv.* **2019**, *5* (11), 1–9. <https://doi.org/10.1126/sciadv.aaw5643>.
- (8) Pham, Q. N.; Zhang, S.; Montazeri, K.; Won, Y. Droplets on Slippery Lubricant-Infused Porous Surfaces: A Macroscale to Nanoscale Perspective. *Langmuir* **2018**, *34* (47), 14439–14447. <https://doi.org/10.1021/acs.langmuir.8b02765>.
- (9) Wong, T. S.; Kang, S. H.; Tang, S. K. Y.; Smythe, E. J.; Hatton, B. D.; Grinthal, A.; Aizenberg, J. Bioinspired Self-Repairing Slippery Surfaces with Pressure-Stable Omniprophobicity. *Nature* **2011**, *477* (7365), 443–447. <https://doi.org/10.1038/nature10447>.
- (10) Wang, Z.; Heng, L.; Jiang, L. Effect of Lubricant Viscosity on the Self-Healing Properties and Electrically Driven Sliding of Droplets on Anisotropic Slippery Surfaces. *J. Mater. Chem. A* **2018**, *6* (8), 3414–3421. <https://doi.org/10.1039/c7ta10439a>.

- (11) Hou, X.; Hu, Y.; Grinthal, A.; Khan, M.; Aizenberg, J. Liquid-Based Gating Mechanism with Tunable Multiphase Selectivity and Antifouling Behaviour. *Nature* **2015**, *519* (7541), 70–73. <https://doi.org/10.1038/nature14253>.
- (12) Epstein, A. K.; Wong, T. S.; Belisle, R. A.; Boggs, E. M.; Aizenberg, J. Liquid-Infused Structured Surfaces with Exceptional Anti-Biofouling Performance. *Proc. Natl. Acad. Sci. U. S. A.* **2012**, *109* (33), 13182–13187. <https://doi.org/10.1073/pnas.1201973109>.
- (13) Wang, N.; Xiong, D.; Pan, S.; Wang, K.; Shi, Y.; Deng, Y. Robust Superhydrophobic Coating and the Anti-Icing Properties of Its Lubricants-Infused-Composite Surface under Condensing Condition. *New J. Chem.* **2017**, *41* (4), 1846–1853. <https://doi.org/10.1039/c6nj02824a>.
- (14) Wilson, P. W.; Lu, W.; Xu, H.; Kim, P.; Kreder, M. J.; Alvarenga, J.; Aizenberg, J. Inhibition of Ice Nucleation by Slippery Liquid-Infused Porous Surfaces (SLIPS). *Phys. Chem. Chem. Phys.* **2013**, *15* (2), 581–585. <https://doi.org/10.1039/c2cp43586a>.
- (15) Anand, S.; Paxson, A. T.; Dhiman, R.; Smith, J. D.; Varanasi, K. K. Enhanced Condensation on Lubricant-Impregnated Nanotextured Surfaces. *ACS Nano* **2012**, *6* (11), 10122–10129. <https://doi.org/10.1021/nn303867y>.
- (16) Yao, X.; Hu, Y.; Grinthal, A.; Wong, T. S.; Mahadevan, L.; Aizenberg, J. Adaptive Fluid-Infused Porous Films with Tunable Transparency and Wettability. *Nat. Mater.* **2013**, *12* (6), 529–534. <https://doi.org/10.1038/nmat3598>.
- (17) Baumli, P.; D'Acunzi, M.; Hegner, K. I.; Naga, A.; Wong, W. S. Y.; Butt, H.-J.; Vollmer, D. The Challenge of Lubricant-Replenishment on Lubricant-Impregnated Surfaces. *Adv. Colloid Interface Sci.* **2021**, *287*, 102329. <https://doi.org/10.1016/j.cis.2020.102329>.
- (18) Smith, J. D.; Dhiman, R.; Anand, S.; Reza-Garduno, E.; Cohen, R. E.; McKinley, G. H.; Varanasi, K. K. Droplet Mobility on Lubricant-Impregnated Surfaces. *Soft Matter* **2013**, *9* (6), 1772–1780. <https://doi.org/10.1039/c2sm27032c>.
- (19) Cao, M.; Guo, D.; Yu, C.; Li, K.; Liu, M.; Jiang, L. Water-Repellent Properties of Superhydrophobic and Lubricant-Infused “Slippery” Surfaces: A Brief Study on the Functions and Applications. *ACS Appl. Mater. Interfaces* **2016**, *8* (6), 3615–3623. <https://doi.org/10.1021/acsami.5b07881>.
- (20) Chen, X.; Wen, G.; Guo, Z. What Are the Design Principles, from the Choice of Lubricants and Structures to the Preparation Method, for a Stable Slippery Lubricant-Infused Porous Surface? *Mater. Horizons* **2020**, *7* (7), 1697–1726. <https://doi.org/10.1039/d0mh00088d>.
- (21) Kreder, M. J.; Daniel, D.; Tetreault, A.; Cao, Z.; Lemaire, B.; Timonen, J. V. I.; Aizenberg, J. Film Dynamics and Lubricant Depletion by Droplets Moving on

- Lubricated Surfaces. *Phys. Rev. X* **2018**, *8* (3), 31053. <https://doi.org/10.1103/PhysRevX.8.031053>.
- (22) Butt, H. J.; Pham, J. T.; Kappl, M. Forces between a Stiff and a Soft Surface. *Curr. Opin. Colloid Interface Sci.* **2017**, *27*, 82–90. <https://doi.org/10.1016/j.cocis.2016.09.007>.
- (23) Style, R. W.; Wettnaufer, J. S.; Dufresne, E. R. Surface Tension and the Mechanics of Liquid Inclusions in Compliant Solids. *Soft Matter* **2015**, *11* (4), 672–679. <https://doi.org/10.1039/c4sm02413c>.
- (24) Style, R. W.; Hyland, C.; Boltyanskiy, R.; Wettnaufer, J. S.; Dufresne, E. R. Surface Tension and Contact with Soft Elastic Solids. *Nat. Commun.* **2013**, *4* (1), 2728. <https://doi.org/10.1038/ncomms3728>.
- (25) Pham, J. T.; Schellenberger, F.; Kappl, M.; Butt, H.-J. From Elasticity to Capillarity in Soft Materials Indentation. *Phys. Rev. Mater.* **2017**, *1* (1), 015602. <https://doi.org/10.1103/PhysRevMaterials.1.015602>.
- (26) Karpitschka, S.; Das, S.; van Gorcum, M.; Perrin, H.; Andreotti, B.; Snoeijer, J. H. Droplets Move over Viscoelastic Substrates by Surfing a Ridge. *Nat. Commun.* **2015**, *6* (1), 7891. <https://doi.org/10.1038/ncomms8891>.
- (27) Müller, P.; Saúl, A. Elastic Effects on Surface Physics. *Surf. Sci. Rep.* **2004**, *54* (5–8), 157–258. <https://doi.org/10.1016/j.surfrep.2004.05.001>.
- (28) Masurel, R.; Roché, M.; Limat, L.; Ionescu, I.; Dervaux, J. Elastocapillary Ridge as a Noninteger Disclination. *Phys. Rev. Lett.* **2019**, *122* (24), 1–6. <https://doi.org/10.1103/PhysRevLett.122.248004>.
- (29) Liang, H.; Cao, Z.; Wang, Z.; Dobrynin, A. V. Surface Stresses and a Force Balance at a Contact Line. *Langmuir* **2018**, *34* (25), 7497–7502. <https://doi.org/10.1021/acs.langmuir.8b01680>.
- (30) Shuttleworth, R. The Surface Tension of Solids. *Proc. Phys. Soc. Sect. A* **1950**, *63* (5), 444.
- (31) Style, R. W.; Boltyanskiy, R.; Che, Y.; Wettnaufer, J. S.; Wilen, L. A.; Dufresne, E. R. Universal Deformation of Soft Substrates near a Contact Line and the Direct Measurement of Solid Surface Stresses. *Phys. Rev. Lett.* **2013**, *110* (6), 066103. <https://doi.org/10.1103/PhysRevLett.110.066103>.
- (32) Park, S. J.; Weon, B. M.; Lee, J. S.; Lee, J.; Kim, J.; Je, J. H. Visualization of Asymmetric Wetting Ridges on Soft Solids with X-Ray Microscopy. *Nat. Commun.* **2014**, *5* (1), 4369. <https://doi.org/10.1038/ncomms5369>.
- (33) Urata, C.; Dunderdale, G. J.; England, M. W.; Hozumi, A. Self-Lubricating Organogels (SLUGs) with Exceptional Syneresis-Induced Anti-Sticking Properties

- against Viscous Emulsions and Ices. *J. Mater. Chem. A* **2015**, *3* (24), 12626–12630. <https://doi.org/10.1039/c5ta02690c>.
- (34) Yeong, Y. H.; Wang, C.; Wynne, K. J.; Gupta, M. C. Oil-Infused Superhydrophobic Silicone Material for Low Ice Adhesion with Long-Term Infusion Stability. *ACS Appl. Mater. Interfaces* **2016**, *8* (46), 32050–32059. <https://doi.org/10.1021/acsami.6b11184>.
- (35) Jensen, K. E.; Sarfati, R.; Style, R. W.; Boltyanskiy, R.; Chakrabarti, A.; Chaudhury, M. K.; Dufresne, E. R. Wetting and Phase Separation in Soft Adhesion. *Proc. Natl. Acad. Sci. U. S. A.* **2015**, *112* (47), 14490–14494. <https://doi.org/10.1073/pnas.1514378112>.
- (36) Karpitschka, S.; Pandey, A.; Lubbers, L. A.; Weijts, J. H.; Botto, L.; Das, S.; Andreotti, B.; Snoeijer, J. H. Liquid Drops Attract or Repel by the Inverted Cheerios Effect. *Proc. Natl. Acad. Sci. U. S. A.* **2016**, *113* (27), 7403–7407. <https://doi.org/10.1073/pnas.1601411113>.
- (37) Roy, R.; Seiler, R. L.; Weibel, J. A.; Garimella, S. V. Droplets on Soft Surfaces Exhibit a Reluctance to Coalesce Due to an Intervening Wetting Ridge. *Adv. Mater. Interfaces* **2020**, 2000731.
- (38) Gerber, J.; Lendenmann, T.; Eghlidi, H.; Schutzius, T. M.; Poulikakos, D. Wetting Transitions in Droplet Drying on Soft Materials. *Nat. Commun.* **2019**, *10* (1), 4776. <https://doi.org/10.1038/s41467-019-12093-w>.
- (39) Cao, Z.; Dobrynin, A. V. Polymeric Droplets on Soft Surfaces: From Neumann's Triangle to Young's Law. *Macromolecules* **2015**, *48* (2), 443–451. <https://doi.org/10.1021/ma501672p>.
- (40) Style, R. W.; Che, Y.; Park, S. J.; Weon, B. M.; Je, J. H.; Hyland, C.; German, G. K.; Power, M. P.; Wilen, L. A.; Wettlaufer, J. S.; Dufresne, E. R. Patterning Droplets with Durotaxis. *Proc. Natl. Acad. Sci. U. S. A.* **2013**, *110* (31), 12541–12544. <https://doi.org/10.1073/pnas.1307122110>.
- (41) Nandi, S.; Winter, H. H. Swelling Behavior of Partially Cross-Linked Polymers: A Ternary System. *Macromolecules* **2005**, *38* (10), 4447–4455. <https://doi.org/10.1021/ma048335e>.
- (42) Hourlier-Fargette, A.; Antkowiak, A.; Chateauminois, A.; Neukirch, S. Role of Uncrosslinked Chains in Droplets Dynamics on Silicone Elastomers. *Soft Matter* **2017**, *13* (19), 3484–3491. <https://doi.org/10.1039/c7sm00447h>.
- (43) Xu, Q.; Wilen, L. A.; Jensen, K. E.; Style, R. W.; Dufresne, E. R. Viscoelastic and Poroelastic Relaxations of Soft Solid Surfaces. *arXiv* **2020**, 2006.09767.

- (44) Zhao, M.; Lequeux, F.; Narita, T.; Roché, M.; Limat, L.; Dervaux, J. Growth and Relaxation of a Ridge on a Soft Poroelastic Substrate. *Soft Matter* **2017**, *14* (1), 61–72. <https://doi.org/10.1039/c7sm01757j>.
- (45) Glover, J. D.; Pham, J. T. Capillary-Driven Indentation of a Microparticle into a Soft, Oil-Coated Substrate. *Soft Matter* **2020**, *16* (25), 5812–5818. <https://doi.org/10.1039/d0sm00296h>.
- (46) Xue, L.; Pham, J. T.; Iturri, J.; Del Campo, A. Stick-Slip Friction of PDMS Surfaces for Bioinspired Adhesives. *Langmuir* **2016**, *32* (10), 2428–2435. <https://doi.org/10.1021/acs.langmuir.6b00513>.
- (47) Cai, Z.; Pham, J. T. How Swelling, Cross-Linking, and Aging Affect Drop Pinning on Lubricant-Infused, Low Modulus Elastomers. *ACS Appl. Polym. Mater.* **2021**. <https://doi.org/10.1021/acsapm.1c01455>.
- (48) Wong, W. S. Y.; Hauer, L.; Naga, A.; Kaltbeitzel, A.; Baumli, P.; Berger, R.; D'Acunzi, M.; Vollmer, D.; Butt, H.-J. Adaptive Wetting of Polydimethylsiloxane. *Langmuir* **2020**, *36* (26), 7236–7245. <https://doi.org/10.1021/acs.langmuir.0c00538>.
- (49) Chen, Y.; Askounis, A.; Koutsos, V.; Valluri, P.; Takata, Y.; Wilson, S. K.; Sefiane, K. On the Effect of Substrate Viscoelasticity on the Evaporation Kinetics and Deposition Patterns of Nanosuspension Drops. *Langmuir* **2020**, *36* (1), 204–213. <https://doi.org/10.1021/acs.langmuir.9b02965>.
- (50) Liu, Q.; Suo, Z. Osmocapillary Phase Separation. *Extrem. Mech. Lett.* **2016**, *7*, 27–33. <https://doi.org/10.1016/j.eml.2016.02.001>.
- (51) Pezzulla, M.; Shillig, S. A.; Nardinocchi, P.; Holmes, D. P. Morphing of Geometric Composites via Residual Swelling. *Soft Matter* **2015**, *11* (29), 5812–5820. <https://doi.org/10.1039/c5sm00863h>.
- (52) Hourlier-Fargette, A.; Dervaux, J.; Antkowiak, A.; Neukirch, S. Extraction of Silicone Uncrosslinked Chains at Air-Water-Polydimethylsiloxane Triple Lines. *Langmuir* **2018**, *34* (41), 12244–12250. <https://doi.org/10.1021/acs.langmuir.8b02128>.
- (53) Lee, J. N.; Park, C.; Whitesides, G. M. Solvent Compatibility of Poly(Dimethylsiloxane)-Based Microfluidic Devices. *Anal. Chem.* **2003**, *75* (23), 6544–6554. <https://doi.org/10.1021/ac0346712>.
- (54) Glover, J. D.; McLaughlin, C. E.; McFarland, M. K.; Pham, J. T. Extracting Uncrosslinked Material from Low Modulus Sylgard 184 and the Effect on Mechanical Properties. *J. Polym. Sci.* **2020**, *58* (2), 343–351. <https://doi.org/10.1002/pol.20190032>.

- (55) Young, R. J.; Lovell, P. A. *Introduction to Polymers*, 3rd editio.; CRC Press, 2011. <https://doi.org/10.1201/9781439894156>.
- (56) Rubinstein, M.; Colby, R. H. *Polymer Physics*; 2003.
- (57) Du, P.; Lin, I. K.; Lu, H.; Zhang, X. Extension of the Beam Theory for Polymer Bio-Transducers with Low Aspect Ratios and Viscoelastic Characteristics. *J. Micromechanics Microengineering* **2010**, *20* (9). <https://doi.org/10.1088/0960-1317/20/9/095016>.
- (58) Wang, B.; Krause, S. Properties of Dimethylsiloxane Microphases in Phase-Separated Dimethylsiloxane Block Copolymers. *Macromolecules* **1987**, *20* (9), 2201–2208. <https://doi.org/10.1021/ma00175a026>.
- (59) Pritchard, R. H.; Lava, P.; Debruyne, D.; Terentjev, E. M. Precise Determination of the Poisson Ratio in Soft Materials with 2D Digital Image Correlation. *Soft Matter* **2013**, *9* (26), 6037–6045.
- (60) Neumann, A. W.; Good, R. J.; Hope, C. J.; Sejpal, M. An Equation-of-State Approach to Determine Surface Tensions of Low-Energy Solids from Contact Angles. *J. Colloid Interface Sci.* **1974**, *49* (2), 291–304. [https://doi.org/10.1016/0021-9797\(74\)90365-8](https://doi.org/10.1016/0021-9797(74)90365-8).
- (61) Butt, H.; Graf, K.; Kappl, M. *Physics and Chemistry of Interfaces*, 3rd editio.; Wiley-VCH, 2013.
- (62) Schellenberger, F.; Xie, J.; Encinas, N.; Hardy, A.; Klapper, M.; Papadopoulos, P.; Butt, H. J.; Vollmer, D. Direct Observation of Drops on Slippery Lubricant-Infused Surfaces. *Soft Matter* **2015**, *11* (38), 7617–7626. <https://doi.org/10.1039/c5sm01809a>.
- (63) Daniel, D.; Timonen, J. V. I.; Li, R.; Velling, S. J.; Kreder, M. J.; Tetreault, A.; Aizenberg, J. Origins of Extreme Liquid Repellency on Structured, Flat, and Lubricated Hydrophobic Surfaces. *Phys. Rev. Lett.* **2018**, *120* (24), 244503. <https://doi.org/10.1103/PhysRevLett.120.244503>.
- (64) Wang, J.; Wang, L.; Sun, N.; Tierney, R.; Li, H.; Corsetti, M.; Williams, L.; Wong, P. K.; Wong, T. S. Viscoelastic Solid-Repellent Coatings for Extreme Water Saving and Global Sanitation. *Nat. Sustain.* **2019**, *2* (12), 1097–1105. <https://doi.org/10.1038/s41893-019-0421-0>.
- (65) Keiser, A.; Keiser, L.; Clanet, C.; Quéré, D. Drop Friction on Liquid-Infused Materials. *Soft Matter* **2017**, *13* (39), 6981–6987. <https://doi.org/10.1039/c7sm01226h>.
- (66) Mukherjee, R.; Habibi, M.; Rashed, Z. T.; Berbert, O.; Shi, X.; Boreyko, J. B. Oil-Impregnated Hydrocarbon-Based Polymer Films. *Sci. Rep.* **2018**, *8* (1), 11698. <https://doi.org/10.1038/s41598-018-29823-7>.

- (67) Cui, J.; Daniel, D.; Grinthal, A.; Lin, K.; Aizenberg, J. Dynamic Polymer Systems with Self-Regulated Secretion for the Control of Surface Properties and Material Healing. *Nat. Mater.* **2015**, *14* (8), 790–795. <https://doi.org/10.1038/nmat4325>.
- (68) Zheng, W.; Zhang, W.; Jiang, X. Precise Control of Cell Adhesion by Combination of Surface Chemistry and Soft Lithography. *Adv. Healthc. Mater.* **2013**, *2* (1), 95–108. <https://doi.org/10.1002/adhm.201200104>.
- (69) Sotiri, I.; Tajik, A.; Lai, Y.; Zhang, C. T.; Kovalenko, Y.; Nemr, C. R.; Ledoux, H.; Alvarenga, J.; Johnson, E.; Patanwala, H. S.; Timonen, J. V. I.; Hu, Y.; Aizenberg, J.; Howell, C. Tunability of Liquid-Infused Silicone Materials for Biointerfaces. *Biointerphases* **2018**, *13* (6), 06D401. <https://doi.org/10.1116/1.5039514>.
- (70) Van Gorcum, M.; Andreotti, B.; Snoeijer, J. H.; Karpitschka, S. Dynamic Solid Surface Tension Causes Droplet Pinning and Depinning. *Phys. Rev. Lett.* **2018**, *121* (20), 208003. <https://doi.org/10.1103/PhysRevLett.121.208003>.
- (71) Zhao, M.; Dervaux, J.; Narita, T.; Lequeux, F.; Limat, L.; Roché, M. Geometrical Control of Dissipation during the Spreading of Liquids on Soft Solids. *Proc. Natl. Acad. Sci. U. S. A.* **2018**, *115* (8), 1748–1753. <https://doi.org/10.1073/pnas.1712562115>.
- (72) Clough, J. M.; Creton, C.; Craig, S. L.; Sijbesma, R. P. Covalent Bond Scission in the Mullins Effect of a Filled Elastomer: Real-Time Visualization with Mechanoluminescence. *Adv. Funct. Mater.* **2016**, *26* (48), 9063–9074. <https://doi.org/10.1002/adfm.201602490>.
- (73) Rubinstein, M.; Colby, R. H. M\_Rubinstein,\_Ralph\_H\_Colby,\_Polymer.Pdf. 2003.
- (74) Jerison, E. R.; Xu, Y.; Wilen, L. A.; Dufresne, E. R. Deformation of an Elastic Substrate by a Three-Phase Contact Line. *Phys. Rev. Lett.* **2011**, *106* (18), 186103. <https://doi.org/10.1103/PhysRevLett.106.186103>.
- (75) Marchand, A.; Das, S.; Snoeijer, J. H.; Andreotti, B. Contact Angles on a Soft Solid: From Young's Law to Neumann's Law. *Phys. Rev. Lett.* **2012**, *109* (23), 1–5. <https://doi.org/10.1103/PhysRevLett.109.236101>.
- (76) Preston, D. J.; Song, Y.; Lu, Z.; Antao, D. S.; Wang, E. N. Design of Lubricant Infused Surfaces. *ACS Appl. Mater. Interfaces* **2017**, *9* (48), 42383–42392. <https://doi.org/10.1021/acsami.7b14311>.
- (77) Sett, S.; Yan, X.; Barac, G.; Bolton, L. W.; Miljkovic, N. Lubricant-Infused Surfaces for Low-Surface-Tension Fluids: Promise versus Reality. *ACS Appl. Mater. Interfaces* **2017**, *9* (41), 36400–36408. <https://doi.org/10.1021/acsami.7b10756>.

- (78) Banpurkar, A. G.; Nichols, K. P.; Mugele, F. Electrowetting-Based Microdrop Tensiometer. *Langmuir* **2008**, *24* (19), 10549–10551. <https://doi.org/10.1021/la801549p>.
- (79) Mchale, G.; Orme, B. V; Wells, G. G.; Ledesma-aguilar, R. Apparent Contact Angles on Lubricant-Impregnated Surfaces / SLIPS : From Superhydrophobicity to Electrowetting. *Langmuir* **2019**, *35* (11), 4197–4204. <https://doi.org/10.1021/acs.langmuir.8b04136>.
- (80) Xu, Q.; Wilen, L. A.; Jensen, K. E.; Style, R. W.; Dufresne, E. R. Viscoelastic and Poroelastic Relaxations of Soft Solid Surfaces. *Phys. Rev. Lett.* **2020**, *125* (23), 238002. <https://doi.org/10.1103/PhysRevLett.125.238002>.
- (81) Paul C, H.; Timothy P, L. *Polymer Chemistry*, Second.; CRC Press, 2007.
- (82) Marzocca, A. J. Evaluation of the Polymer-Solvent Interaction Parameter  $\chi$  for the System Cured Styrene Butadiene Rubber and Toluene. *Eur. Polym. J.* **2007**, *43* (6), 2682–2689. <https://doi.org/10.1016/j.eurpolymj.2007.02.034>.
- (83) Horta, A.; Pastoriza, M. A. The Interaction Parameter of Crosslinked Networks and Star Polymers. *Eur. Polym. J.* **2005**, *41* (12), 2793–2802.
- (84) Milner, S. T.; Lacasse, M. D.; Graessley, W. W. Why  $\chi$  Is Seldom Zero for Polymer - Solvent Mixtures. *Macromolecules* **2009**, *42* (3), 876–886. <https://doi.org/10.1021/ma801091b>.
- (85) Rubinstein, M.; Ralph H, C. *Polymer Physics*; OUP Oxford, 2003.
- (86) Gilra, N.; Cohen, C.; Briber, R. M.; Bauer, B. J.; Hedden, R. C.; Panagiotopoulos, A. Z. A SANS Study of the Conformational Behaviour of Linear Chains in Compressed and Uncompressed End-Linked Elastomers. *Macromolecules* **2001**, *34* (22), 7773–7782. <https://doi.org/10.1021/ma010018+>.
- (87) Li, G.; Prasad, S.; Dhinojwala, A. Dynamic Interfacial Tension at the Oil / Surfactant - Water Interface. *Langmuir* **2007**, *23* (20), 9929–9932. <https://doi.org/10.1021/la7014463>.
- (88) Pu, G.; Severtson, S. J. Dependence of Wetting Behavior on the Thickness of Highly Viscoelastic Films. *J. Phys. Chem. C* **2011**, *115* (38), 18729–18735. <https://doi.org/10.1021/jp205662v>.
- (89) Bostwick, J. B.; Shearer, M.; Daniels, K. E. Elastocapillary Deformations on Partially-Wetting Substrates: Rival Contact-Line Models. *Soft Matter* **2014**, *10* (37), 7361–7369. <https://doi.org/10.1039/c4sm00891j>.
- (90) Carré, A.; Gastel, J.-C.; Shanahan, M. E. R. Viscoelastic Effects in the Spreading of Liquids. *Nature* **1996**, *379* (6564), 432–434. <https://doi.org/10.1038/379432a0>.

- (91) Berman, J. D.; Randeria, M.; Style, R. W.; Xu, Q.; Nichols, J. R.; Duncan, A. J.; Loewenberg, M.; Dufresne, E. R.; Jensen, K. E. Singular Dynamics in the Failure of Soft Adhesive Contacts. *Soft Matter* **2019**, *15* (6), 1327–1334. <https://doi.org/10.1039/c8sm02075b>.
- (92) Chakrabarti, A.; Porat, A.; Raphaël, E.; Salez, T.; Chaudhury, M. K. Elastowetting of Soft Hydrogel Spheres. *Langmuir* **2018**, *34* (13), 3894–3900. <https://doi.org/10.1021/acs.langmuir.8b00368>.
- (93) Pham, J. T.; Paven, M.; Wooh, S.; Kajiya, T.; Butt, H. J.; Vollmer, D. Spontaneous Jumping, Bouncing and Trampolining of Hydrogel Drops on a Heated Plate. *Nat. Commun.* **2017**, *8* (1), 905. <https://doi.org/10.1038/s41467-017-01010-8>.
- (94) Golovin, K.; Tuteja, A. A Predictive Framework for the Design and Fabrication of Icephobic Polymers. *Sci. Adv.* **2017**, *3* (9), e1701617. <https://doi.org/10.1126/sciadv.1701617>.
- (95) Cai, Z.; Skabev, A.; Morozova, S.; Pham, J. T. Fluid Separation and Network Deformation in Wetting of Soft and Swollen Surfaces. *Commun. Mater.* **2021**, *2* (1), 21. <https://doi.org/10.1038/s43246-021-00125-2>.
- (96) Lavielle, N.; Asker, D.; Hatton, B. D. Lubrication Dynamics of Swollen Silicones to Limit Long Term Fouling and Microbial Biofilms. *Soft Matter* **2021**, *17* (4), 936–946. <https://doi.org/10.1039/d0sm01039a>.
- (97) Chuah, Y. J.; Koh, Y. T.; Lim, K.; Menon, N. V.; Wu, Y.; Kang, Y. Simple Surface Engineering of Polydimethylsiloxane with Polydopamine for Stabilized Mesenchymal Stem Cell Adhesion and Multipotency. *Sci. Rep.* **2016**, *5* (1), 18162. <https://doi.org/10.1038/srep18162>.
- (98) Tibbitt, M. W.; Anseth, K. S. Hydrogels as Extracellular Matrix Mimics for 3D Cell Culture. *Biotechnol. Bioeng.* **2009**, *103* (4), 655–663. <https://doi.org/10.1002/bit.22361>.
- (99) Kotikian, A.; McMahan, C.; Davidson, E. C.; Muhammad, J. M.; Weeks, R. D.; Daraio, C.; Lewis, J. A. Untethered Soft Robotic Matter with Passive Control of Shape Morphing and Propulsion. *Sci. Robot.* **2019**, *4* (33), 86–1226. <https://doi.org/10.1126/scirobotics.aax7044>.
- (100) Cao, Y.; Tan, Y. J.; Li, S.; Lee, W. W.; Guo, H.; Cai, Y.; Wang, C.; Tee, B. C.-K. Self-Healing Electronic Skins for Aquatic Environments. *Nat. Electron.* **2019**, *2* (2), 75–82. <https://doi.org/10.1038/s41928-019-0206-5>.
- (101) Byun, J.; Lee, Y.; Yoon, J.; Lee, B.; Oh, E.; Chung, S.; Lee, T.; Cho, K.-J.; Kim, J.; Hong, Y. Electronic Skins for Soft, Compact, Reversible Assembly of Wirelessly Activated Fully Soft Robots. *Sci. Robot.* **2018**, *3* (18). <https://doi.org/10.1126/scirobotics.aas9020>.

- (102) Hönes, R.; Lee, Y.; Urata, C.; Lee, H.; Hozumi, A. Antiadhesive Properties of Oil-Infused Gels against the Universal Adhesiveness of Polydopamine. *Langmuir* **2020**, *36* (16), 4496–4502. <https://doi.org/10.1021/acs.langmuir.0c00062>.
- (103) Urata, C.; Nagashima, H.; Hatton, B. D.; Hozumi, A. Transparent Organogel Films Showing Extremely Efficient and Durable Anti-Icing Performance. *ACS Appl. Mater. Interfaces* **2021**, *13* (24), 28925–28937. <https://doi.org/10.1021/acsami.1c06815>.
- (104) Zhang, P.; Zhao, C.; Zhao, T.; Liu, M.; Jiang, L. Recent Advances in Bioinspired Gel Surfaces with Superwettability and Special Adhesion. *Adv. Sci.* **2019**, *6* (18), 1900996. <https://doi.org/10.1002/advs.201900996>.
- (105) Peppou-Chapman, S.; Hong, J. K.; Waterhouse, A.; Neto, C. Life and Death of Liquid-Infused Surfaces: A Review on the Choice, Analysis and Fate of the Infused Liquid Layer. *Chem. Soc. Rev.* **2020**, *49* (11), 3688–3715. <https://doi.org/10.1039/d0cs00036a>.
- (106) Style, R. W.; Dufresne, E. R. Static Wetting on Deformable Substrates, from Liquids to Soft Solids. *Soft Matter* **2012**, *8* (27), 7177–7184. <https://doi.org/10.1039/c2sm25540e>.
- (107) Yao, X.; Dunn, S. S.; Kim, P.; Duffy, M.; Alvarenga, J.; Aizenberg, J. Fluorogel Elastomers with Tunable Transparency, Elasticity, Shape-Memory, and Antifouling Properties. *Angew. Chemie - Int. Ed.* **2014**, *53* (17), 4418–4422. <https://doi.org/10.1002/anie.201310385>.
- (108) Dussan V., E. B. On the Ability of Drops or Bubbles to Stick to Non-Horizontal Surfaces of Solids. Part 2. Small Drops or Bubbles Having Contact Angles of Arbitrary Size. *J. Fluid Mech.* **1985**, *151*, 1–20. <https://doi.org/10.1017/S0022112085000842>.
- (109) Exstrand, C. W.; Kumagai, Y. Liquid Drops on an Inclined Plane: The Relation between Contact Angles, Drop Shape, and Retentive Force. *J. Colloid Interface Sci.* **1995**, *170* (2), 515–521. <https://doi.org/10.1006/jcis.1995.1130>.
- (110) Sedev, R. V.; Petrov, J. G.; Neumann, A. W. Effect of Swelling of a Polymer Surface on Advancing and Receding Contact Angles. *J. Colloid Interface Sci.* **1996**, *180* (1), 36–42. <https://doi.org/10.1006/jcis.1996.0271>.
- (111) ElSherbini, A. I.; Jacobi, A. M. Retention Forces and Contact Angles for Critical Liquid Drops on Non-Horizontal Surfaces. *J. Colloid Interface Sci.* **2006**, *299* (2), 841–849. <https://doi.org/10.1016/j.jcis.2006.02.018>.
- (112) ElSherbini, A. I.; Jacobi, A. M. Liquid Drops on Vertical and Inclined Surfaces: I. An Experimental Study of Drop Geometry. *J. Colloid Interface Sci.* **2004**, *273* (2), 556–565. <https://doi.org/10.1016/j.jcis.2003.12.067>.

- (113) Gao, N.; Geyer, F.; Pilat, D. W.; Wooh, S.; Vollmer, D.; Butt, H. J.; Berger, R. How Drops Start Sliding over Solid Surfaces. *Nat. Phys.* **2018**, *14* (2), 191–196. <https://doi.org/10.1038/nphys4305>.
- (114) Adera, S.; Alvarenga, J.; Shneidman, A. V.; Zhang, C. T.; Davitt, A.; Aizenberg, J. Depletion of Lubricant from Nanostructured Oil-Infused Surfaces by Pendant Condensate Droplets. *ACS Nano* **2020**, *14* (7), 8024–8035. <https://doi.org/10.1021/acsnano.9b10184>.
- (115) Grundke, K.; Michel, S.; Knispel, G.; Grundler, A. Wettability of Silicone and Polyether Impression Materials: Characterization by Surface Tension and Contact Angle Measurements. *Colloids Surfaces A Physicochem. Eng. Asp.* **2008**, *317* (1–3), 598–609. <https://doi.org/10.1016/j.colsurfa.2007.11.046>.
- (116) Tian, Y.; Ina, M.; Cao, Z.; Sheiko, S. S.; Dobrynin, A. V. How to Measure Work of Adhesion and Surface Tension of Soft Polymeric Materials. *Macromolecules* **2018**, *51* (11), 4059–4067. <https://doi.org/10.1021/acs.macromol.8b00738>.
- (117) Ina, M.; Cao, Z.; Vatankhah-Varnoosfaderani, M.; Everhart, M. H.; Daniel, W. F. M.; Dobrynin, A. V.; Sheiko, S. S. From Adhesion to Wetting: Contact Mechanics at the Surfaces of Super-Soft Brush-like Elastomers. *ACS Macro Lett.* **2017**, *6* (8), 854–858. <https://doi.org/10.1021/acsmacrolett.7b00419>.
- (118) Gelest. *Silicone Fluids: Stable Inert Media*; 2012.
- (119) Shanahan, M. E. R.; Carre, A. Viscoelastic Dissipation in Wetting and Adhesion Phenomena. *Langmuir* **1995**, *11* (4), 1396–1402. <https://doi.org/10.1021/la00004a055>.
- (120) Long, D.; Ajdari, A.; Leibler, L. Static and Dynamic Wetting Properties of Thin Rubber Films. *Langmuir* **1996**, *12* (21), 5221–5230. <https://doi.org/10.1021/la9604700>.
- (121) Van Gorcum, M.; Karpitschka, S.; Andreotti, B.; Snoeijer, J. H. Spreading on Viscoelastic Solids: Are Contact Angles Selected by Neumann’s Law? *Soft Matter* **2020**, *16* (5), 1306–1322. <https://doi.org/10.1039/c9sm01453e>.
- (122) Forsberg, P. S. H.; Priest, C.; Brinkmann, M.; Sedev, R.; Ralston, J. Contact Line Pinning on Microstructured Surfaces for Liquids in the Wenzel State. *Langmuir* **2010**, *26* (2), 860–865. <https://doi.org/10.1021/la902296d>.
- (123) Kajiyama, T.; Daerr, A.; Narita, T.; Royon, L.; Lequeux, F.; Limat, L. Advancing Liquid Contact Line on Visco-Elastic Gel Substrates: Stick-Slip vs. Continuous Motions. *Soft Matter* **2013**, *9* (2), 454–461. <https://doi.org/10.1039/c2sm26714d>.
- (124) Lhermerout, R.; Davitt, K. Controlled Defects to Link Wetting Properties to Surface Heterogeneity. *Soft Matter* **2018**, *14* (42), 8643–8650. <https://doi.org/10.1039/C8SM01715H>.

- (125) Hauer, L.; Cai, Z.; Vollmer, D.; Pham, J. T. Phase Separation in Wetting Ridges of Sliding Drops on Soft and Swollen Surfaces. *ArXiv* **2022**, 1–13.

## VITA

### Education

University of Kentucky, Doctor of Philosophy, Fall 2018 - Spring 2023 (expected)

University of Akron, Master of Science, Fall 2016 - Spring 2018

East China University of Science and Technology, Bachelor of Science, Fall 2012 - Spring 2016

### Publications

[1] L. Hauer\*, Z. Cai\*, D. Vollmer, J. T. Pham. “Phase Separation in Wetting Ridges of Sliding Drops on Soft and Swollen Surfaces”. arXiv, (2022).

[2] D. R. Darby, Z. Cai, C. Mason, J. T. Pham. “Modulus and adhesion of Sylgard 184, Solaris, and Ecoflex 00-30 silicone elastomers with varied mixing ratios”. *Journal of Applied Polymer Science*, (2022).

[3] Z. Cai, J. T. Pham. “How swelling, crosslinking, and aging affect drop pinning on lubricant-infused soft elastomers”. *ACS Applied Polymer Materials*, (2022).

[4] S. Torabi, Z Cai, J. T. Pham, C. Trinkle. “Hydrophobic surface patterning with soft, wax-infused micro-stamps”. *Journal of Colloid and Interface Science*, (2022)

- [5] Z. Cai, A. Skabeev, S. Morozova, J. T. Pham. "Fluid separation and network deformation in wetting of soft and swollen surfaces." *Communications Materials (Nature)*, 2, 21, (2021).

\* These authors contributed equally.

#### Honors

- [1] Langmuir Graduate Student Oral Presentation Awards (Second Prize), ACS Colloid and Surface Science Symposium, Colorado School of Mines, Golden, CO. 07.2022
- [2] Outstanding Graduate Student Awards, Materials Science and Engineering Department, University of Kentucky. 05.2022